3D printing of cellulose derivatives based-biogel matrices as the drug delivery system and support structure

by

Yiliang Cheng

A thesis submitted to the graduate faculty

in partial fulfillment of the requirements for the degree of

MASTER OF SCIENCE

Major: Food Science and Technology

Program of Study Committee:
Xiaolei Shi, Co-major Professor
Nuria C. Acevedo, Co-major Professor
Hantang Qin, Co-major Professor

The student author, whose presentation of the scholarship herein was approved by the program of study committee, is solely responsible for the content of this thesis. The Graduate College will ensure this thesis is globally accessible and will not permit alterations after a degree is conferred.

Iowa State University

Ames, Iowa

2020

TABLE OF CONTENTS

Page

LIST OF FIGURES

Page

LIST OF TABLES

Page

NOMENCLATURE

3D	Three-Dimensional
ABS	Acrylonitrile Butadiene Styrene
AM	Additive Manufacturing
CMEC	Carboxy Methyl Ethyl Cellulose
DS	Degree of Substitution
FDM	Fused Deposition Modeling
HME	Hot Melt Extrusion
HPMC	Hydroxypropyl Methylcellulose
MC	Methylcellulose
PLA	Polylactic Acid
SSE	Semi-Solid Extrusion

ACKNOWLEDGMENTS

I would like to thank my committee chair, Dr. Xiaolei Shi, and my committee members, Dr. Nuria Acevedo, and Dr. Hantang Qin, for their guidance and support throughout the course of this research. Many thanks for Dr. Shi for giving me the valuable opportunity to go back to school and helping me to find my enthusiasm in research. All of my committee members showed their patience, erudition, and kindness during the journey of my master's degree. They are all wonderful and inspiring mentors that make meaningful impacts on my life.

In addition, I would also like to thank my friends, colleagues, and the department faculty and staff for making my time at Iowa State University a wonderful experience. My lab mates, Chih-Chun, Xuepeng, Xiaohui, Xiao, and Hunter, they have all generously provided support and helped with my research.

I also want to offer my appreciation to my dear and loving families. They are people who understand me best in the world and consistently gave me unconditional love to support my research.

ABSTRACT

Within the last decade, three-dimensional (3D) printing has attracted an unprecedented interest as a promising technology due to its high flexibility and cost-effectiveness. The hydrogels and colloids prepared by biopolymers such as cellulose derivatives have been considered as the most critical materials for the development of 3D printing technology, due to their biodegradability and biocompatibility. In this work, two types of cellulose derivatives, hydroxypropyl methylcellulose (HPMC) and methylcellulose (MC), were selected as the potential materials to assess their printability by using semi-solid extrusion (SSE) based 3D printer. The HPMC and MC in their powder forms are also widely used in the conventional pharmaceutical industry; however, in this study, they were prepared into hydrogels for 3D printing purpose. The 3D printed tablets contained two solid ingredients, cellulose derivatives as the excipient and theophylline as the active pharmaceutical ingredient (API). The therapeutic paste was prepared by combining various doses of theophylline (0, 75, 100, 125mg) with different concentrations of excipients (8, 10, and 12%). The paste was then 3D printed into semi-solid tablets under optimized printing conditions under ambient temperature. The HPMC and MC based hydrogels showed a shear-thinning behavior, which is suitable for the extrusion-based 3D printing. The concentration and type of excipient played predominate roles in determining the 3D printing potential, which was related to the rheological and textural properties. The results of apparent viscosity, yield stress, storage modulus, and hardness showed a significant increase with the increase in excipient concentration. For tablets with different excipients, the MC A4M 12% (w/w) based tablets showed the best printing quality and shape retention ability, followed by HPMC K4M 12% (w/w) based tablets. The tan δ values of these tablets with optimal printability fell in the range between 0.2 and 0.7, which indicated the solid-like property. The

increased concentration of excipient also significantly increased the magnitude of storage modulus. The results of flow behavior and oscillation sweep tests could be used to predict the printability of potential materials for 3D printing purposes using the current platform.

The SEM images demonstrated that the cross-linked hydrogel matrix exhibited a porous three-dimensional structure, which had the potential to encapsulate the theophylline particles within its microstructure. The *in vitro* dissolution test showed that the release of all tablets regardless of the excipient type was extended over 12 hours. After the dissolution test, the matrices of MC A4M based tablets were still kept in their original structures, which indicated that MC A4M formed the porous microstructure to delay the release through the barrier effect. The release profiles of all these cellulose derivative-based tablets were well fitted into first-order and Korsmeyer-Peppas models, which showed non-Fickian diffusion. 3D printed HPMC matrix release the theophylline by both diffusion and erosion mechanisms. The findings in these studies will support the development of patient-tailored and extended-release tablets by using the SSE based 3D printing technology.

In addition, the 3D printable characteristics of HPMC K4M hydrogel also showed the potential to fabricate a biodegradable support structure in the manufacturing industry. Similar to the 3D printed tablets, the printed geometries with HPMC K4M 12% (w/w) concentration also showed the optimal 3D printing quality and mechanical strength after the printing process. This material is feasible to be 3D printed into geometries with different infill density (100%, 75%, and 50%) and different patterns (rectilinear and Hilbert curve). Since HPMC is produced from renewable resource, the cellulose derivative polymers could be used to replace the petroleum-based materials in the 3D printing application.

CHAPTER 1. GENERAL INTRODUCTION

Thesis Organization

This thesis begins with a review of the literature focusing on using 3D printing technologies for food fabrication and drug delivery systems. The physical properties (solubility and sol-gel behavior, etc.) and application of cellulose derivatives in pharmaceutical fields were also involved. Three manuscripts in the format of journal publications are included in this thesis following the literature review. The manuscript authors are from the Department of Food Science and Human Nutrition and the Department of Industrial and Manufacturing Systems Engineering. Drs. Xiaolei Shi and Dr. Hantang Qin are the corresponding authors for all of the manuscripts.

Literature Review

3D printing technology

3D printing or additive manufacturing (AM) is a process for building a 3D object by successively adding material layer by layer under digital control (Gokhare, Raut, & Shinde, 2017). Since the first mention of 3D printing for a patent application in the 1980s, it has become the first choice of the industry for rapid prototyping (Sharma & Goel, 2019). In the past 40 years, 3D printing technology has already been applied in various fields, such as medicine, tissue engineering, fashion design, manufacturing engineering, construction, and the computer industry (Gokhare et al., 2017). 3D printing is a multi-step process that could be achieved by different methods with various fabrication steps. The common techniques include selective laser sintering, binder deposition, stereolithography, inkjet printing, and extrusion-based printing (Algahtani, Mohammed, & Ahmad, 2019; Gokhare et al., 2017). The extrusion-based printing technique was mainly used for prototyping in manufacturing due to flexibility and material availability (Algahtani et al., 2019). The extrusion-based 3D printing was classified into two process

categories (**Fig. 1.1**), which are fused deposition modeling (FDM) and semi-solid extrusion (SSE) (Solanki, Tahsin, Shah, & Serajuddin, 2018).

The FDM method was first developed in the late 1980s and was particularly of interest in the various fields. For this method, the thermoplastic polymers (e.g., Acrylonitrile Butadiene Styrene (ABS) or Polylactic Acid (PLA)) are first extruded and shaped into filament or wire, then fed into the FDM-based 3D printer. The nozzle head or printer heater heats the polymer materials into a viscoelastic form, which allows the molten materials to be extruded and fused with the previously printed layers (Chaunier, Leroy, Della Valle, & Lourdin, 2016; Gokhare et al., 2017). Similar to the FDM-based 3D printers, SSE-based printers also achieve the printing process by using extrusion so that it can be considered as an alternative technique for the extrusion-based method. SSE 3D printing typically uses the pressure or screw gear rotation to fabricate the semi-solid materials into filament through a nozzle, and the material is kept in a syringe before extrusion (Algahtani et al., 2019). The main difference between these two process categories is the state of the printable materials. Before printing, FDM-based printers require the production of filaments, which contain thermoplastic polymers, while SSE-based printers require the semi-solid state materials to be loaded into printer syringe and then extruded through the printer nozzle (Azad et al., 2020; Vithani et al., 2019). To make the thermoplastic-contained filaments to be liquefied and extrudable, FDM-printers need to use a heater to melt the filaments, and the operating temperature is typically higher than 150°C (Melocchi et al., 2015). For SSE-based printers, the excellent printing performance mostly depends on the viscosity and flow behavior of the semi-solid state materials. Since the printing materials are extrudable at ambient temperature, there is no requirement for tuning the operating temperature during 3D printing (Algahtani et al., 2019). Therefore, SSE-based 3D printers function under a broader range of

temperatures, such as printing chocolates at an operating temperature between 31°C and 47°C and printing cement-based materials under ambient temperature (Lanaro et al., 2017; Valente, Sibai, & Sambucci, 2019). Thus, SSE-based 3D printing is widely applied in bio-tissue print, such as organ repair and bone tissue scaffolds (AnilKumar et al., 2019; Khalil, Nam, & Sun, 2005). Additionally, the semi-solid state materials are more suitable for SSE-based 3D printers (e.g., hydrogels) due to the well-controlled viscoelastic response. The cross-linked hydrogel solutions or bio-inks behave like a viscous liquid during extrusion and show the ability to avoid deformation due to the stable cross-linked networks (Dankar, Haddarah, Omar, Sepulcre, & Pujolà, 2018; Vancauwenberghe, Verboven, Lammertyn, & Nicolaï, 2018).

3D printing for food production

Previous research and achievements showed that 3D printing technology is gradually becoming a potential manufacturing technology in many fields of the industry due to its advantages such as simple process, cost-effectiveness and customization freedom (Chaunier, Della, Lourdin, & Leroy, 2018; Rattanakit, Moulton, Santiago, Liawruangrath, & Wallace, 2012). Examples of 3D printing applied to human activity fields include the food and pharmaceutical industry. 3D printing technology in the food industry has the potential to produce customized food with complex design and personalized nutritional content (Godoi, Prakash, & Bhandari, 2016). Based on the selection of materials and processes, there are three leading 3D printing technologies currently in use for food fabrication: extrusion printing, inkjet printing, and powder binding deposition. The best-developed technology is extrusion 3D printing because of the low-cost and proper resolution of printed objects (H. Chen, Xie, Chen, & Zheng, 2019). There are typically two kinds of food materials that could be printable for extrusion-based 3D printers: molten materials (cheese and chocolate, etc.) and semi-solid state materials (pastes and gels, etc.) (Derossi, Caporizzi, Azzollini, & Severini, 2018; Le Tohic et al., 2018). For molten

materials, the rigid materials are first melted and then extruded through the printer nozzle or head under pressure. Then the extruded filaments are deposited onto the previous layer and then adhere to each other. Cornell University explored chocolate 3D printing by using a Fab@home Fabrication system, and many food 3D printer companies (Foodini, TNO, etc.) are developing 3D printing systems for chocolate fabrication as well (Godoi et al., 2016). Lanaro et al. (2017) designed a melt extrusion 3D printer to print chocolate into a complex structure over 90 mm height with the assistance of air cooling. The materials within the printer were heated to around 47 °C in a syringe and then cooled down to about 20 °C to prevent object collapse. Another publication also showed the potential of using extrusion printing to generate the complex structures of processed cheese with both low and high printing speed after melting cheese at 75°C (Le Tohic et al., 2018).

Semi-solid state food materials are a choice for extrusion printing, especially when printing thermal sensitive materials like proteins (egg yolk, soy protein isolate), vegetables, fruits, and peanut butter (Anukiruthika, Moses, & Anandharamakrishnan, 2019; J. Chen et al., 2019; Dankar et al., 2018; Derossi et al., 2018; Lille, Nurmela, Nordlund, Metsä-Kortelainen, & Sozer, 2018; Severini, Derossi, Ricci, Caporizzi, & Fiore, 2018). Semi-solid state extrusion is also appropriate for thermoset polymers, such as the hydrogels formed with cross-linking, to fabricate the matrix for encapsulation/entrapment of other active ingredients (Khaled, Burley, Alexander, & Roberts, 2014). The fabrication of food is performed at an ambient or slightly elevated temperature when using the extrusion 3D printers. However, not all of the consumable materials are 3D printable since materials can only achieve the shape fidelity of printed objects with proper physical properties. So the addition of other ingredients could be used to improve the material’s printability (Lipton, Cutler, Nigl, Cohen, & Lipson, 2015). Hydrogels made by

polymer-based materials had been selected to prevent deformation due to the gel-forming ability, such as pectin, gelatin, xanthan gum, and fish protein (J. Chen et al., 2019; Kim et al., 2018; Vancauwenberghe et al., 2018; L. Wang, Zhang, Bhandari, & Yang, 2018). Also, the addition of thickener or gelling agents such as starch could lead to increases of viscosity and water holding capacity and improve the printability as a result (Anukiruthika et al., 2019; H. Chen et al., 2019; F. Yang, Zhang, Bhandari, & Liu, 2018). The shear-thinning behavior is one of the most critical indicators for food materials to produce a self-supporting structure (H. Chen et al., 2019; J. Chen et al., 2019; Liu, Zhang, Bhandari, & Yang, 2018).

3D printing in the area of pharmaceuticals

3D printing in the drug delivery system has recently attracted considerable interest in medications to make a new type of drug delivery system. The principal benefits of using 3D printing technology in the pharmaceutical field include enhanced productivity, increased cost efficiency, and customized medication dose (Kotta, Nair, & Alsabeelah, 2018). Similar to the technologies for 3D food printing, various techniques had been developed for 3D pharmaceutical printing. The first FDA approved 3D printed medicine, Spritam®, became available to patients in 2015. Unlike the conventional pill fabricated by compression technology, the loose layer-by-layer 3D printed structure allowed the Spritam® pill to disintegrate in the mouth with just a sip of water to benefit the patients with difficulty in swallowing, especially epilepsy patients (Solanki et al., 2018). Even though the Spritam® pill is one of the most successful examples prepared by binder jet printing technology, the most popular and common methodology for 3D tablets printing is the extrusion-based method, especially the FDM technology (Chai et al., 2017; Solanki et al., 2018; Tan, Maniruzzaman, & Nokhodchi, 2018).

Regarding the FDM technology, the active pharmaceutical ingredient (API) first is prepared by mixing with the thermoplastic polymers, and then the mixtures are processed into

filaments by using hot-melt extrusion (HME) technology. During the printing process, the heater of the FDM-based printer applied a high temperature (typically over 180 °C) to make the prepared filaments to be liquefied and extruded through the printer's nozzle (Q. Li et al., 2018). FDM has become the most prevalent technology for tablets fabrication in the pharmaceutical field due to the advantages of low-cost, customizable, and relatively high printing resolution (Algahtani et al., 2019; Norman, Madurawe, Moore, Khan, & Khairuzzaman, 2017). However, previous studies of FDM in the drug delivery system exhibited several limitations. Firstly, the high-temperature processes (usually over 150°C) during both HEM and FDM were only compatible and suitable for thermally stable APIs (Huang et al., 2017). Previous studies demonstrated as well that thermal degradation may have still occurred even though the API passed through the hot printer nozzle very quickly in a span of a few seconds (Goyanes, Buanz, Hatton, Gaisford, & Basit, 2015). Secondly, the excipient selection of FDM filament making is limited. Most of the published research used thermoplastic polymers, such as ABS, PLA, and PVA, as the excipient materials for FDM printing. However, these materials are not FDA approved polymers for food and pharmaceutical usage (Jamróz, Szafraniec, Kurek, & Jachowicz, 2018; Smith et al., 2018). These limitations could be overcome by using biodegradable hydrogels as the excipient and fabricating the dosage forms by SSE-based 3D printing technology. The unique characteristic of SSE-based 3D printing is that the materials' printability is typically provided by the gel-forming ability through the selected excipients, so that the printing material could be fabricated without the thermal process. The potential excipients, which showed gel-forming ability, include hydroxypropyl methylcellulose (HPMC) or microcrystalline cellulose (MCC), etc. (Khaled et al., 2018, 2014; Khaled, Burley, Alexander, Yang, & Roberts, 2015b, 2015a; Q. Li et al., 2018). However, the study of SSE technology for tablets fabrication is still in

its infancy. There is no standard SSE 3D printing model to fabricate the tablets or a predictable parameter that can be used to select proper excipient for extrusion. Several publications have reported that the 3D printing is related to the viscoelastic properties of the materials; however, the mathematic model between the rheological properties of the printing materials and the printability/mechanical properties of the 3D printed objects has not been well established (Q. Li et al., 2018; Rattanakit et al., 2012).

Derivation of cellulose

Cellulose is the most abundant polymer, followed by chitin, on the surface of the Earth (Sanandiya, Vijay, Dimopoulou, Dritsas, & Fernandez, 2018). Cellulose is an essential structural component in plants, and it can be extracted from the plant cell wall materials. The chemical structure of natural cellulose is a long chain composed of repeating β-1, 4-linked D-glucose units ranging from several hundred to over ten thousand monomers (Bhatia, 2016). The molecular structure of powdered cellulose is a linear unbranched polysaccharide, as shown in **Fig. 1.2** (Marques-Marinho & Vianna-Soares, 2013). Based on the different orientations of the cellulose molecule chains, there are two different types of cellulose allomorphs, cellulose I (parallel), and cellulose II (antiparallel). Once extracted from the fibrous plants, such as wood or cotton, and processed into powder, cellulose could be used as filler/binder in tablets fabrication for both granulation and direct compression processes in the pharmaceutical industry (Ogaji, Nep, & Audu-Peter, 2012).

The inter-molecular hydrogen bonds between hydroxyl groups lead to the aggregation of the crystalline form of cellulose. But the natural cellulose material is insoluble in water due to the firm, intermolecular, hydrogen bonding in the chemical structure (Nasatto et al., 2015). The process of cellulose derivatization allows chemical and physical replacement of the hydroxyl groups on the D-glucopyranose units. Once the hydrogen groups are partially substituted by the

hydrophobic groups, the strong hydrogen bonds are prevented, and the solubility of cellulose in water increases consequently (L. Li et al., 2001). There are three different approaches for derivatization: etherification, esterification, and cross-linking or graft copolymerization (Bhatia, 2016). Esterification is the first and most common technique to yield cellulose derivatives, and the yield products included cellulose nitrate, cellulose acetate (simplest cellulose ester), and cellulose sulfate (Y. Wang, Wang, Xie, & Zhang, 2018). Etherification can also be used to replace the primary hydroxyl groups on the cellulose backbone to yield ether derivatives such as MC (simplest cellulose ether), HPMC, and carboxymethylcellulose (Fox, Li, Xu, & Edgar, 2011). The different derivatives can be yielded depending on the replaced R groups during etherification (**Fig. 1.3**). The degree of substitution (DS) presents the average number of substituent groups attached to each D-glucose units along the backbone (Marques-Marinho & Vianna-Soares, 2013). DS affects cellulose derivatives' physical properties such as solubility, hydrophobicity, molecular weight, and crystallization inhibition (Marques-Marinho & Vianna-Soares, 2013; Y. Yang, Bi, Dürig, & Ingredients, 2016).

Mischnick et al. (2010) claimed that the primary purpose of cellulose etherification is to improve water solubility, which could provide the potential for cellulose derivatives to work as a desirable excipient in pharmaceuticals and food applications. The appropriate type of cellulose derivatives can form a hydrogel once dissolved in water to control the drug release by diffusion through the hydrogel or by aqueous swelling or shrinking (L. Li et al., 2001; Mischnick & Momcilovic, 2010). The excipients which were used in this thesis are two different kinds of cellulose derivatives, MC and HPMC. HPMC is the most predominant semisynthetic excipient compared with other cellulose derivative-based excipients. It has already been widely applied in the pharmaceutical industry as capsules shells, disintegrants, binders, protective coatings, and

hydrophilic matrixes to control the release profiles of APIs in the traditional pharmaceutical industry, i.e., compressed tablet production (Debotton & Dahan, 2016; Marques-Marinho & Vianna-Soares, 2013; Ogaji et al., 2012). The HPMC-based hydrophilic matrices have been widely applied in pharmaceuticals as an excipient in controlled release drug delivery systems (Jayasree et al., 2014). The HPMC matrices prevent the diffusion or erosion of the dissolution medium through hydrated layers to dissolve solid pharmaceutical dosages (Bhatia, 2016; Ramachandran, Chen, & Etzler, 1999). MC is provided mainly as a powder, and it cannot be metabolized or digested in the gastrointestinal tract. These properties make MC a common additive for pharmaceuticals such as thickeners, binders, emulsifiers, and stabilizers. It was also used as the alternative of gelatin to produce the capsule from non-animal sources (Nasatto et al., 2015).

Approximately 27-32% of hydroxyl groups in MC are substituted for the methyl ether (CH_3O) form. The general degree of polymerization and molecular weights of MC is in the range of 50 to 1,000 and 10,000 to 220,000 Da, respectively. The hydroxyl groups in HPMC are substituted for both methoxyl (OCH_3) and hydroxypropyl groups [$OCH_2CH(OH)CH_3$]. There are various grades of HPMC with different viscosities and extents of substitution. The molecular weights of HPMC are in the range of 10,000 to 1,500,000 Da (Marques-Marinho & Vianna-Soares, 2013).

The solubility of MC is closely related to the DS value since the higher DS value indicated the lower fraction of polar hydroxyl groups. When MC contacts cold water, it will form a gel layer to inhibit the complete dissolution and decrease the dissolution rate (Nasatto et al., 2015). Nasatto et al. (2015) indicated a proper way to prepare a homogeneous MC solution by dissolving the MC powder firstly in hot water around 75 °C and then cooling down to around

5 °C with continuous stirring. The cellulose ethers aqueous solution could transform into a homogeneous hydrogel with proper concentration when following these proposed procedures.

Sol-gel behavior of MC and HPMC

The formation of MC gels included a two-stage process and showed both increases in turbidity and viscosity (**Fig. 1.4**) (Nasatto et al., 2015). The hydrophobic interaction between highly methylated glucose zones prompted the first stage during the MC gelation process, which was called “clear loose gel” or “pre-gel”. The second stage was accompanied by an increased turbidity and phase separation, so it was called “turbid strong gel”. The increased turbidity and storage modulus (G') indicated the generation of gel structure formed by the phase separation of hydrophobic parts from the hydrophilic matrix during heating (L. Li et al., 2001). Besides, the created MC solutions were stable at room temperature and would show syneresis processes at high temperatures (over 70°C) (Nasatto et al., 2015). Likewise, HPMC gels were also formed as a result of the formation of hydrophobic aggregations at high temperatures (L. Li et al., 2001). The main difference between MC and HPMC was the degree of substitution and substituted groups. In the case of HPMC, the substituted methyl group remained the dominant substituent, but there were some of the hydroxyl groups that had been replaced by more polar and larger hydroxypropyl groups (Haque, Richardson, Morris, Gidley, & Caswell, 1993).

When a natural or synthetic polymer was cross-linked into a three-dimensional network by chemical or physical bonds once swelling in water, the formed system was called hydrogel, which could hold a large volume of water (L. Li et al., 2001). As semisynthetic polymers, MC and HPMC powder could be dissolved into hot water and formed firm hydrogels during cooling down.

Cellulose derivatives applications in the pharmaceutical field

Solid oral dosage forms (e.g., tablets and capsules) were the most common and convenient pharmaceutical routes of drug delivery in clinical practice (Debotton & Dahan, 2016). These drug products usually contained two types of substances: excipient and active pharmaceutical ingredient (API). The excipient was an inactive material that served as the medium for drug delivery and essential functions of excipients in pharmaceuticals, including using them as a tablet binder, lubricant anti-adhesive agent, viscosity enhancer, or tablet disintegrant, etc. (Karolewicz, 2016). Selecting the optimal excipients was critical to ensuring the safety and stability of APIs and providing profitability of time and therapeutic efficacy. The excipients could be divided into three major categories depending on their components: natural, semisynthetic, and synthetic excipients. The natural excipients were mostly natural polymeric materials such as cellulose, pectin, collagen, and gum acacia. Those polymers that were naturally derived but chemically modified were semi-synthetic excipients, such as MC, HPMC, and carboxymethyl ethylcellulose (CMEC). Examples of synthetic excipient included the organic chemicals which were derived from oil or rock, such as poly (vinyl pyrrolidone) and poly (acrylic acid) (Domínguez-Robles et al., 2019; Jayasree et al., 2014; Ogaji et al., 2012). Compared with the synthetic excipients, the natural and semisynthetic excipients provided a series of advantages such as low cost, low toxicity, relative abundance, biocompatibility, and biodegradable profiles (Bhatia, 2016; Ogaji et al., 2012). The most widely used excipients were cellulose and its derivatives, which had attracted lots of attention from both industrial and academic communities (Domínguez-Robles et al., 2019; Karolewicz, 2016).

Hypothesis of this Research

Our central hypothesis for this study is that the cellulose derivatives-based polymers, i.e., HPMC and MC, could be used as excipients for SSE 3D printing of a drug delivery system. To

be more specific, we expect that the rheological properties of 3D printing materials could be used to predict the 3D printability and mechanical properties of 3D printed objects. We hypothesize that the increases of the excipient concentration and API dosage could influence the rheological properties of the printing materials, and thus impact the shape retention ability and printing quality of the 3D printed tablets. The printed tablets could serve as microscale hydrogel-based matrices to control the API release rate over time by modifying the formulation.

Objective

The study of SSE technology for tablets fabrication is still in its infancy. To fill the knowledge gap, this research aimed to explore the feasibility of using an SSE-based 3D printer to fabricate sustained-release tablets by pursuing three objectives: 1) to investigate the effect of the concentration of excipient and the dosage of theophylline on the tablets physical properties (rheological, textural, and microstructural properties); 2) to build the relationship between semi-solid materials' printability (extrudability and shape retention ability) and rheological parameters (yield stress, dynamic modulus, and apparent viscosity); 3) to explore the drug loading capacity and drug release profile through the microscale cellulose derivative-based matrices.

References

Algahtani, M. S., Mohammed, A. A., & Ahmad, J. (2019). Extrusion-Based 3D Printing for Pharmaceuticals: Contemporary Research and Applications. *Current Pharmaceutical Design*, *24*(42), 4991–5008. https://doi.org/10.2174/1381612825666190110155931

AnilKumar, S., Allen, S. C., Tasnim, N., Akter, T., Park, S., Kumar, A., … Joddar, B. (2019). The applicability of furfuryl-gelatin as a novel bioink for tissue engineering applications. *Journal of Biomedical Materials Research - Part B Applied Biomaterials*, *107*(2), 314–323. https://doi.org/10.1002/jbm.b.34123

Anukiruthika, T., Moses, J. A., & Anandharamakrishnan, C. (2019). 3D printing of egg yolk and white with rice flour blends. *Journal of Food Engineering*, *265*(August 2019), 109691. https://doi.org/10.1016/j.jfoodeng.2019.109691

Azad, M. A., Olawuni, D., Kimbell, G., Badruddoza, A. Z. M., Hossain, M. S., & Sultana, T. (2020). *Polymers for extrusion-based 3D printing of pharmaceuticals: A holistic materials–process perspective*. *Pharmaceutics* (Vol. 12). https://doi.org/10.3390/pharmaceutics12020124

Bhatia, S. (2016). *Natural Polymer Drug Delivery Systems*. *Natural Polymer Drug Delivery Systems*. Springer. https://doi.org/10.1007/978-3-319-41129-3

Chai, X., Chai, H., Wang, X., Yang, J., Li, J., Zhao, Y., … Xiang, X. (2017). Fused deposition modeling (FDM) 3D printed tablets for intragastric floating delivery of domperidone. *Scientific Reports*, *7*(1), 1–9. https://doi.org/10.1038/s41598-017-03097-x

Chaunier, L., Della, G., Lourdin, D., & Leroy, E. (2018). Material extrusion of plant biopolymers : Opportunities & challenges for 3D printing, *21*(January 2017), 220–233. https://doi.org/10.1016/j.addma.2018.03.016

Chaunier, L., Leroy, E., Della Valle, G., & Lourdin, D. (2016). Plasticized protein for 3D printing by fused deposition modeling. *AIP Conference Proceedings*, *1769*(2016). https://doi.org/10.1063/1.4963611

Chen, H., Xie, F., Chen, L., & Zheng, B. (2019). Effect of rheological properties of potato, rice and corn starches on their hot-extrusion 3D printing behaviors. *Journal of Food Engineering*, *244*(September 2018), 150–158. https://doi.org/10.1016/j.jfoodeng.2018.09.011

Chen, J., Mu, T., Goffin, D., Blecker, C., Richard, G., Richel, A., & Haubruge, E. (2019). Application of soy protein isolate and hydrocolloids based mixtures as promising food material in 3D food printing. *Journal of Food Engineering*, *261*(December 2018), 76–86. https://doi.org/10.1016/j.jfoodeng.2019.03.016

Dankar, I., Haddarah, A., Omar, F. E. L., Sepulcre, F., & Pujolà, M. (2018). 3D printing technology: The new era for food customization and elaboration. *Trends in Food Science and Technology*, *75*, 231–242. https://doi.org/10.1016/j.tifs.2018.03.018

Debotton, N., & Dahan, A. (2016). Applications of Polymers as Pharmaceutical Excipients in Solid Oral Dosage Forms. *Medicinal Research Reviews*, *30*(1), 1–22. https://doi.org/10.1002/med

Derossi, A., Caporizzi, R., Azzollini, D., & Severini, C. (2018). Application of 3D printing for customized food. A case on the development of a fruit-based snack for children. *Journal of Food Engineering*, *220*, 65–75. https://doi.org/10.1016/j.jfoodeng.2017.05.015

Domínguez-Robles, J., Stewart, S. A., Rendl, A., González, Z., Donnelly, R. F., & Larrañeta, E. (2019). Lignin and cellulose blends as pharmaceutical excipient for tablet manufacturing via direct compression. *Biomolecules*, *9*, 423. https://doi.org/10.3390/biom9090423

Fox, S. C., Li, B., Xu, D., & Edgar, K. J. (2011). Regioselective esterification and etherification of cellulose: A review. *Biomacromolecules*, *12*(6), 1956–1972. https://doi.org/10.1021/bm200260d

Godoi, F. C., Prakash, S., & Bhandari, B. R. (2016). 3d printing technologies applied for food design: Status and prospects. *Journal of Food Engineering*, *179*, 44–54. https://doi.org/10.1016/j.jfoodeng.2016.01.025

Gokhare, V. G., Raut, D. N., & Shinde, D. K. (2017). A Review paper on 3D-Printing Aspects and Various Processes Used in the 3D-Printing. *International Journal of Engineering Research & Technology (IJERT)*, *6*(06), 953–958.

Goyanes, A., Buanz, A. B. M., Hatton, G. B., Gaisford, S., & Basit, A. W. (2015). 3D printing of modified-release aminosalicylate (4-ASA and 5-ASA) tablets. *European Journal of Pharmaceutics and Biopharmaceutics*, *89*, 157–162. https://doi.org/10.1016/j.ejpb.2014.12.003

Haque, A., Richardson, R. K., Morris, E. R., Gidley, M. J., & Caswell, D. C. (1993). Thermogelation of methylcellulose. Part II: effect of hydroxypropyl substituents. *Carbohydrate Polymers*, *22*(3), 175–186. https://doi.org/10.1016/0144-8617(93)90138-T

Huang, S., O'Donnell, K. P., Delpon de Vaux, S. M., O'Brien, J., Stutzman, J., & Williams, R. O. (2017). Processing thermally labile drugs by hot-melt extrusion: The lesson with gliclazide. *European Journal of Pharmaceutics and Biopharmaceutics*, *119*, 56–67. https://doi.org/10.1016/j.ejpb.2017.05.014

Jamróz, W., Szafraniec, J., Kurek, M., & Jachowicz, R. (2018). 3D printing in pharmaceutical and medical applications. *Pharmaceutical Research*, *35*(9), 1–22.

Jayasree, J., Sivaneswari, S., Hemalatha, G., Preethi, N., Mounika, B., & Murthy, S. V. (2014). Role of various natural, synthetic and semi-synthetic polymers on drug release kinetics of losartan potassium oral controlled release tablets. *International Journal of Pharmaceutical Investigation*, *4*(4), 183. https://doi.org/10.4103/2230-973x.143118

Karolewicz, B. (2016). A review of polymers as multifunctional excipients in drug dosage form technology. *Saudi Pharmaceutical Journal*, *24*(5), 525–536. https://doi.org/10.1016/j.jsps.2015.02.025

Khaled, S. A., Alexander, M. R., Irvine, D. J., Wildman, R. D., Wallace, M. J., Sharpe, S., … Roberts, C. J. (2018). Extrusion 3D Printing of Paracetamol Tablets from a Single Formulation with Tunable Release Profiles Through Control of Tablet Geometry. *AAPS PharmSciTech*, *19*(8), 3403–3413. https://doi.org/10.1208/s12249-018-1107-z

Khaled, S. A., Burley, J. C., Alexander, M. R., & Roberts, C. J. (2014). Desktop 3D printing of controlled release pharmaceutical bilayer tablets. *International Journal of Pharmaceutics*, *461*(1–2), 105–111. https://doi.org/10.1016/j.ijpharm.2013.11.021

Khaled, S. A., Burley, J. C., Alexander, M. R., Yang, J., & Roberts, C. J. (2015a). 3D printing of five-in-one dose combination polypill with defined immediate and sustained release profiles. *Journal of Controlled Release*, *217*, 308–314. https://doi.org/10.1016/j.jconrel.2015.09.028

Khaled, S. A., Burley, J. C., Alexander, M. R., Yang, J., & Roberts, C. J. (2015b). 3D printing of tablets containing multiple drugs with defined release profiles. *International Journal of Pharmaceutics*, *494*(2), 643–650. https://doi.org/10.1016/j.ijpharm.2015.07.067

Khalil, S., Nam, J., & Sun, W. (2005). Multi-nozzle deposition for construction of 3D biopolymer tissue scaffolds. *Rapid Prototyping Journal*, *11*(1), 9–17. https://doi.org/10.1108/13552540510573347

Kim, H. W., Lee, J. H., Park, S. M., Lee, M. H., Lee, I. W., Doh, H. S., & Park, H. J. (2018). Effect of Hydrocolloids on Rheological Properties and Printability of Vegetable Inks for 3D Food Printing. *Journal of Food Science*, *83*(12), 2923–2932. https://doi.org/10.1111/1750-3841.14391

Kotta, S., Nair, A., & Alsabeelah, N. (2018). 3D Printing Technology in Drug Delivery: Recent Progress and Application. *Current Pharmaceutical Design*, *24*(42), 5039–5048. https://doi.org/10.2174/1381612825666181206123828

Lanaro, M., Forrestal, D. P., Scheurer, S., Slinger, D. J., Liao, S., Powell, S. K., & Woodruff, M. A. (2017). 3D printing complex chocolate objects: Platform design, optimization and evaluation. *Journal of Food Engineering*, *215*, 13–22. https://doi.org/10.1016/j.jfoodeng.2017.06.029

Le Tohic, C., O'Sullivan, J. J., Drapala, K. P., Chartrin, V., Chan, T., Morrison, A. P., … Kelly, A. L. (2018). Effect of 3D printing on the structure and textural properties of processed cheese. *Journal of Food Engineering*, *220*, 56–64. https://doi.org/10.1016/j.jfoodeng.2017.02.003

Li, L., Thangamathesvaran, P. M., Yue, C. Y., Tam, K. C., Hu, X., & Lam, Y. C. (2001). Gel Network Structure of Methylcellulose in Water. *Langmuir*, *17*(26), 8062–8068. https://doi.org/10.1021/la010917r

Li, Q., Guan, X., Cui, M., Zhu, Z., Chen, K., Wen, H., … Pan, W. (2018). Preparation and investigation of novel gastro-floating tablets with 3D extrusion-based printing. *International Journal of Pharmaceutics*, *535*(1–2), 325–332. https://doi.org/10.1016/j.ijpharm.2017.10.037

Lille, M., Nurmela, A., Nordlund, E., Metsä-Kortelainen, S., & Sozer, N. (2018). Applicability of protein and fiber-rich food materials in extrusion-based 3D printing. *Journal of Food Engineering*, *220*, 20–27. https://doi.org/10.1016/j.jfoodeng.2017.04.034

Lipton, J. I., Cutler, M., Nigl, F., Cohen, D., & Lipson, H. (2015). Additive manufacturing for the food industry. *Trends in Food Science and Technology*, *43*(1), 114–123. https://doi.org/10.1016/j.tifs.2015.02.004

Liu, Z., Zhang, M., Bhandari, B., & Yang, C. (2018). Impact of rheological properties of mashed potatoes on 3D printing. *Journal of Food Engineering*, *220*, 76–82. https://doi.org/10.1016/j.jfoodeng.2017.04.017

Marques-Marinho, F., & Vianna-Soares, C. (2013). Cellulose and Its Derivatives Use in the Pharmaceutical Compounding Practice. In T. van de Ven & L. Godbout (Eds.), *Cellulose - Medical, Pharmaceutical and Electronic Applications* (1st ed.). InTech. https://doi.org/10.5772/56637

Melocchi, A., Parietti, F., Loreti, G., Maroni, A., Gazzaniga, A., & Zema, L. (2015). 3D printing by fused deposition modeling (FDM) of a swellable/erodible capsular device for oral pulsatile release of drugs. *Journal of Drug Delivery Science and Technology*, *30*, 360–367. https://doi.org/10.1016/j.jddst.2015.07.016

Mischnick, P., & Momcilovic, D. (2010). *Chemical Structure Analysis of Starch and Cellulose Derivatives*. *Advances in Carbohydrate Chemistry and Biochemistry* (Vol. 64). Elsevier Inc. https://doi.org/10.1016/S0065-2318(10)64004-8

Nasatto, P. L., Pignon, F., Silveira, J. L. M., Duarte, M. E. R., Noseda, M. D., & Rinaudo, M. (2015). Methylcellulose, a cellulose derivative with original physical properties and extended applications. *Polymers*, *7*(5), 777–803. https://doi.org/10.3390/polym7050777

Norman, J., Madurawe, R. D., Moore, C. M. V., Khan, M. A., & Khairuzzaman, A. (2017). A new chapter in pharmaceutical manufacturing: 3D-printed drug products. *Advanced Drug Delivery Reviews*, *108*, 39–50. https://doi.org/10.1016/j.addr.2016.03.001

Ogaji, I. J., Nep, E. I., & Audu-Peter, J. D. (2012). Advances in Natural Polymers as Pharmaceutical Excipients. *Pharmaceutica Analytica Acta*, *03*(146), 1–16. https://doi.org/10.4172/2153-2435.1000146

Ramachandran, S., Chen, S., & Etzler, F. (1999). Rheological characterization of hydroxypropylcellulose gels. *Drug Development and Industrial Pharmacy*, *25*(2), 153–161. https://doi.org/10.1081/DDC-100102155

Rattanakit, P., Moulton, S. E., Santiago, K. S., Liawruangrath, S., & Wallace, G. G. (2012). Extrusion printed polymer structures : A facile and versatile approach to tailored drug delivery platforms. *International Journal of Pharmaceutics*, *422*(1–2), 254–263. https://doi.org/10.1016/j.ijpharm.2011.11.007

Sanandiya, N. D., Vijay, Y., Dimopoulou, M., Dritsas, S., & Fernandez, J. G. (2018). Large-scale additive manufacturing with bioinspired cellulosic materials. *Scientia Horticulturae*, *8*(8642), 1–8. https://doi.org/10.1038/s41598-018-26985-2

Severini, C., Derossi, A., Ricci, I., Caporizzi, R., & Fiore, A. (2018). Printing a blend of fruit and vegetables. New advances on critical variables and shelf life of 3D edible objects. *Journal of Food Engineering*, *220*, 89–100. https://doi.org/10.1016/j.jfoodeng.2017.08.025

Sharma, S., & Goel, S. A. (2019). Three-Dimensional Printing and its Future in Medical World. *Journal of Medical Research and Innovation*, *3*(1), 1–8. https://doi.org/10.15419/jmri.141.Publication

Smith, D., Kapoor, Y., Hermans, A., Nofsinger, R., Kesisoglou, F., Gustafson, T. P., & Procopio, A. (2018). 3D printed capsules for quantitative regional absorption studies in the GI tract. *International Journal of Pharmaceutics*, *550*(1–2), 418–428. https://doi.org/10.1016/j.ijpharm.2018.08.055

Solanki, N. G., Tahsin, M., Shah, A. V, & Serajuddin, A. T. M. (2018). Formulation of 3D Printed Tablet for Rapid Drug Release by Fused Deposition Modeling: Screening Polymers for Drug Release, Drug-Polymer Miscibility and Printability. *Journal of Pharmaceutical Sciences*, *107*(1), 390–401. https://doi.org/10.1016/j.xphs.2017.10.021

Tan, D. K., Maniruzzaman, M., & Nokhodchi, A. (2018). Advanced pharmaceutical applications of hot-melt extrusion coupled with fused deposition modelling (FDM) 3D printing for personalised drug delivery. *Pharmaceutics*, *10*(4). https://doi.org/10.3390/pharmaceutics10040203

Valente, M., Sibai, A., & Sambucci, M. (2019). Extrusion-Based Additive Manufacturing of Concrete Products: Revolutionizing and Remodeling the Construction Industry. *Journal of Composites Science*, *3*(3), 88. https://doi.org/10.3390/jcs3030088

Vancauwenberghe, V., Verboven, P., Lammertyn, J., & Nicolaï, B. (2018). Development of a coaxial extrusion deposition for 3D printing of customizable pectin-based food simulant. *Journal of Food Engineering*, *225*, 42–52. https://doi.org/10.1016/j.jfoodeng.2018.01.008

Vithani, K., Goyanes, A., Jannin, V., Basit, A. W., Gaisford, S., & Boyd, B. J. (2019). An Overview of 3D Printing Technologies for Soft Materials and Potential Opportunities for Lipid-based Drug Delivery Systems. *Pharmaceutical Research*, *36*(1). https://doi.org/10.1007/s11095-018-2531-1

Wang, L., Zhang, M., Bhandari, B., & Yang, C. (2018). Investigation on fish surimi gel as promising food material for 3D printing. *Journal of Food Engineering*, *220*, 101–108. https://doi.org/10.1016/j.jfoodeng.2017.02.029

Wang, Y., Wang, X., Xie, Y., & Zhang, K. (2018). Functional nanomaterials through esterification of cellulose: a review of chemistry and application. *Cellulose*, *25*(7), 3703–3731. https://doi.org/10.1007/s10570-018-1830-3

Yang, F., Zhang, M., Bhandari, B., & Liu, Y. (2018). Investigation on lemon juice gel as food material for 3D printing and optimization of printing parameters. *LWT - Food Science and Technology*, *87*, 67–76. https://doi.org/10.1016/j.lwt.2017.08.054

Yang, Y., Bi, V., Dürig, T., & Ingredients, A. S. (2016). The Impact of Hydroxypropyl Methylcellulose and Methylcellulose Molecular Weight and Degree of Substitution on Crystallization Inhibition of Felodipine in Aqueous Media. *Pharmaceutical Technology Report*, *04*, 1–5.

Figures

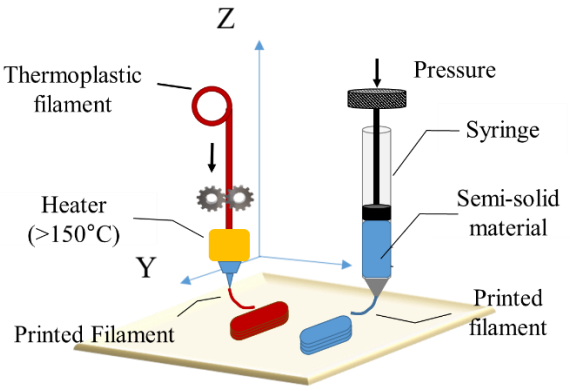

Figure 1.1 Two standard techniques related to the extrusion-based methodology: fused deposition modeling (FDM) (left) and semi-solid extrusion (SSE) (right).

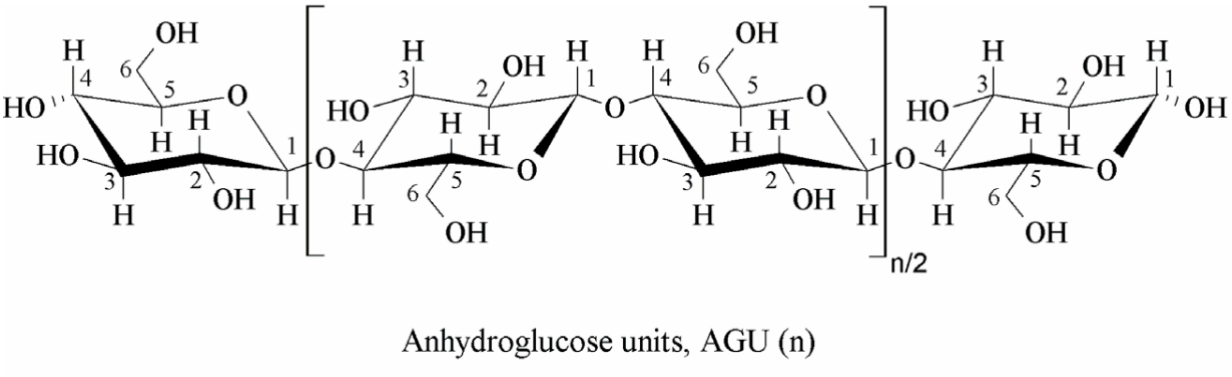

Figure 1.2 Chemical structure of powdered cellulose (n ≈ 500) or microcrystalline cellulose (n ≈ 220) (Marques-Marinho & Vianna-Soares, 2013).

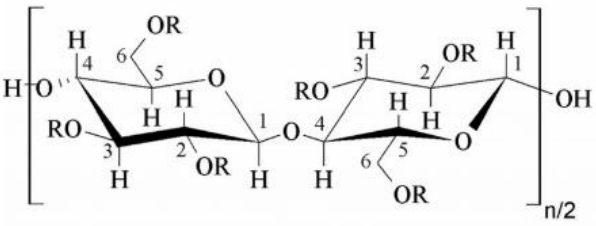

Cellulose ethers	R groups
Methylcellulose	H, CH_3
Ethylcellulose	H, CH_2CH_3
Hydroxyethylmethylcellulose	H, CH_3, $[CH_2CH_2O]_nH$
Hydroxypropylcellulose	H, $[CH_2CH(CH_3)O]_nH$
Carboxymethylcellulose	H, CH_2COONa

Figure 1.3 Chemical structure of cellulose ether derivatives (Marques-Marinho & Vianna-Soares, 2013).

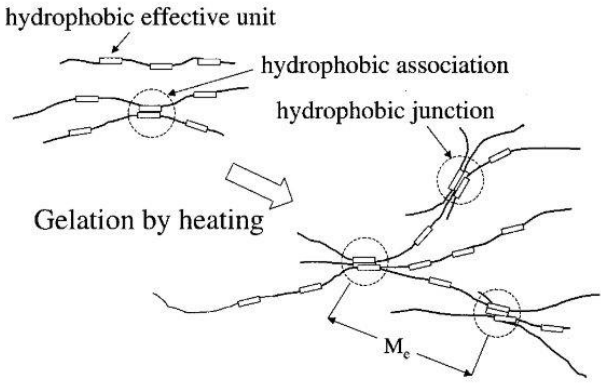

Figure 1.4 Schematic drawing showing gelation through the hydrophobic effective units of MC chains (L. Li et al., 2001) . Reprinted (adapted) with permission from (Li, L., Thangamathesvaran, P.M., Yue, C.Y., Tam, K.C., Hu, X., Lam, Y.C., 2001. Gel Network Structure of Methylcellulose in Water. Langmuir 17, 8062–8068.). Copyright (2020) American Chemical Society.

CHAPTER 2. DEVELOPMENT OF METHYLCELLULOSE-BASED SUSTAINED-RELEASE DOSAGE BY SEMI-SOLID EXTRUSION ADDITIVE MANUFACTURING IN DRUG DELIVERY SYSTEM

Yiliang Cheng[a], Hantang Qin[b]*, Nuria Acevedo[a], Xiaolei Shi[a]*

[a] Food Science and Human Nutrition Department, Iowa State University, Ames, IA, 50011, USA

[b] Industrial and Manufacturing Systems Engineering Department, Iowa State University, Ames, IA, 50011, USA

Modified from a manuscript accepted to *Journal of Biomedical Materials Research Part B: Applied Biomaterials*

Abstract

The objective of this study is to fabricate customized dosage forms using extrusion-based 3D printing for the sustained delivery of theophylline. The therapeutic paste was prepared by combining various doses of theophylline (0, 75, 100, 125mg) with different concentrations of methylcellulose (MC) A4M (8, 10, and 12%). The paste was then 3D printed into semi-solid tablets under optimized printing conditions. The rheological properties of printing pastes were related to the 3D printability. Our results indicated that to be 3D printed using the current platform, the storage modulus (G') of the printing paste should be higher than the loss modulus (G") during the frequency sweep (0.1-600 rad/s), and the tanδ should fall in the range of 0.25-0.27 at 0.63 rad/s. The printed tablets formulated with 10% MC showed the highest overall quality, considering the aspects of resolution, texture, and shape retention regardless of the dosage. The scanning electron microscopy (SEM) images indicated that the cross-linked structure of MC A4M formed the micro-scale porous microstructure, which has the potential to

embed the theophylline, thus delayed the release through the barrier effect. The *in vitro* dissolution test revealed that the 3D printed tablets exhibited a sustained release during the first 12 hours. The findings in this study will support the development of customized, personalized medicine with improved efficacy.

Introduction

Additive manufacturing, i.e., 3D printing technology, has become the focus of interest in the areas of engineering and processing in the global market. The development and application of 3D printing are increasing due to their advantages of rapid fabrication, hyper-personalization, reduced waste, and lifecycle sustainability [1,2]. Nowadays, 3D printing technology has opened up a new chapter of opportunities for customized pharmaceutical applications, which provides ease of fabricating personalized medication doses, rather than relying on a standard set of dosages [3,4]. The rapid prototyping technology can finish the tablet fabrication in a short time using small and portable equipment, like the bench-top printers [5,6]. Besides the customized dosage forms, 3D printing for tablet fabrication also achieved the implementation of complicated structure and adjustable design, such as polypills and density controllable meshed structures for the gastro retentive drug delivery system [7,8].

Among different methods, material extrusion-based 3D printing, including fused deposition modeling (FDM) and semi-solid extrusion (SSE), has been broadly applied in pharmaceutical manufacturing due to the advantages that include low-cost, customizable, and acceptable printing resolution for pharmaceutical production [9,10]. Even though FDM based 3D printing has become the most prevalent technology of tablet fabrication in the pharmaceutical field, the wide use of FDM has been restricted because it requires a high-temperature process (usually over 150°C) for operation. Thus, the FDM approach only compatible and suitable for thermally stable active pharmaceutical ingredients (API) [11,12]. The low-temperature FDM 3D

printing currently decreased the printing temperature to 90ºC, but the printing process still requires the hot-melt extrusion (HME) process to prepare the drug-loaded filaments before printing, and needs to operate the fabrication process of tablets with thermal treatment [13,14]. The SSE based 3D printing technology is an alternative approach that may be considered to overcome the limitations of the FDM approach. The customized dosage forms could also be fabricated by using SSE approach, which uses pressure or screw gear rotation directly, rather than using thermal process [15]. However, the study of SSE for the fabrication of 3D printed tablets is still in its infancy. There is not a standard SSE based 3D printing model to fabricate semi-solid matrices with a pharmaceutical-grade excipient to load APIs, and limited design of geometry to extend the release profile to improve therapeutic efficacy. Without this knowledge, the widespread use of SSE based 3D printing for manufacturing customized and personalized dosage forms will be limited. The knowledge gap on the investigation of the SSE 3D printing process and extended-release dosage formulation needs to be further explored.

The aim of this work was to explore the feasibility of using an SSE-based 3D printer to prepare for the sustained release tablets in the semi-solid state. Unlike the FDM approach, which utilizes thermoplastic filaments and heats over melting temperature to make material extrudable, the SSE approach utilizes pressurized air or rotating screw gear to press semi-solid material into filaments without deformation or collapse [9]. Thus, the selection of excipient plays a significant role in the performance of SSE 3D printing. The print material should exhibit desirable printability including extrudability and shape retention ability. There are few reports on the investigation of 3D printed tablets with the SSE approach, and some research indicated that the viscosity of the material is critically important for the successful extrusion process [8,16,17]. This study was designed to fill the knowledge gap by using rheological properties to predict the

printability of a potential excipient and revealing the drug loading capacity with the demonstration of a 3D printed tablet's microstructure. In the previous study, methylcellulose (MC) A4M exhibited the shear-thinning flow behavior and successfully printed by an SSE-based 3D printer to fabricate the biodegradable support structure and exhibited prominent shape retention ability under different concentrations [18]. The shear thinning has already been determined as one of the most critical characteristics to assess the printability of bio-ink materials for tissue engineering applications [19,20]. The pharmaceutical grade MC was also used as the excipient to control the release of API like in traditional pharmacy [21]. The MC A4M consists of a higher percentage of methoxyl groups and the dominated methoxyl groups provide a relatively higher level of hydrophobic properties to prevent MC A4M dissolution [22]. This characteristic may make MC A4M have the potential to build a gel barrier as micro-scale capsules to delay the API release over time as a biodegradable and food grade polymer. Therefore it has the potential to be used for 3D printing without additional shape stabilizers or binders.

In this study, the therapeutic paste was prepared by premixing MC A4M with theophylline, which is a model API. The objective of this study was to develop a sustained drug release system using MC A4M hydrogel as the matrix to fabricate the 3D printed tablets. The physical, mechanical, and rheological properties, as well as the release profiles of the 3D printed tablets with different MC concentrations and theophylline dosages were analyzed to understand their effects on the printability, shape retention ability, drug loading capacity, and release profile.

Materials

The theophylline (99+ %) was obtained from Acros (New Jersey, USA), and the excipient material, MC A4M, was donated by J. Rettenmaier & Söhne (Schoolcraft, MI). For MC A4M, the degree of substitution for the methoxyl groups and hydroxyethoxyl groups are

27.5-31.5% and 5%, respectively. The molecular weight ranges from 20,000- 380,000, and the dissolving and gelling temperatures are 0-5°C and 49°C, respectively. The 4M terminology indicates the viscosity of this material is in the range of 3,000-5,600 mPa·s, when it is measured in 2% solution at 20°C under 20 rpm.

Preparation of the therapeutic paste

The therapeutic paste was prepared by uniformly mixing the theophylline and MC A4M powders into deionized water at 70°C. The mixed materials were cooled to ambient temperature and then centrifuged at 3000 rpm, for 10 min to remove potential air bubbles trapped within the mixture. The concentrations of MC A4M were 8, 10, and 12% (w/w). For each concentration, the theophylline dosages were predetermined at 0, 75, 100, and 125 mg (±5 % deviation) per tablet, based on the average 1.4 g.

Rheological characterization

The rheological characterization experiments were carried out using a Discovery HR-2 rotational rheometer (TA Instruments, New Castle, DE) with cone and plate geometry (2° cone angle, 40 mm diameter, serial # 109675). All of the tests were set at 20°C with a 1 mm gap size between the geometry and steel Peltier plate. The sample and geometry plates were covered by a solvent trap to avoid water evaporation. The flow curves were fitted to the Herschel-Bulkley model($\tau = \tau_0 + K\dot{\gamma}^n$), where τ means shear stress (Pa), τ_0 is yield stress (Pa), $\dot{\gamma}$ is shear rate (1/s), *K* is the consistency index (Pa·s^2), and n is the flow behavior index. The yield stress value (Pa) was determined through the oscillatory stress sweep test which increased oscillatory stress in log mode from 1 to 1000%, while the frequency was kept constant at 1 Hz. This test was used to determine the linear viscoelastic region (LVR) and to estimate yield stress values (Pa). The endpoint of the LVR can be considered as the yield stress, i.e., the stress required to make the printable material flow [23]. Once the estimated value of yield stress is measured, the value of K

and n can be calculated by changing the model equation into a log function [24]. Dynamic viscoelastic properties tests were carried out by keeping the strain constant at 0.1, and increased angular frequency oscillated from 0.1 to 600 rad/s in logarithmic sweep mode. All rheological properties tests were conducted in triplicates.

Tablets 3D printing process

The customized 3D printer used for this study was described in a previous publication, and the extrusion process was driven by a stepper motor [18]. An extrusion-based syringe was configured on the platform of the Velleman K8200 3D printer (Velleman Inc.) for 3D printing purposes. The tablet structure was designed by using the SolidWorks software, which was saved as .stl file with a fixed dimension (20.37 × 8.35 × 6.61 mm). To assess the dimension uniformity, 12 printed tablets were randomly selected and weighed. The printer settings were as follows: speed was 5 mm/s, nozzle diameter was 0.437 mm, the volumetric flow rate was 0.75 mm^3/s, extrusion multilayer was 0.125, and layer number was eight layers for each tablet. The printing process was operated for 6 minutes under ambient temperature. The expected weight of each 3D printed tablet was 1.40 g with a deviation of 5 %. To assess the weight uniformity, 36 printed tablets were selected and weighed.

Textural profile analysis

Textural profile analysis (TPA) is conducted in the double compression test mode. The test was conducted using a TA.XT plusC texture analyzer (Texture Technologies Corp. and Stable Micro Systems, Ltd. Hamilton, MA) under ambient temperature, which was configured with a 35-mm diameter compression plate and compressed the tablets to 50% strain deformation. The pre-test and post-test speeds were 1.5 mm/s, the compression rate is 1.0 mm/s, and the delay time between the first and second compression was 5 s with 5 g trigger force. Force versus time graphs was generated from the instrument software for hardness, adhesiveness, cohesiveness,

and springiness. TPA tests were conducted in triplicate by measuring three tablets with the same formulation because of the large deformation.

Scanning Electron Microscopy (SEM)

The surface morphology of freezing dried tablets was observed by scanning electronic microscopy (SEM), JCM-6000 (Jeol, Japan). All tablets were freeze-dried by the Virtis Genesis SQ freeze dryer at -40 °C for 12 hours, and then coated with gold (SBC-12 Sputter coater). The average size of pores and clusters on the tablets' surfaces were acquired by measuring 5 representative pores with Image J Software (Java 1.8.0).

***In vitro* dissolution test**

The dissolution test of 3D printed semi-solid state tablets was carried out using the DT 126 light dissolution tester (Erweka, Germany) by adopting the USP dissolution apparatus 2 paddle method. The dissolution media (500 mL) were 0.1 M hydrochloric acid for the first 2 hours and phosphate buffer (pH 7.0) for the next 22 hours. The media temperature was maintained at 37 ± 0.5 °C. The paddle rotation speed was 100 rpm. Media samples were collected and analyzed at 1, 2, 3, 4, 6, 8, 12, and 24 hours during the test. In order to reduce variation, there were two separate batches of therapeutic pastes prepared for each formula as the replication. Then the dissolution profile of two printed tablets from the same batch was measured, and dissolution tests were performed in quadruplicate. The theophylline concentration contained in the filtrated solution (0.45μm polypropylene syringe filter) was determined using reverse-phase HPLC. The Ultimate3000 HPLC system was configured with a C18 column (5 μm, 120Å, 4.6 × 100 MM, make: Thermo Fisher Scientific, Waltham, MA) and a UV/Visible detector (Thermo Fisher Scientific, Waltham, MA) at a wavelength of 272 nm. The mobile phase was water/acetonitrile (96:4 v/v), at a flow rate of 1.2mL/min. The injection volume was set at

20 µl with retention time for 12 min, and the column temperature was maintained at 30 ºC. All the HPLC injections were carried out in duplicate.

Chromatographs were collected by Chromeleon™ Chromatography Data System Software 7 (Thermo Fisher Scientific, Waltham, MA). The baseline was locally calculated for each signal in the specific retention interval. The areas under the signal line were calculated by using peak integration. The concentrations of theophylline were calculated by linear interpolation. The calibration curve was obtained by plotting the ratio of peak area (y) versus known theophylline concentration (x) range of 10 -250 ppm. The linear equation of the calibration curve was $y = 0.9018x + 0.7955$ with the coefficient of determination (R2) over 0.99.

Drug release kinetics

The drug release data obtained from the *in vitro* dissolution test were fitted using several kinds of kinetic models (zero-, first-order, Korsmeyer-Peppas, and higuchi model). The calculation equations and methods were mentioned in the published paper by Dash [25].

Statistical analysis

Statistical analysis was performed using JMP Pro 14 software (Cary, NC). Comparison between different formulations was analyzed using a one-way analysis of variance (ANOVA) with a significance level of $p < 0.05$. Tukey's HSD (Honestly Significant Difference) test was used to determine significant differences between means.

Results

Rheological properties

The flow behavior and apparent viscosity curves of 12 different tablet formulas are shown in **Fig. 2.1**. All the pastes showed shear-thinning behavior, i.e., as the shear rate increased, the apparent viscosity decreased simultaneously. At the same concentration, the sample with higher dosage showed significantly higher apparent viscosity and stress. For the materials of the

same dosages, as the concentration of MC A4M also increased, the apparent viscosity and stress also increased significantly. The paste formula containing 12% (w/w) MC A4M with 125 mg dosage showed the highest apparent viscosity value (3183 Pa·s at 1 rad/s) compared with other formulations.

The Herschel-Bulkley fluid behavior model was the best fit for the flow behavior of printing materials with the highest R^2 (>0.99). The model fitting parameters for all the samples are listed in **Table 2.1**: consistency index (*K*), and flow behavior index (n). The *K* values increased significantly with increased levels of MC A4M concentration and theophylline dosage. All the n values of the 12 different material formulas were less than 1, but there is no significant difference between most of the means. Yield stress τ_0 is another critical parameter to compose the fluid behavior model equation, and the estimated values were determined by the LVR method and shown in **Fig. 2.2**. When the MC A4M concentration increased, the yield stress values increased significantly. Although no significant difference regarding yield stress could be seen between four dosage treatments for 8 and 10% (w/w), the yield stress of MC A4M 12% (w/w) was in fact significantly reduced when theophylline was added into the paste.

Fig. 2.3 shows the results obtained by frequency sweeps studies. The storage modulus (G') is always statistically higher than the loss modulus (G") without showing a crossover. The magnitude of both G' and G" simultaneously increased once the drug dosage or concentration of MC A4M increased. Similar to flow behavior and apparent viscosity curves (**Fig. 2.1**), the dosages were not that significant in the magnitude of both G' and G" compared with concentration. The paste formula containing 12% (w/w) MC A4M with 125 mg dosage showed highest G' and G" value (5,418 Pa and 1,216 Pa at 1 rad/s, respectively) compared with other formulations. Another parameter evaluated loss tangent (tanδ) is the ratio of G"/G'. For all the

prepared materials, G' is always higher than G" when angular frequency increased, i.e., tanδ was always less than 1, as shown in **Fig. 2.3**. Furthermore, the magnitude of tanδ decreased as concentration and dosage increased: the range for MC A4M 8% (w/w) is 0.3-0.35, 0.23-0.29 for 10% (w/w), and 0.20-0.25 for 12% (w/w).

Tablets printability performance and SEM images

Fig. 2.4 shows the photographs of 3D printed tablets fabricated by an extrusion-based 3D printer. The opacity level of pure MC A4M tablets (control group) increased as the MC A4M concentration increased. All the tablets that contain theophylline showed a milky white color, which can be attributed to the white color of theophylline drug powder. The printed tablet length averaged 21.38 ± 0.76 mm, width averaged 10.01 ± 0.51 mm, and height averaged 0.698 ± 0.74 mm (n = 12). And the printed tablet mass for all averaged 1.37 ± 0.09 g (n = 36). All printed tablets with MC A4M 8% (w/w) (**Fig. 2.4A**) showed deformation because of the sticky surface, and the average mass of these tablets was 1.39 ± 0.07 g (n = 12). The tablets with 10% (w/w) (**Fig. 2.4B**) concentration showed compact and uniform surfaces, and they are easily moved from the print bed when touched by the fingers without any deformation. The average mass of these tablets (MC 10%) was 1.41 ± 0.06 g (n = 12). However, the extruded filaments of MC 12% (w/w) tablets (**Fig. 2.4C**) were too brittle to be continuously extruded. Even though the printed surfaces are flat and smooth for the control tablet, the filaments were broken several times during the printing process, especially for high dosage formulations. The mass of MC 12% based tablets averaged in 1.33 ± 0.12 g (n = 12), which was hard to be kept the tablet mass in an acceptable variation.

The SEM images revealed more of the surface morphology of the printed tablets (**Fig. 2.5**). The side view of the surface of the tablet (**Fig. 2.6A**) showed the fabrication is a layer-by-layer process and each layer is formed by extruding the therapeutic paste from the printer nozzle.

The control groups of MC A4M with different concentrations showed the porous net structure. The average length and width of the oblong shape pores are 192 μm and 84 μm, respectively. These microscale pores have composed a net structure of MC A4M hydrogel which contained high water content before sublimation. Once the dosage of theophylline increased, the particle clusters are observed on the surface of the MC A4M net structure. The tablets containing 125 mg doses showed more cluster aggregation of theophylline particles. The average length of the single square particle and particle cluster were 20 μm and 95 μm, respectively. The SEM cross-section image (**Fig. 2.6B**) of the printed tablet showed theophylline clusters were attached within the porous structure between the printed MC A4M layers, and the averaged pore size was 102 μm.

Textural profile analysis

The textural test results for printed tablets are shown in **Table 2.2**. When compared among all the formulations, theophylline dosage showed a less significant impact on hardness. The increased dosage led to a decrease in the absolute value of adhesiveness when compared MC 8% (w/w) groups, but MC A4M 12% (w/w) groups showed an opposite trend. Printed tablets formulated with 8% (w/w) MC 75 and 100 mg, 10% (w/w) MC A4M 100 and 125 mg, and 12% (w/w) MC with any API dosage showed relatively lower adhesiveness (< 300 g·s) compared to the other formulations. The difference among these groups is not significant. The increased concentration and dosage both decreased the cohesiveness and springiness of tablets. The formulas MC 10% (w/w) 125 mg, and MC 12% (w/w) 100, 125 mg groups had both the lowest cohesiveness and adhesiveness absolute values.

***In vitro* dissolution test**

The drug release profiles from *in vitro* dissolution tests of the nine different formulas are shown in **Fig. 2.7**. During the first two hours (with acidic dissolution media), all printed tablets

showed over 45% release of the total drug amount in the 0.1M HCl media. By comparing the different formulations, the MC 8% (w/w) 75 mg dosage tablets exhibited the highest release percentage (61%) on average. The MC 10% and 12% (w/w) with 125 mg dosage tablets both showed the lowest release percentage (50%) on average. For the tablets at the same concentration, the release percentage was significantly lower for the tablets with higher dosage. But there was no significant difference in the release percentage between the tablets with different MC A4M concentrations at fixed theophylline dosage. All the 3D printed tablets had released over 90% of theophylline after 12 hours. The dissolution results showed the profile of theophylline release from all tablets at over 99% after the 24 hours dissolution test. Besides, after the theophylline particles had been completely released into the solution, we observed that the MC A4M based tablet matrices still kept the original shape and integrity after soaking without deformation, collapse, or dissolve. All of these tablets showed similar appearances to tablets with control treatment after the dissolution test.

Discussion

The effects of MC A4M concentration and API dosage on extrudability and printability through the 3D printing process can be related to the viscoelastic and shear-thinning characterization [19, 26]. To be eligible for 3D printing, the material should be continuously and homogeneously extruded through the nozzle without fracture or lumpy texture. Also, once 3D printed in the designed shape, the extruded filaments should have both sufficiently strong mechanical strength and interfacial strength to support subsequently printed filaments without delamination, sagging, or fusion [27]. The rheological properties indicated that within the range of theophylline dosage and MC concentration we selected for this study, the addition of MC A4M and theophylline was beneficial to 3D printability. This is indicated by the corresponding increasing tendency of yield stress, K, and G' values which benefits the shape retention capacity

of printed tablets. The value of tanδ decreased as the concentration and dosage increased which indicated the value difference between G' and G" also increased, and solid-like property became pronounced which reflected stronger mechanical strength [28, 29].

The actual dimensions of printed tablets are slightly larger than the designed dimensions is due to the die swell phenomenon in polymer extrusion [30]. In the comparison of tablet appearances, the tablets with the lowest concentration (8% w/w) showed poorest overall quality regarding the physical and mechanical properties of printed tablets. Although the material under this concentration was extrudable, the printing material was too sticky to the touch and easily deformed after 3D printing. Thus, the printed tablets formulated with 8% MC showed more susceptibility to sagging and deformation after printing than samples at higher concentrations (**Fig. 2.4**). This condition is improved for the higher concentration groups, which had less sticky surfaces and better tablet shape retention and integrity. However, the optimal printability of therapeutic paste cannot be achieved by further increase in the concentration or dosage. The extruded filaments of MC 12% (w/w) were easily broken and hard to be continuously extruded, even at the maximum pressure that can be applied to the extruder. Thus, the weight uniformity of MC 12% (w/w) tablets was worse than tablets with other two concentration levels. The poor extrudability and fluidity was related to the high magnitude of yield stress and G', and the relatively low value of tanδ [31, 32]. Accordingly, 10% (w/w) was determined as the optimal concentration for MC as the 3D printing materials, regardless of theophylline dosages. Pastes at this concentration can be easily extruded from the nozzle without breakage due to relatively low viscosity, and K. This printed paste also had better shape retention and minimum visible defects with relatively high G' and yield stress [33]. When using the current printing parameters to print MC 10% (w/w) tablets, the corresponding yield stress range is 440-570 Pa, and the apparent

viscosity range is approximately 3200-6300 Pa·s at the shear rate of 0.1 s-1. The corresponding magnitudes for G', G" at 0.63 rad/s are approximately 1800-3200 Pa and 450-850 Pa, respectively. The tanδ should fall in the range of 0.25-0.27 at 0.63 rad/s. The overall results are comparable to the findings from previous research that used lemon juice gel and potato starch as reference materials. Based on their observations, the corresponded apparent viscosity, G', G", and tanδ are 8079.3 Pa·s, 4924 Pa, and 760 Pa, and 0.155 under the same condition of shear rate and angular frequency [34]. The optimal parameter values and magnitudes were analogous to those data obtained from rheological determination.

The TPA result can be used to indicate the effect of the formulation change on the mechanical properties of 3D printed tablets. As the MC concentration increased, the hardness also increased. This trend is also indicated from the SEM images, which showed a more compact net structure and more aggregation of particle clusters with increased concentration and dosage [35]. Since the MC based hydrogel was formed by the hydrophobic aggregation between methyl groups, the increased MC concentration could provide more available methyl groups and enhance the gel strength after the gelation process [36,37]. Thus, MC concentration plays a predominant role over the effect of theophylline dosage in the hardness properties of printed tablets. As for adhesiveness, a high absolute value of adhesiveness indicates that the surface of printed tablets is stickier during compression [38]. Even though the adhesiveness of MC 10 and 12% at low dosage are still high, these tablets' surfaces were actually not too sticky to handle them. One reason for this is because the low water content and relatively high G' value made the filament less moist and brought more solid-like texture. The increased concentration and dosage both decreased the cohesiveness and springiness of tablets, making the printed tablets easier to breakdown and lose some of the elasticity [39].

When comparing the effect of tablet formulations on the rheological and textural properties, the difference was more related to the concentration of MC A4M rather than the dosage of theophylline. One of the possible explanations is that the cross-linked structure of MC A4M worked as a three dimensional porous matrix to embed the theophylline, and theophylline was not involved in the matrix formation as confirmed by the SEM images as shown in **Fig. 2.5**. When mixed with the water over gelling temperature, the powder-like MC A4M material firstly dissolved into solvent as a liquid then converted into a semi-solid state as a hydrogel. The gelation formed as the self-aggregation between methyl groups and water because of the relative hydrophobic property which then resulted in a three-dimensional network as the major matrix [36]. MC-based tablets could work as the microscale semi-solid barrier and provide porous matrices for theophylline particle aggregation. Since the pore sizes are larger than theophylline particles, this matrix showed the potential to embed the theophylline and delay the release through the barrier effect.

As shown in **Fig. 2.7**. The *in vitro* dissolution test revealed that the 3D printed tablets exhibited an effective retardance of drug release during the first 12 hours. With the increase of theophylline dose, the 3D printed tablets exhibited significant delay of release during the dissolution test over 24 hours. The significantly higher drug release rate for low dosage forms is probably due to the higher porosity and lower theophylline density when the tablets are printed with relatively low drug infill, as shown in **Fig. 2.5** [40]. The increased MC A4M concentration conferred shape retention ability and elastic property (increased G' and yield stress) and also brought stronger net structure by increased hydrogen bonding formation, which trapped theophylline particles into a stronger and denser gel barrier [41]. The poor solubility of the MC A4M based matrix after soaking over 24 hours could be explained by the presence of methoxyl

substitutions. The dominated methoxyl groups provided a relatively higher level of hydrophobic properties to prevent MC A4M dissolution [22]. Based on the result of release profiles, all these 3D printed tablets were best fitted by first-order and Korsmeyer-Peppas with the highest R^2 values between 0.97 to 0.99 (**Table 2.3**). The equation of first-order revealed that the change of drug release rate depended only on the theophylline dosage over time [42]. In addition, the values of release exponent n showed a range of 0.44 to 0.47 when fitted into the Korsmeyer-Peppas model, which indicated the release of theophylline from the 3D printed tablets followed both drug diffusion and matrix swelling as non-Fickian or anomalous transport [42].

When comparing the theophylline dissolution result with a previously published study, comparable release profiles were observed for the tablets prepared by the conventional compression method and our 3D printing process. The majority of drug release (>80%) took place gradually during the first 12 hours at the same paddle rotation speed (100 rpm) [43]. Another research explored that the best release kinetic models for theophylline released from the tablets prepared with direct compression were also first-order and Korsmeyer Peppas with anomalous drug transport mechanism. These similarities between the *in vitro* dissolution test results indicated that the SSE-based 3D printed tablets had the potential to offer the comparable transport mechanism and release behavior as the convention method prepared tablets. A similar extended release profile was also observed when comparing the 3D printed tablet fabricated with different extrusion-based printing methods. Pietrzak et al. explored the release pattern of theophylline from FDM based 3D printed tablets was extended over 16 hours, and the faster release pattern was also observed in the tablets contained lower theophylline does [44]. But the sizes of these FDM based 3D printed tablets in Pietrzak's research are not fixed, so faster release patterns may also cause by the increased surface/mass ratio with the smaller tablets. These

results proved that semi-solid extrusion 3D printing is a potential technology to fabricate methylcellulose-based tablets and extend the release of theophylline with different dosages. Compared to the conventional tablet manufacturing conducted by the compression or granulation method, SSE technology is a cost-effective approach as it saves up to 80% usage of excipients. The reason is that the 3D printing materials are hydrogels prepared by high amount of water, instead of excipient powders. The 3D printed semi-solid tablets can be further processed by dehydration method, such as freeze-drying, to make the solid tablets for its potential to be used as a fast-release delivery system. This potential will be tested and verified by our research group as the next step in the near future.

Conclusion

This study demonstrated the rheological properties could be used to predict the extrudability and shape retention of semi-solid materials for 3D printing purpose. By adjusting the excipient concentration and the API dosage, the physical and mechanical properties of 3D printed tablets could be manipulated. The 3D printed tablets with 10% MC is an optimized delivery system with drug loading capacity of 75-125 mg. Considering the advantages such as low process temperature (ambient temperature), rapid fabrication, customized dosage, and controllable textural and release profiles, the 3D printed matrix fabricated with methylcellulose hydrogels could be applied as a promising delivery system. With further development, this delivery system has a potential to deliver other active ingredients, such as bioactive compounds, substrates of oral immunotherapy, living cells, and probiotics, thus may promote the development of pharmaceuticals, nutraceuticals, and food products in the future.

References

1. Gokhare VG, Raut DN, Shinde DK. A Review paper on 3D-Printing Aspects and Various Processes Used in the 3D-Printing. International Journal of Engineering Research & Technology (IJERT). 2017;6(06):953–958.

2. Lin H, Shi L, Wang D. A rapid and intelligent designing technique for patient-specific and 3D-printed orthopedic cast. 3D Printing in Medicine. 2016;2(1).

3. Pravin S, Sudhir A. Integration of 3D printing with dosage forms: A new perspective for modern healthcare. Biomedicine and Pharmacotherapy. 2018;107:146–154.

4. Liu J, Sun L, Xu W, Wang Q, Yu S, Sun J. Current advances and future perspectives of 3D printing natural-derived biopolymers. Carbohydrate Polymers. 2019;207:297–316.

5. Skowyra J, Pietrzak K, Alhnan MA. Fabrication of extended-release patient-tailored prednisolone tablets via fused deposition modelling (FDM) 3D printing. European Journal of Pharmaceutical Sciences. 2015;68:11–17.

6. Tan DK, Maniruzzaman M, Nokhodchi A. Advanced pharmaceutical applications of hot-melt extrusion coupled with fused deposition modelling (FDM) 3D printing for personalised drug delivery. Pharmaceutics. 2018;10(4).

7. Khaled SA, Burley JC, Alexander MR, Yang J, Roberts CJ. 3D printing of five-in-one dose combination polypill with defined immediate and sustained release profiles. Journal of Controlled Release. 2015;217:308–314.

8. Li Q, Guan X, Cui M, Zhu Z, Chen K, Wen H, Jia D, Hou J, Xu W, Yang X, et al. Preparation and investigation of novel gastro-floating tablets with 3D extrusion-based printing. International Journal of Pharmaceutics. 2018;535(1–2):325–332.

9. Algahtani MS, Mohammed AA, Ahmad J. Extrusion-Based 3D Printing for Pharmaceuticals: Contemporary Research and Applications. Current Pharmaceutical Design. 2019;24(42):4991–5008.

10. Norman J, Madurawe RD, Moore CMV, Khan MA, Khairuzzaman A. A new chapter in pharmaceutical manufacturing: 3D-printed drug products. Advanced Drug Delivery Reviews. 2017;108:39–50.

11. Goyanes A, Buanz ABM, Hatton GB, Gaisford S, Basit AW. 3D printing of modified-release aminosalicylate (4-ASA and 5-ASA) tablets. European Journal of Pharmaceutics and Biopharmaceutics. 2015;89:157–162.

12. Alhijjaj M, Belton P, Qi S. An investigation into the use of polymer blends to improve theprintability of and regulate drug release from pharmaceutical soliddispersions prepared via fused deposition modeling (FDM) 3D printing.pdf. European Journal of Pharmaceutics and Biopharmaceutics. 2016;108:111–125.

13. Okwuosa TC, Stefaniak D, Arafat B, Isreb A, Wan KW, Alhnan MA. A Lower Temperature FDM 3D Printing for the Manufacture of Patient-Specific Immediate Release Tablets. Pharmaceutical Research. 2016;33(11):2704–2712.

14. Kollamaram G, Croker DM, Walker GM, Goyanes A, Basit AW, Gaisford S. Low temperature fused deposition modeling (FDM) 3D printing of thermolabile drugs. International Journal of Pharmaceutics. 2018;545(1–2):144–152.

15. Conceição J, Farto-Vaamonde X, Goyanes A, Adeoye O, Concheiro A, Cabral-Marques H, Manuel Sousa Lobo J, Alvarez-Lorenzo C. Hydroxypropyl-β-cyclodextrin-based fast dissolving carbamazepine printletsprepared by semisolid extrusion 3D printing.pdf. Carbohydrate Polymers. 2019;221:52–62.

16. Rattanakit P, Moulton SE, Santiago KS, Liawruangrath S, Wallace GG. Extrusion printed polymer structures : A facile and versatile approach to tailored drug delivery platforms. International Journal of Pharmaceutics. 2012;422(1–2):254–263.

17. Khaled SA, Burley JC, Alexander MR, Yang J, Roberts CJ. 3D printing of tablets containing multiple drugs with defined release profiles. International Journal of Pharmaceutics. 2015;494(2):643–650.

18. Polamaplly P, Cheng Y, Shi X, Manikandan K, Zhang X, Kremer GE, Qin H. 3D printing and characterization of hydroxypropyl methylcellulose and methylcellulose for biodegradable support structures. Polymer. 2019;173:119–126.

19. AnilKumar S, Allen SC, Tasnim N, Akter T, Park S, Kumar A, Chattopadhyay M, Ito Y, Suggs LJ, Joddar B. The applicability of furfuryl-gelatin as a novel bioink for tissue engineering applications. Journal of Biomedical Materials Research - Part B Applied Biomaterials. 2019;107(2):314–323.

20. Luo Y, Wei X, Huang P. 3D bioprinting of hydrogel-based biomimetic microenvironments. Journal of Biomedical Materials Research - Part B Applied Biomaterials. 2019;107(5):1695–1705.

21. Nasatto PL, Pignon F, Silveira JLM, Duarte MER, Noseda MD, Rinaudo M. Methylcellulose, a cellulose derivative with original physical properties and extended applications. Polymers. 2015;7(5):777–803.

22. Yang Y, Bi V, Dürig T, Ingredients AS. The Impact of Hydroxypropyl Methylcellulose and Methylcellulose Molecular Weight and Degree of Substitution on Crystallization Inhibition of Felodipine in Aqueous Media. Pharmaceutical Technology Report. 2016;04:1–5.

23. De Graef V, Depypere F, Minnaert M, Dewettinck K. Chocolate yield stress as measured by oscillatory rheology. Food Research International. 2011;44(9):2660–2665.

24. Mullineux G. Non-linear least squares fitting of coefficients in the Herschel-Bulkley model. Applied Mathematical Modelling. 2008;32(12):2538–2551.

25. Dash S, Murthy PN, Nath L, Chowdhury P. Kinetic modeling on drug release from controlled drug delivery systems. Acta Poloniae Pharmaceutica - Drug Research. 2010;67(3):217–223.

26. Costakis Jr WJ, Rueschhoff LM, Diaz-cano AI, Youngblood JP, Trice RW. Additive manufacturing of boron carbide via continuous filament direct ink writing of aqueous ceramic suspensions. Journal of the European Ceramic Society. 2016;36(14):3249–3256.

27. Li H, Tan YJ, Leong KF, Li L. 3D Bioprinting of Highly Thixotropic Alginate/Methylcellulose Hydrogel with Strong Interface Bonding. ACS Applied Materials and Interfaces. 2017;9(23):20086–20097.

28. Cernencu AI, Lungu A, Stancu IC, Serafim A, Heggset E, Syverud K, Iovu H. Bioinspired 3D printable pectin-nanocellulose ink formulations. Carbohydrate Polymers. 2019;220:12–21.

29. Barki AM, Bocquet L, Stevenson A. Linking Rheology and Printability for Dense and Strong Ceramics by Direct Ink Writing. Scientific Reports. 2017;7(6017):1–10.

30. Henderson AM, Rudin A. Effects of die temperature on extrudate swell in screw extrusion. Journal of Applied Polymer Science. 1986;31(2):353–365.

31. Amborski LE, Mecca TD. A study of polymer film brittleness. Journal of Applied Polymer Science. 1960;4(12):332–342.

32. Liu Z, Zhang M, Bhandari B, Yang C. Impact of rheological properties of mashed potatoes on 3D printing. Journal of Food Engineering. 2018;220:76–82.

33. Zhang M, Vora A, Han W, Wojtecki RJ, Maune H, Le ABA, Thompson LE, McClelland GM, Ribet F, Engler AC, et al. Dual-Responsive Hydrogels for Direct-Write 3D Printing. Macromolecules. 2015;48(18):6482–6488.

34. Yang F, Zhang M, Bhandari B, Liu Y. Investigation on lemon juice gel as food material for 3D printing and optimization of printing parameters. LWT - Food Science and Technology. 2018;87:67–76.

35. Ding C, Zhang M, Li G. Rheological properties of collagen/hydroxypropyl methylcellulose (COL/HPMC) blended solutions. Journal of Applied Polymer Science. 2014;131(7):1–10.
36. Joshi SC. Sol-gel behavior of hydroxypropyl methylcellulose (HPMC) in ionic media including drug release. Materials. 2011;4(10):1861–1905.

37. Li L, Thangamathesvaran PM, Yue CY, Tam KC, Hu X, Lam YC. Gel Network Structure of Methylcellulose in Water. Langmuir. 2001;17(26):8062–8068.

38. Hashemi Sanatgar R, Campagne C, Nierstrasz V. Investigation of the adhesion properties of direct 3D printing of polymers and nanocomposites on textiles: Effect of FDM printing process parameters. Applied Surface Science. 2017;403:551–563.

39. Kim HW, Bae H, Park HJ. Reprint of: Classification of the printability of selected food for 3D printing: Development of an assessment method using hydrocolloids as reference material. Journal of Food Engineering. 2018;220:28–37.

40. Solanki NG, Tahsin M, Shah A V, Serajuddin ATM. Formulation of 3D Printed Tablet for Rapid Drug Release by Fused Deposition Modeling: Screening Polymers for Drug Release, Drug-Polymer Miscibility and Printability. Journal of Pharmaceutical Sciences. 2018;107(1):390–401.

41. Zhang J, Yang W, Vo AQ, Feng X, Ye X, Kim DW, Repka MA. Hydroxypropyl methylcellulose-based controlled release dosage by melt extrusion and 3D printing: Structure and drug release correlation. Carbohydrate Polymers. 2017;177:49–57.

42. Bruschi ML, editor. Mathematical models of drug release. In: Strategies to Modify the Drug Release from Pharmaceutical Systems. 2015. p. 63–86.

43. Hayashi T, Kanbe H, Okada M, Suzuki M, Ikeda Y, Onuki Y, Kaneko T, Sonobe T. Formulation study and drug release mechanism of a new theophylline sustained-release preparation. International Journal of Pharmaceutics. 2005;304(1–2):91–101.

44. Pietrzak K, Isreb A, Alhnan MA. A flexible-dose dispenser for immediate and extended release 3D printed tablets. European Journal of Pharmaceutics and Biopharmaceutics. 2015;96:380–387.

Tables and Figures

Table 2.1 Herschel-Bulkley model parameters for the curves of MC A4M with the addition of different theophylline dosage (0, 75, 100, 125 mg) at different concentration (8, 10, 12% w/w). Means that have no superscript in common are significantly different from each other (Tukey's HSD, $P<0.05$). Values are presented as mean ± SD (n=3). (*K*: consistency index; n: flow behavior index).

Dosage (mg)	**MC 8% (w/w)**		**MC 10% (w/w)**		**MC 12% (w/w)**	
	K (Pa·s^n)	n	*K* (Pa·s^n)	n	*K* (Pa·s^n)	n
0	654.2±20.1^{g}	0.34^{a}	943.7±88.9^{ef}	0.33^{ab}	1550.7±37.0^{c}	0.31^{abc}
75	868.7±28.8^{f}	0.31^{abc}	1091.2±57.5^{e}	0.32^{ab}	1946.1±10.0^{b}	0.29^{bc}
100	903.8±58.4^{f}	0.33^{ab}	1336.2±133.5^{d}	0.31^{abc}	2135.8±32.3^{a}	0.28^{bc}
125	1090.9±31.3^{e}	0.31^{abc}	1580.6±16.23^{c}	0.29^{bc}	2218.9±75.3^{a}	0.27^{c}

Table 2.2 Textural profile analysis parameters for MC A4M with the addition of different theophylline dosage (0, 75, 100, 125 mg) at different concentration (8, 10, 12% w/w). Means that have no superscript in common are significantly different from each other (Tukey's HSD, $P<0.05$). Values are presented as mean ± SD (n=3).

Concentration % (w/w)	Dosage (mg)	Hardness (g)	Adhesiveness (g·s)	Cohesiveness	Springiness
8%	0	121.4 ± 31.6^{g}	-206.5 ± 33.0^{abc}	0.9 ± 0.1^{a}	0.9 ± 0.0^{a}
	75	157.4 ± 16.7^{g}	-270.2 ± 33.8^{abcd}	0.9 ± 0.0^{a}	0.9 ± 0.0^{a}
	100	216.4 ± 21.6^{fg}	-345.0 ± 41.1^{abcd}	0.8 ± 0.1^{ab}	0.9 ± 0.0^{ab}
	125	510.5 ± 119.3^{cd}	-501.2 ± 120.1^{cd}	0.7 ± 0.0^{bcd}	0.9 ± 0.0^{ab}
10%	0	296.5 ± 58.2^{efg}	-420.8 ± 27.3^{bcd}	0.8 ± 0.1^{ab}	0.9 ± 0.0^{ab}
	75	400.0 ± 27.2^{def}	-525.5 ± 50.1^{d}	0.7 ± 0.0^{bc}	0.9 ± 0.0^{ab}
	100	418.6 ± 47.6^{de}	-285.4 ± 197.6^{abcd}	0.5 ± 0.1^{cde}	0.7 ± 0.2^{bcd}
	125	564.9 ± 115.4^{bcd}	-98.8 ± 33.2^{a}	0.4 ± 0.0^{e}	0.4 ± 0.0^{d}
12%	0	453.5 ± 44.6^{de}	-570.6 ± 266.2^{d}	0.7 ± 0.1^{bcd}	0.8 ± 0.2^{abc}
	75	681.9 ± 92.2^{abc}	-298.2 ± 75.8^{abcd}	0.5 ± 0.1^{de}	0.6 ± 0.1^{cd}
	100	721.7 ± 61.0^{ab}	-142.9 ± 38.3^{ab}	0.4 ± 0.0^{e}	0.5 ± 0.1^{d}
	125	812.3 ± 52.8^{a}	-114.1 ± 11.3^{ab}	0.4 ± 0.0^{e}	0.5 ± 0.0^{d}

Table 2.3 Results of fitting *in vitro* release profile to different kinetic models

Concentration % (w/w)	Dosage (mg)	Zero-order (R^2)	First-order (R^2)	Korsmeyer-Peppas (R^2)	Release exponent n	Higuchi (R^2)
8%	75	0.68	0.99	0.97	0.47	0.93
	100	0.76	0.97	0.99	0.47	0.96
	125	0.79	0.99	0.99	0.44	0.97
10%	75	0.73	0.98	0.98	0.44	0.95
	100	0.77	0.98	0.99	0.47	0.97
	125	0.80	0.99	0.99	0.45	0.98
12%	75	0.72	0.99	0.98	0.46	0.95
	100	0.78	0.98	0.99	0.47	0.97
	125	0.79	0.99	0.99	0.44	0.98

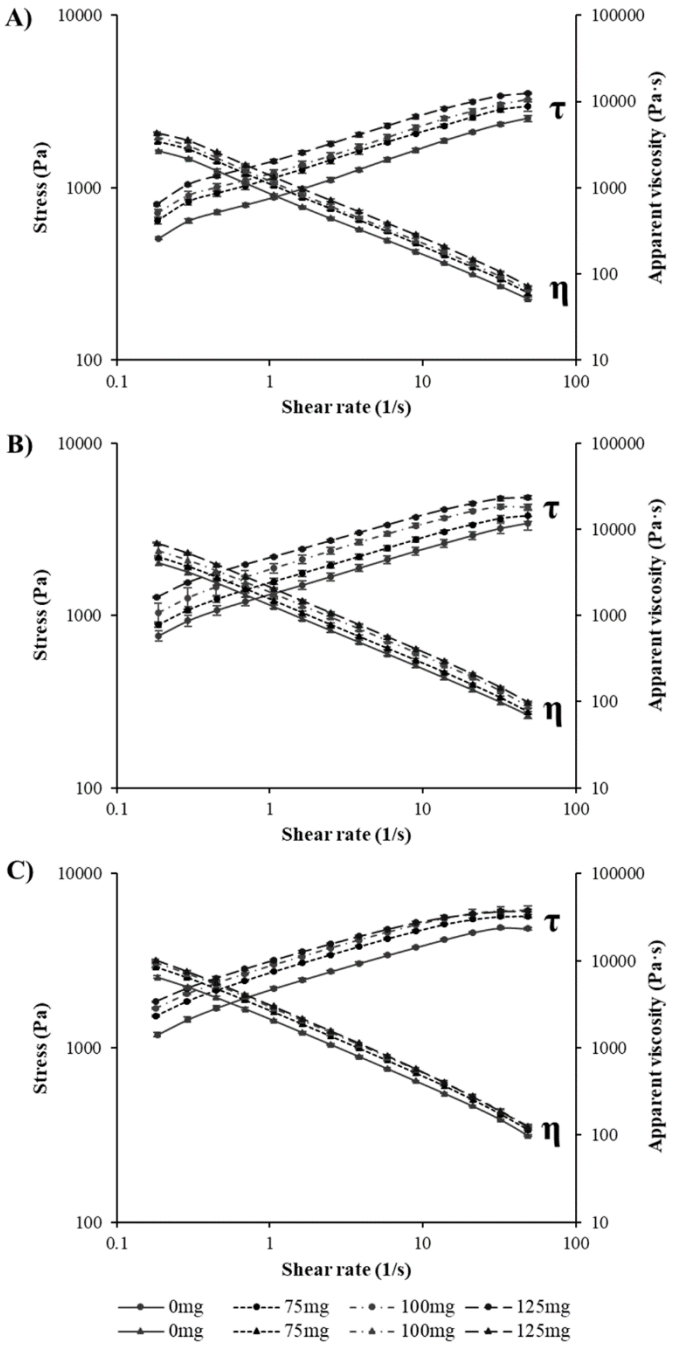

Figure 2.1 Shear stress (τ) and apparent viscosity (η) versus shear rate profiles of MC A4M with different theophylline dosages (0, 75, 100, 125 mg) at different MC concentrations A) 8%, B) 10%, and C) 12% (w/w).

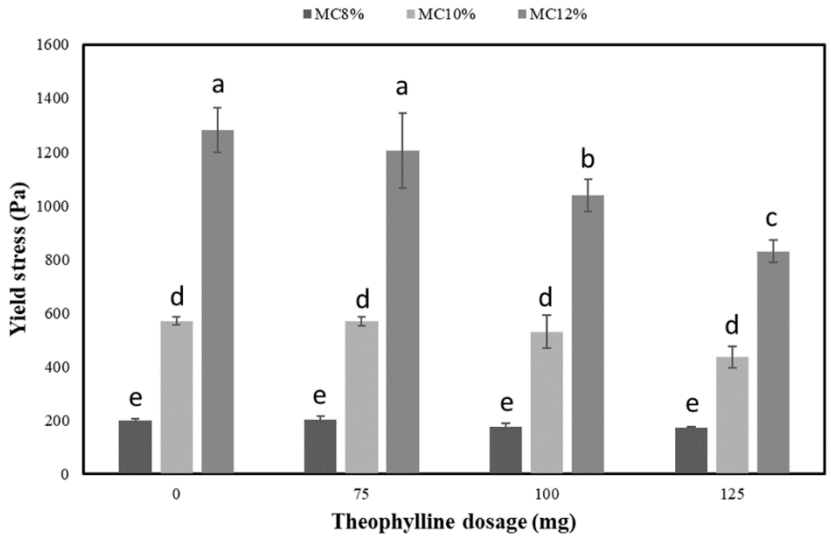

Figure 2.2 Estimated yield stress (determined through the oscillatory stress sweep test - linear viscoelastic region) of MC A4M samples with varying concentrations and theophylline dosages.

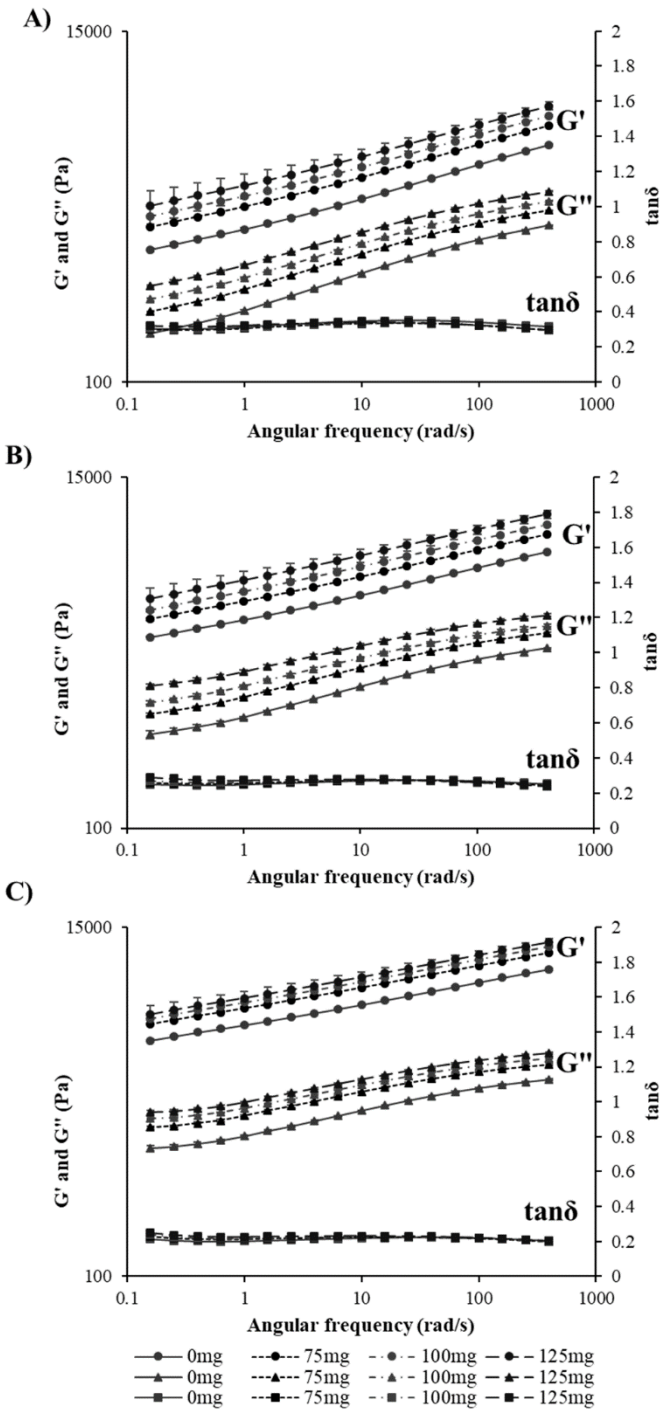

Figure 2.3 Storage modulus (G'), loss modulus (G") and tanδ versus frequency profile of MC A4M with different theophylline dosages (0, 75, 100, 125 mg) at different MC concentrations: a) 8%, b) 10%, c) 12% (w/w).

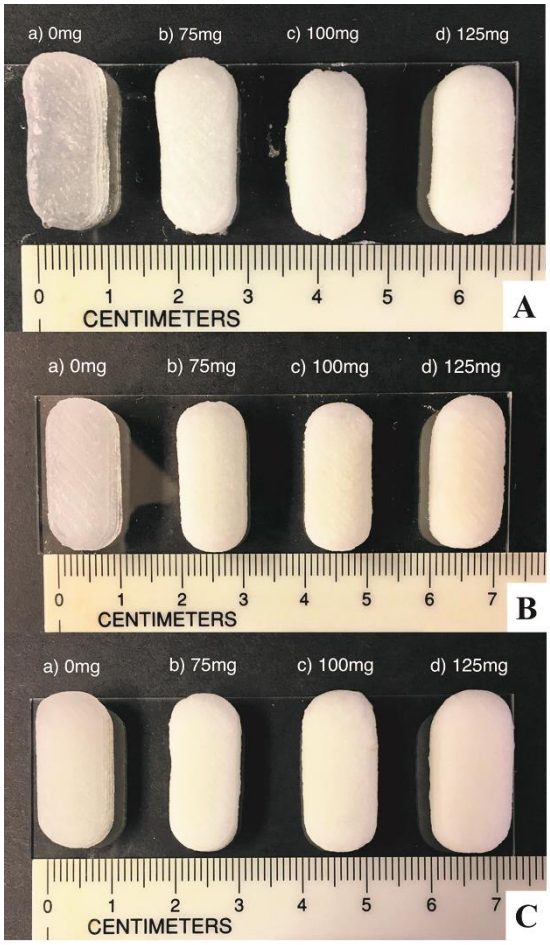

Figure 2.4 The appearance of printed tablets with different MC A4M concentrations: A) 8%, B) 10%, C) 12% (w/w), and theophylline dosages: a) 0, b) 75, c) 100, d) 125mg.

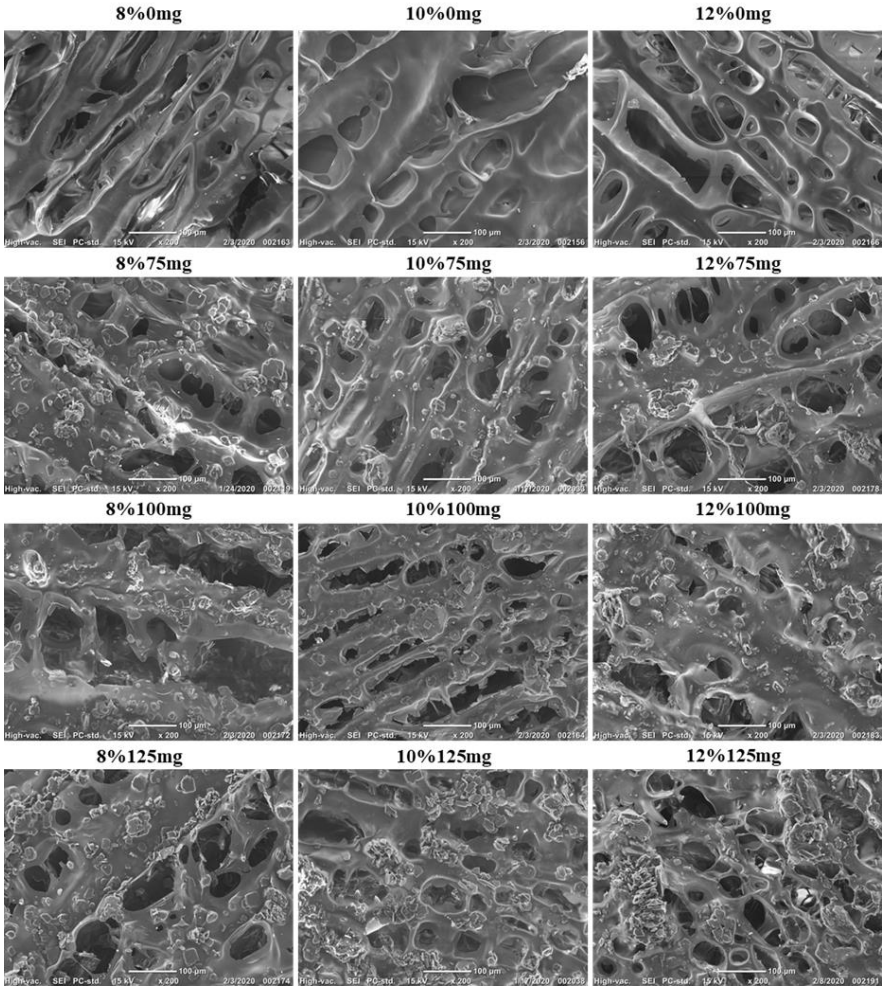

Figure 2.5 SEM image of the printed tablets' top surface with different formulations.

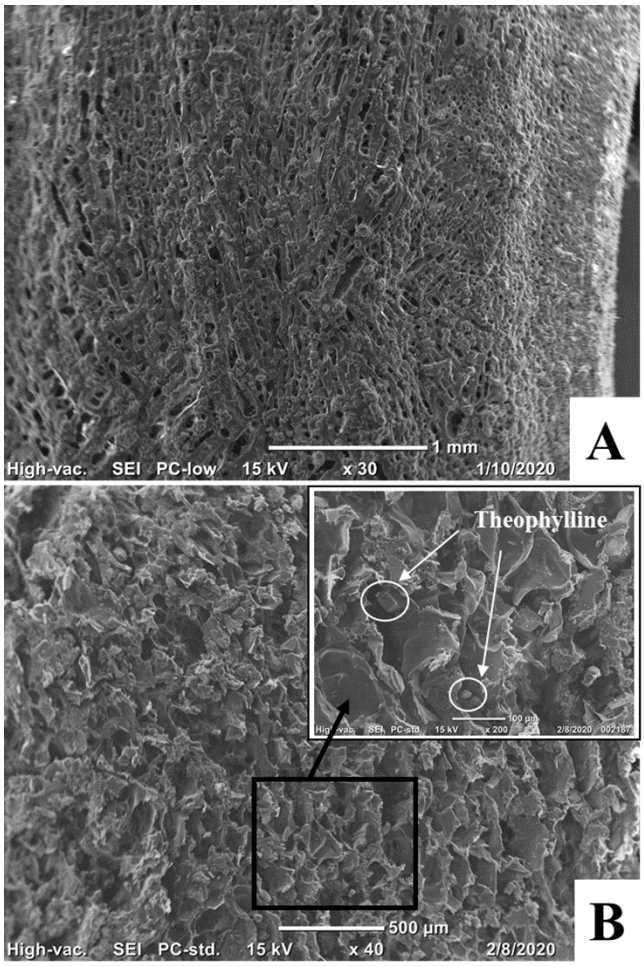

Figure 2.6 A) SEM image of the printed tablet' side surface with MC10% 125mg formulation and B) SEM cross-section image of printed tablet with MC10% 125 mg.

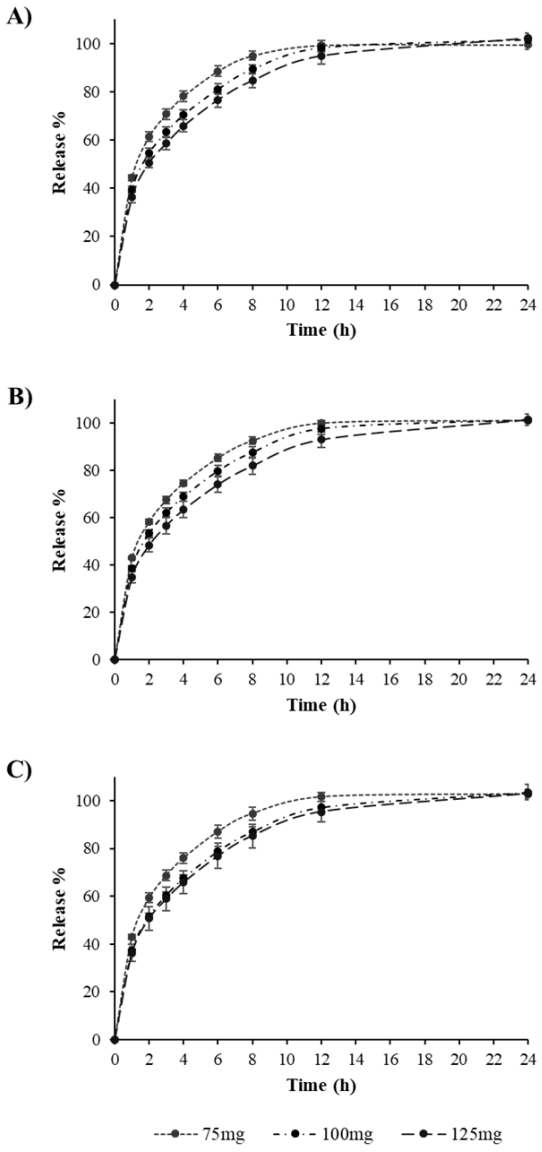

Figure 2.7 The cumulative release profiles of theophylline from 3D printed tablets at different dosages (75, 100, 125 mg) with different MC A4M concentrations: A) 8%, B) 10%, C) 12% (w/w).

CHAPTER 3. 3D PRINTING OF EXTENDED-RELEASE TABLETS OF THEOPHYLLINE USING HYDROXYPROPYL METHYLCELLULOSE (HPMC) HYDROGELS

Yiliang Cheng[a], Hantang Qin[b]*, Nuria Acevedo[a], Xuepeng Jiangb, Xiaolei Shi[a]*

[a] Food Science and Human Nutrition Department, Iowa State University, Ames, IA, 50011, USA

[b] Industrial and Manufacturing Systems Engineering Department, Iowa State University, Ames, IA, 50011, USA

Modified from a manuscript under review to *International Journal of Pharmaceutics*

Abstract

Extrusion-based three dimensional (3D) printing has been used for rapid and reliable tailoring of the drug dosage and the release profile to provide customized medicine. An extrusion (SSE) based 3D printer was used to prepare the semi-solid tablets with different drug loading dosages (75, 100, 125 mg) under ambient temperature. The active pharmaceutical ingredients, theophylline, was uploaded within the hydrogels, prepared by hydroxypropyl methylcellulose (HPMC) K4M or E4M. The HPMC concentrations were adjusted to different levels (10 and 12% w/w) to fulfill the requirements for 3D printing. Rheological and textural properties, as well as release profiles, were significantly affected by the excipient concentrations and types, regardless of theophylline doses. The printing material should exhibit shear-thinning behavior and a loss factor ($\tan\delta = G''/G'$) between 0.2 and 0.7, especially for 3D printing purposes using the current platform. The SEM images demonstrated that the hydrogel matrix exhibited a porous structure, which had the potential to encapsulate the theophylline particles within its microstructure. The *in vitro* dissolution test showed that the release of all tablets was extended over 12 hours, and the

release profiles were well fitted into first-order and Korsmeyer-Peppas models. The release exponent (n values) of the Korsmeyer-Peppas model is between 0.45 and 0.89, which revealed that the 3D printed HPMC matrix release the theophylline by diffusion and erosion mechanisms. These results demonstrated the potential of using the SSE based 3D printing to develop extended-release tablets with flexible dosage combinations.

Introduction

The oral tablet is the most common type of pharmaceutical dosage form to deliver active pharmaceutical ingredients (APIs) into the human body (Domínguez-Robles et al., 2019). The conventional method for tablet fabrication is compression, which presses or compacts the mixture of APIs and excipients from powders into solid doses (Gambhire et al., 2007). The conventional pharmaceutical industries would benefit from continuous production and large-scale manufacturing for tablet fabrication. However, these large manufacturing facilities and multiple-step processes are not suitable for customized dosage forms, considering the high expenses of equipment changeover and the requirement of trained personnel. Thus, most of the oral tablets on the market provide a predetermined dose of each APIs and fixed design of tablets shapes (Acosta-Vélez and Wu, 2016; Khaled et al., 2015a). To improve the efficacy and safety of a therapeutic substance, the worldwide demand for personalized and tailored pharmaceutical tablets has been continually rising in the past few years. As the pharmaceutical industry personalizes the drug delivery system, 3D printing technology has attracted much attention for use as a novel pharmaceutical manufacturing technique to fabricate patient-tailored medicines (Goyanes et al., 2015a; Skowyra et al., 2015).

Compared to the conventional tablets manufacturing technique, recent research has demonstrated that 3D printing offers high flexibility and complexity in the design of release profiles and tablets structures to accommodate patient needs (Norman et al., 2017). Recent

advances include the development of using computer software (e.g., computer-aided design (CAD)) to fabricate the complex structures of tablets such as multi-compartmental dosage forms (Genina et al., 2017; Maroni et al., 2017) and multi-component polypills (Khaled et al., 2015b, 2015a). These dosage forms were used to deliver APIs individually from a single personalized tablet with different release profiles. The drug release profiles could also be controlled by varying the 3D printing settings (infill percentage, porosity, etc.) (Goyanes et al., 2015a; Solanki et al., 2018), and tablet geometries (shape and the ratio between surface area and volume, etc.) (Goyanes et al., 2015b; Khaled et al., 2018; Kyobula et al., 2017), as well as excipient types (Melocchi et al., 2015) to enhance the specific therapeutic benefits. The findings of these studies support that using 3D printing in the pharmaceutical industry could rapidly and reliably tailor the drug combination and release profile based on the metabolic responses and pathophysiology of patients (Acosta-Vélez and Wu, 2016; Kadry et al., 2018; Sadia et al., 2016; Skowyra et al., 2015). Besides, the fabrication process could be finished by using the highly adjustable and portable desktop devices, rather than the large manufacturing facilities (Khaled et al., 2014; Trenfield et al., 2018).

Along with the development of technology, the first FDA approved 3D printed medicine, Spritam®, has become available to epilepsy patients in 2015 (Kotta et al., 2018). Unlike the conventional method for compressed pill production, 3D binder jet printers could bind the high dose of API (up to 1000 mg) into a small low-density pill. The highly porous structure allows the Spritam® pill disintegrate in the mouth with just a sip of water, benefiting the patients who struggle with swallowing, especially epilepsy patients (Jamróz et al., 2018; Solanki et al., 2018; Tan et al., 2018). In addition to binder jet printing technology, there are several different types of 3D printing technology: extrusion-based, selective laser sintering (SLS), and stereolithography

(SLA), and inkjet printing, etc (G. et al., 2016; Trenfield et al., 2018). Among these, a growing trend of using extrusion-based 3D printing in pharmaceutical fields has been noticed around the world which including two different printing techniques: fused deposition modeling (FDM) and semi-solid extrusion (SSE). The FDM technology is typically used to fabricate objects with thermoplastic materials, such as polyvinylpyrrolidone (PVP) (Kollamaram et al., 2018), polyvinyl alcohol (PVA) (Pietrzak et al., 2015), and polylactic acid (PLA) (Water et al., 2015); however, these materials are not suitable for tablet formulation. To overcome these limitations, the SSE technique was developed for fabricating patient-tailored tablets in the semi-solid state. Compared to the FDM technique, the printing process of the SSE technique does not require high operation temperature. So it has been widely implemented in 3D printing for tissue engineering and food processing to load bioactive and thermo-sensitive compounds, such as living cells (AnilKumar et al., 2019; Khalil et al., 2005), vitamins (Kim et al., 2018) and proteins (J. Chen et al., 2019), probiotics, and enzymes. The starting materials for the SSE-based 3D printer are usually semi-solid inks like gels or pastes, which were prepared by a high amount of water to save the usage of excipients (Khaled et al., 2015a; Li et al., 2018). Therefore, SSE 3D printing is also considered a cost-effective manufacturing process. Several publications have reported that the printing quality depended on the viscoelastic properties and flow behavior of the printing ink (Azad et al., 2020; Li et al., 2018). However, the study of SSE technology for tablets fabrication is still in its infancy. The relationship between the rheological properties of the printing materials and the printability of the 3D printed tablets have not been well established. Additionally, the drug loading capacity provided by the hydrogel-based matrix should also be investigated better to understand the release profiles of the 3D printed tablets.

This study aimed to investigate the effect of the rheological and physical properties of hydrogel-API bioinks on the printability and printing quality of 3D printed tablets. Two different types of FDA-approved biopolymers, hydroxypropyl methylcellulose (HPMC) K4M and E4M, were selected as excipients to deliver theophylline due to their encapsulation capacity and 3D printing ability (Cheng et al., 2020). The impact of excipient concentrations and theophylline dosages on the *in vitro* drug release profile and the parameters of release kinetics were also investigated. The knowledge of the relations among rheological properties, 3D printability, and printing quality, and release kinetics are necessary for the successful application of 3D printing in the area of pharmaceuticals.

Material and methods

Materials

Two kinds of excipient materials, HPMC K4M and E4M, was donated by J. Rettenmaier & Söhne (Schoolcraft, MI). Theophylline, which is the API, was purchased from Acros (New Jersey, USA). For HPMC K4M, the degrees of substitution for the methoxyl group and hydroxypropyl group are 19-24% and 4-12%, respectively. The dissolving and gelling temperatures are 25-30°C and 77°C, respectively. For HPMC E4M, the degrees of substitution for the methoxyl group and hydroxypropyl group are 28-30% and 7-12%, respectively. The dissolving and gelling temperatures are 20-25°C and 60°C, respectively. The 4M terminology indicates the viscosity of this material is in the range of 3,000-5,600 mPa·s in the 2% solution at 20°C under 20rpm.

Preparation of the therapeutic paste

The therapeutic pastes were separately prepared by uniformly mixing the theophylline and one type of excipient powders into deionized water at 80°C. The mixed materials were cooled to ambient temperature and then centrifuged at 3000 rpm, for 10 min to remove potential

air bubbles trapped within the mixture. The concentrations of excipients were 10 and 12% (w/w) for both HPMC K4M and E4M powders. For each concentration, the theophylline dosages were predetermined at 0, 75, 100, and 125 mg (±5 % deviation) per tablet. In general, there were 16 different formulas of prepared therapeutic pastes.

Rheological characterization

The rheological characterization experiments were performed by a Discovery HR-2 rotational rheometer (TA Instruments, New Castle, DE) with cone and plate geometry (2° cone angle, 40 mm diameter, serial # 109675). All of the tests were set at 20°C with a 1 mm gap size between the geometry and steel Peltier plate. The sample and geometry plates were covered by a solvent trap to avoid water evaporation. The ramp rate of shear rate was conducted from 0.1 to 60 1/s to determine the flow behavior and apparent viscosity of the therapeutic pastes. The flow curves were fitted to the Herschel-Bulkley model (Equation (1)) as follows

$$\tau = \tau_0 + K\dot{\gamma}^n \quad (1)$$

where τ means shear stress (Pa), τ_0 is yield stress (Pa), $\dot{\gamma}$ is the shear rate (1/s), K is the consistency index (Pa·s^2), and n is the flow behavior index.

The yield stress value (Pa) was determined through the oscillatory stress sweep test by increasing the oscillation stress in log mode from 1 to 1000%, while the frequency was kept constant at 1 Hz. This test was used to determine the linear viscoelastic region (LVR) and to estimate yield stress values (Pa). The endpoint of the LVR can be considered as the yield stress, i.e., the stress required to make the printable material to flow (De Graef et al., 2011). Dynamic viscoelastic properties (storage modulus (G'), loss modulus (G"), and loss tangent (tanδ = G"/G')) were characterized by carrying out frequency sweep tests, which increased the angular frequency

oscillated from 0.1 to 600 rad/s in logarithmic sweep mode and kept the strain constant at 0.1. All rheological properties tests were conducted in triplicates.

Tablets 3D printing process

The customized 3D printer used for this study was described in a previous publication (Polamaplly et al., 2019). A Velleman K8200 3D printer (Velleman Inc.) equipped with an extrusion-based syringe of 0.437 mm diameter nozzle. Tablets were 3D printed with 5 mm/s printing speed and 0.125 extrusion multilayers into eight layers. The printing process was performed under ambient temperature. The average weight of each 3D printed tablet was 1.40 g, with a deviation of 5%, and the average dimensions were 10×21×7 mm.

Textural profile analysis

The physical properties of the printed tablets were analyzed using a TA.XT plusC texture analyzer (Texture Technologies Corp. and Stable Micro Systems, Ltd. Hamilton, MA) under ambient temperature. A 35-mm diameter cylinder probe compressed the tablets to 50% strain deformation with the double compression test mode. The pre-test and post-test speeds were 1.5 mm/s, the compression rate is 1.0 mm/s, and the delay time between the first and second compression was 5 s with 5 g trigger force. Force versus time graphs was generated from the instrument software for hardness, adhesiveness, cohesiveness, and springiness. TPA tests were conducted in triplicate by measuring three tablets with the same formulation because of the large deformation.

Scanning Electron Microscopy (SEM)

The surface morphology of freezing dried tablets was evaluated by scanning electronic microscopy (SEM). Pictures were taken under vacuum using JCM-6000 SEM (Jeol, Japan). All tablets were freeze-dried by the Virtis Genesis SQ freeze dryer at -40 °C for 12 hours and then

coated with gold (SBC-12 Sputter coater). The average size of pores and clusters on the tablets' surfaces were acquired by measuring 10 representative pores with Image J Software (Java 1.8.0).

***In vitro* dissolution test**

The dissolution test of 3D printed semi-solid state tablets was evaluated in 500 mL of 0.1 M hydrochloric acid for the first 2 hours and phosphate buffer (pH 7.0) for the next 10 hours using the USP dissolution apparatus 2 paddle method (DT 126 light dissolution tester (Erweka, Germany) at 100 rpm. The media temperature was maintained at 37 ± 0.5 °C, and media samples were collected and analyzed at 1, 2, 3, 4, 6, 8, and 12 hours during the test. To reduce the variation, there were two separate batches of therapeutic pastes prepared for each formula as the replication. Then the dissolution profile of two printed tablets from the same batch was measured, and dissolution tests were performed in quadruplicate. The theophylline concentration contained in the filtrated solution (0.45μm polypropylene syringe filter) was analyzed using reverse-phase HPLC (Ultimate3000) and a UV/Visible detector at a wavelength of 272 nm. The mobile phase consisting of the 96:4 v/v mixture of water/acetonitrile at a flow rate of 1.2mL/min. The injection volume was set at 20 µl with retention time for 15 min, and the column temperature was maintained at 30 ºC. All the HPLC injections were carried out in duplicate.

Kinetics of drug release

The results of *in vitro* release profile of theophylline obtained from dissolution test were fitted to several kinds of kinetic models: zero-order (Equation (2)), first-order (Equation (3)), Korsmeyer-Peppas (Equation (4)), Higuchi and Hixson-crowell (Dash et al., 2010) to explain the drug release behaviors, and the model with the highest correlation coefficient (R2) should be considered as the optimal fit.

$$Q_t = Q_0 + K_0 t \quad (2)$$

where Q_t is the amount of drug dissolved in time *t*, Q_0 is the initial amount of drug in the solution and K_0 is the zero order release constant.

$$Log\ C = Log\ C_0 - Kt/2.303 \quad (3)$$

where C_0 is the initial concentration of drug, *K* is the first order rate constant, and *t* is the time.

$$\frac{M_t}{M_\infty} = Kt^n \quad (4)$$

where Mt / M∞ is a fraction of drug released at time t, K is the release rate constant, and n is the release exponent.

Statistical analysis

Statistical analysis was performed using JMP Pro 14 software (Cary, NC). Comparison between different formulations was analyzed using a one-way analysis of variance (ANOVA) with a significance level of $p < 0.05$. Tukey's HSD (Honestly Significant Difference) test was used to determine significant differences between means.

Results and discussion

Rheological properties

The flow behavior and apparent viscosity of prepared therapeutic pastes were analyzed by flow ramp tests. The flow curves (**Fig. 3.1**) showed that the apparent viscosity of all the tested samples decreased with the increase of shear rate. Based on the results, HPMC K4M and E4M based pastes both showed shear-thinning behavior, which is also referred to as pseudoplastic behavior. The reduction in apparent viscosity with increased shear rate mimicked the extrusion-based 3D printing conditions where the 3D printing materials were also subjected to high shear rates. During the printing process, the decreased apparent viscosity made the pastes smoothly pass through the syringe and printer nozzle at a high shear rate (J. Chen et al., 2019; Solanki et al., 2018). And the shear rate-depended apparent viscosity could be recovered after removing

high stress or shear rate, which is essential to keep the layer-by-layer deposited shape without deformation (Lille et al., 2018). The pastes with either higher excipient concentration or theophylline dosage showed significantly higher apparent viscosity; however, an exception was observed for 12% E4M, where there was no significant difference in apparent viscosity between 75 and 100 mg dose. Besides, pastes prepared by HPMC K4M showed significantly higher apparent viscosity than E4M-based pastes when compared at the same concentration and dosage. The increased apparent viscosity could lead to the higher viscosity between the two printed filaments next to each other. Thus, it helps the printed structure hold the shape after deposition (Anukiruthika et al., 2019).

Except for the flow behavior, the yield stress is also essential to assess the potential of materials for extrusion-based 3D printing (Cernencu et al., 2019; Liu et al., 2019). The yield stress is the amount of energy or stress necessary to initiate the flow of materials, i.e., an external force larger than the yield stress should be applied to the material so that it can be continuously extruded through the nozzle (Jiang et al., 2018). The estimated yield stress of different excipients and formulas (**Table 3.1**) indicated that the yield stress of pastes significantly increased along with the increase of the excipient concentration. Also, the type of excipients is another significant factor deciding the magnitude of yield stress. The highest yield stress was observed for 12% K4M, followed by 12% E4M, and then 10% (w/w) E4M, regardless of theophylline dosages. The desirable range of yield stress was critical to a successive printing process. For the ease of 3D printing, the magnitude of yield stress for a potential material should not be too high; however, for the 3D printed objects to hold their structure after 3D printing, their resumed yield stress should not be too low. Otherwise, the extruded structure would be too weak to support the

sequentially printed layers if the yield stress of materials was lower than the printed structures' surface tension or gravitational forces (Jiang et al., 2018).

The semi-solid 3D printing materials could exhibit both viscous and elastic properties during extrusion, which could be presented by the dynamic viscoelastic properties (Ramachandran et al., 1999). The key parameters used to determine the viscoelastic properties included storage modulus (G'), loss modulus (G"), and tan δ (ratio of G" to G'), as shown in **Fig. 3.2**. The parameter G' is used to measure the energy that could be stored and recovered, while G" is used to measure the energy dissipated under deformation or extrusion (Gupta et al., 2014). For the therapeutic pastes prepared by K4M, all of the tested formulas showed that the G' was always higher than G" (tan $\delta < 1$), which indicated the pastes with HPMC K4M excipient had elasticity dominating gel-like structures (Lille et al., 2018). However, the results showed that HPMC E4M-based pastes all exhibit the conversion of liquid-like behavior (tan $\delta > 1$) into the solid-like behavior (tan $\delta < 1$) as the angular frequency increases. This conversion was caused by the increased angular frequencies, which left no sufficient time for the materials' structure to be disentangled during stress relaxation (Dooling et al., 2016). The increment of G' and reduction of tan δ that were caused by concentration increase would lead to the stronger mechanical strength and a higher printing resolution of objects (H. Chen et al., 2019; Jiang et al., 2018; Polamaplly et al., 2019). According to the relatively high elasticity, the 12% (w/w) K4M-based pastes may exhibit better shape retention ability and resolution after the 3D printing process (H. Chen et al., 2019; Lille et al., 2018).

Physical and mechanical properties of 3D printed dosage forms

Representative pictures of the 3D printed dosage forms were presented in **Fig. 3.3** to show the appearance of the 3D printed dosage forms. After the layer by layer deposition, all of the HPMC K4M-based tablets showed the desirable shape retention ability and could be

successively extruded into filaments without breaking. Compared with the control group (pure excipient without API), the tablets containing theophylline appeared opaque and milky white, which was caused by the white color of theophylline powder. The filament resolution of printed tablets was enhanced with the increased HPMC K4M concentration. However, the pastes with HPMC K4M 14% (w/w) were too hard to be extruded through the nozzle in the preliminary experiment. The printing difficulty could be explained by the excessively high yield stress (greater than 4000 Pa) of HPMC K4M 12% (w/w) led to the poor extrudability, and too low tan δ caused the poor fluidity (Kuo et al., 2019). For HPMC E4M 10% (w/w) tablets, the increased dimension (width and length) indicated the poor shape retention ability. Although the tablets showed better ability to remain in the printed dimension with higher HPMC E4M concentration, the poor surface resolution of extruded filaments confirmed that the pastes showed more liquid-like behavior and the printed objects were hard to retain the structure after the layer-by-layer deposition. Furthermore, the tablets with excipient HPMC K4M showed better printing quality and resolution when compared with tablets with HPMC E4M. Meanwhile, the HPMC K4M 12% (w/w) tablets showed the desirable printing quality and the optimal printability. The printability was achieved by controlling all of the rheological properties that fell into a proper range to balance between good shape retention ability and extrudability.

The surface morphology of 3D printed dosage forms was analyzed by SEM as illustrated in **Fig. 3.4**. The SEM images of the 3D printed tablets without theophylline (**Fig. 3.4A** and **C**) showed that the tablets were made of the porous structure, with the average pore size of 0.47 x 0.16 mm (length x width). The three-dimensional porous structure was formed during the gelation of HPMC excipient when dissolved into water over gelling temperature. One of the most common method to produce cellulose derivatives is etherification, which replaces the

primary hydroxyl group on the cellulose backbone to yield ether derivatives such as HPMC to improve the water solubility (Fox et al., 2011; Mischnick and Momcilovic, 2010). The substituted methoxyl group disrupted the formation of hydrogen bindings to improve the solubility. Meanwhile, the high temperature of water induced the hydrophobic intermolecular association between methyl groups and water, which caused the aggregation or cluster to form gelation (Joshi, 2011; Li et al., 2001). As the only material used to create a porous structure, the increased concentration of excipient HPMC could provide more available methoxyl groups to interact with water. The increased water absorption and intermolecular association spontaneously enhanced the gel strength and increased the viscosity of printable pastes (Abbas et al., 2013; Roshan and Asef, 2010). The intervention of theophylline (**Fig. 3.4B** and **D**) as a water-soluble solute may decrease the amount of free water to affect the gel strength, but the change of theophylline dosage did not make a remarkable impact on the HPMC-based matrix formation (Roshan and Asef, 2010). The dissolved theophylline came into flakes/clusters with an average size of 0.02 mm. The SEM images showed that the pore sizes of three-dimension HPMC hydrogel structures greater than the dimensions of theophylline. Theophylline flakes/clusters were observed attached to the surface of dehydrated HPMC hydrogel. The highly porous structure would allow the water to penetrate into the matrix, thereby allowing the release of theophylline through water diffusion (Viridén et al., 2011). However, during the fixation steps of the conventional SEM, the 3D printed tablets were freeze-dried to remove the water from the matrix, which may have impacted the distribution of theophylline within the hydrated 3D printed tablets. Thus, the original distribution of theophylline within the hydrated 3D printed tablets were difficult to be observed (Allan-Wojtas et al., 2008).

Both excipient HPMC K4M and E4M showed the gelling ability and could form the matrix to entrap the clusters of theophylline. But these two excipients showed differences in the mechanical properties (**Table 3.2**) when prepared into tablets. Hardness is the term used to describe the force required for a material to deform under compression (Jones et al., 1997). Similar to the effect of excipient concentration and theophylline dosage on yield stress and G', printed tablets with higher concentration and dosage were more hard and rigid, which may be attributed to the increased amount of total solids (Abbas et al., 2013; Roshan and Asef, 2010). According to the results from rheological properties, HPMC K4M-based pastes showed high magnitudes in yield stress and storage modulus; however, the hardness of HPMC E4M-based tablets was higher than K4M-based tablets with the same formula. This inconsistency could be caused by the collapse of HPMC E4M tablets after the 3D printing process due to the poor shape retention ability, which decreased the height of the tablet during the TPA test (Peyron et al., 1997). Adhesiveness is used to measure the attractive forces between the surface of the printed tablet and the test probe, and the higher absolute value of adhesiveness indicated the higher attractive force (Jones et al., 1997). Jones et al. (1997) mentioned that the increased concentration of cellulose derivatives could enhance the molecular interaction between cellulose polymers and the TPA probe. So the absolute value of tablets' adhesiveness increased as the excipient concentration and theophylline dosage increased. The results of cohesiveness and springiness showed a small range, and there was no significant difference ($p>0.05$) in these two parameters between different kinds of excipients. Also, the excipient concentration and theophylline dosage have minimal effect on cohesiveness and springiness.

***In vitro* dissolution profiles and drug release kinetics**

To investigate the drug release profile of the HPMC-based 3D printed tablets, all of the tablets did the *in vitro* dissolution test over 12h, as shown in **Fig. 3.5**. The theophylline release

from printed tablets was extended over 12 h, and the dissolution of the HPMC K4M and E4M matrices was also complete in 12 h. In the first 2 hours, all of the tablets released the theophylline into 0.1M HCl solution over 46%. Then the dissolution rate became lower after the change of dissolution media from HCl solution to phosphate buffer after 2 hours. The release profile obtained for all the printed tablets with the lowest theophylline dosage (75 mg) was higher than the other two dosages. The faster drug release of 75 mg tablets may be attributed to the smaller drug load amount. Even though both HPMC K4M and E4M tablets showed the extended-release profiles over 12 h, the HPMC E4M tablets showed higher release percentages when compared with HPMC K4M tablets with the same formulas. Mitchell et al. (1993) indicated that the drugs are released from the cellulose derivatives-based masteries through two mechanisms: diffusion and erosion. The high amount of substituted methoxyl groups in HMPC E4M weakened the gel strength and fasted the theophylline release through the erosion of the hydrated gel matrixes as well (Gustafsson et al., 1999; Mitchell et al., 1993). In general, the HPMC K4M and E4M-based tablets exhibited the extended-release profile over 12 hours by providing the hydrogel matrices to load theophylline. Once dissolved in water, the 3D printed HPMC matrix could delay the drug release by diffusion through the hydrogel or erosion of the porous structure (Li et al., 2001; Mischnick and Momcilovic, 2010).

The drug release profiles obtained were also plotted into different kinetics models (**Table 3.3**) to investigate the theophylline release kinetics of the 3D printed tablets. All the printed tablets were well fitted into the first-order, Korsmeyer-Peppas, Higuchi, and Hixson-Crowell models with $R2 > 0.9$. The best-fitted model was first-order with the highest R2 value, indicating that the change of drug release rate and kinetics state depended only on the theophylline dosage (Bruschi, 2015). This finding is consistent with previous studies that used HPMC K100M as the

hydrophilic matrix to control the release of nifedipine, glipizide, and guaifenesin, which were also best fitted in the first-order kinetic model (Khaled et al., 2015a, 2014). The drug release profiles of 3D printed tablets were second best fitted into the Korsmeyer-Peppas model, except the HPMC E4M 10% (w/w) tablet with 75 mg dose. Using the Korsmeyer-Peppas model, the release exponent n values for all dosage forms we tested were between 0.45 to 0.89, which indicated that the drug transport mechanism through the HPMC based matrices follows the non-Fickian transport (Dash et al., 2010). Another study has investigated the release profiles of 3D printed gastro-floating tablets prepared by HPMC K4M and E15 as hydrophilic matrices that were also best fitted into the Korsmeyer–Pappas model and showed non-Fickian diffusion through the HPMC tablets (Li et al., 2018). The range of n value also confirmed that drug diffusion and hydrogel erosion were the two predominant release mechanisms of theophylline through 3D printed HPMC tablets (Khaled et al., 2015a). With the knowledge of the release kinetics of the HPMC based tablets, we ensured that the 3D printed tablets have a similar release profile to the theophylline sustained-release tablets prepared by the conventional method (Hayashi et al., 2005). The 3D printed hydrogel matrix also showed the potential to deliver the bioactive or thermal sensitive compounds for further research.

Conclusion

The SSE-based 3D printing is feasible to fabricate the semi-solid tablets under room temperature, which resulted in flexible dosage forms of theophylline exhibiting extended-release profile. It has been established that the rheological properties of the printing pastes can be used to predict the printability of pastes and the quality of 3D printed tablets. The surface morphology of printed tablets revealed that the drug loading capacity of tablets was provided by the three-dimensional network of HPMC hydrogels. The findings built on the rheological properties test and tablets' appearance suggested that excipient type and concentration played the predominant

role in the physical properties of printed tablets. The paste formulas which contained higher excipient concentration and made by HPMC K4M excipient showed relatively high yield stress, storage modulus, and hardness. The *in vitro* dissolution test showed that theophylline release from the 3D printed tablets was extended over 12 hours, and tablets release profiles were well fitted into the first-order and Korsmeyer–Peppas release kinetic models. Considering the advantages of cost-effectiveness, simple process, and customization capability of this novel technique, SSE-based 3D printing technology has the promise for rapid and reliable tailoring of the drug combination to provide personalized medicine.

References

Abbas, G., Irawan, S., Memon, K.R., Kumar, S., Elrayah, A.A.I., 2013. Hydroxypropylmethyl cellulose as a primary viscosifying agent in cement slurry at high temperature. Int. J. Automot. Mech. Eng. 8, 1218–1225. https://doi.org/10.15282/ijame.8.2013.12.0100

Acosta-Vélez, G.F., Wu, B.M., 2016. 3D Pharming : Direct Printing of Personalized Pharmaceutical Tablets Abstract Powder Bed Inkjet 3D Printing. Polym. Sci. 2, 1–10. https://doi.org/10.4172/2471-9935.100011

Allan-Wojtas, P., Truelstrup Hansen, L., Paulson, A.T., 2008. Microstructural studies of probiotic bacteria-loaded alginate microcapsules using standard electron microscopy techniques and anhydrous fixation. LWT - Food Sci. Technol. 41, 101–108. https://doi.org/10.1016/j.lwt.2007.02.003

AnilKumar, S., Allen, S.C., Tasnim, N., Akter, T., Park, S., Kumar, A., Chattopadhyay, M., Ito, Y., Suggs, L.J., Joddar, B., 2019. The applicability of furfuryl-gelatin as a novel bioink for tissue engineering applications. J. Biomed. Mater. Res. - Part B Appl. Biomater. 107, 314–323. https://doi.org/10.1002/jbm.b.34123

Anukiruthika, T., Moses, J.A., Anandharamakrishnan, C., 2019. 3D printing of egg yolk and white with rice flour blends. J. Food Eng. 265, 109691. https://doi.org/10.1016/j.jfoodeng.2019.109691

Azad, M.A., Olawuni, D., Kimbell, G., Badruddoza, A.Z.M., Hossain, M.S., Sultana, T., 2020. Polymers for extrusion-based 3D printing of pharmaceuticals: A holistic materials–process perspective, Pharmaceutics. https://doi.org/10.3390/pharmaceutics12020124

Bruschi, M.L. (Ed.), 2015. Mathematical models of drug release, in: Strategies to Modify the Drug Release from Pharmaceutical Systems. pp. 63–86. https://doi.org/10.1016/b978-0-08-100092-2.00005-9

Cernencu, A.I., Lungu, A., Stancu, I.C., Serafim, A., Heggset, E., Syverud, K., Iovu, H., 2019. Bioinspired 3D printable pectin-nanocellulose ink formulations. Carbohydr. Polym. 220, 12–21. https://doi.org/10.1016/j.carbpol.2019.05.026

Chen, H., Xie, F., Chen, L., Zheng, B., 2019. Effect of rheological properties of potato, rice and corn starches on their hot-extrusion 3D printing behaviors. J. Food Eng. 244, 150–158. https://doi.org/10.1016/j.jfoodeng.2018.09.011

Chen, J., Mu, T., Goffin, D., Blecker, C., Richard, G., Richel, A., Haubruge, E., 2019. Application of soy protein isolate and hydrocolloids based mixtures as promising food material in 3D food printing. J. Food Eng. 261, 76–86. https://doi.org/10.1016/j.jfoodeng.2019.03.016

Cheng, Y., Shi, X., Jiang, X., Wang, X., Qin, H., 2020. Printability of a Cellulose Derivative for Extrusion-Based 3D Printing : The Application on a Biodegradable Support Material. Front. Mater. 7, 3–8. https://doi.org/10.3389/fmats.2020.00086

Dash, S., Murthy, P.N., Nath, L., Chowdhury, P., 2010. Kinetic modeling on drug release from controlled drug delivery systems. Acta Pol. Pharm. - Drug Res. 67, 217–223.

De Graef, V., Depypere, F., Minnaert, M., Dewettinck, K., 2011. Chocolate yield stress as measured by oscillatory rheology. Food Res. Int. 44, 2660–2665. https://doi.org/10.1016/j.foodres.2011.05.009

Domínguez-Robles, J., Stewart, S.A., Rendl, A., González, Z., Donnelly, R.F., Larrañeta, E., 2019. Lignin and cellulose blends as pharmaceutical excipient for tablet manufacturing via direct compression. Biomolecules 9, 423. https://doi.org/10.3390/biom9090423

Dooling, L.J., Buck, M.E., Zhang, W. Bin, Tirrell, D.A., 2016. Programming Molecular Association and Viscoelastic Behavior in Protein Networks. Adv. Mater. 28, 4651–4657. https://doi.org/10.1002/adma.201506216

Fox, S.C., Li, B., Xu, D., Edgar, K.J., 2011. Regioselective esterification and etherification of cellulose: A review. Biomacromolecules 12, 1956–1972. https://doi.org/10.1021/bm200260d

G., B.O., S., G. V., K., S.B., C., D.R., A., G.S., S., G.P., 2016. 3D Printing & Pharmaceutical Manufacturing: Opportunities and Challenges. Int. J. Bioassays 5, 4723. https://doi.org/10.21746/ijbio.2016.01.006

Gambhire, M.N., Ambade, K.W., Kurmi, S.D., Kadam, V.J., Jadhav, K.R., 2007. Development and in vitro evaluation of an oral floating matrix tablet formulation of diltiazem hydrochloride. AAPS PharmSciTech 8, E166–E174. https://doi.org/10.1208/pt0803073

Genina, N., Boetker, J.P., Colombo, S., Harmankaya, N., Rantanen, J., Bohr, A., 2017. Anti-tuberculosis drug combination for controlled oral delivery using 3D printed compartmental dosage forms : From drug product design to in vivo testing. J. Control. Release 268, 40–48. https://doi.org/10.1016/j.jconrel.2017.10.003

Goyanes, A., Buanz, A.B.M., Hatton, G.B., Gaisford, S., Basit, A.W., 2015a. 3D printing of modified-release aminosalicylate (4-ASA and 5-ASA) tablets. Eur. J. Pharm. Biopharm. 89, 157–162. https://doi.org/10.1016/j.ejpb.2014.12.003

Goyanes, A., Robles Martinez, P., Buanz, A., Basit, A.W., Gaisford, S., 2015b. Effect of geometry on drug release from 3D printed tablets. Int. J. Pharm. 494, 657–663. https://doi.org/10.1016/j.ijpharm.2015.04.069

Gupta, S.S., Meena, A., Parikh, T., Serajuddin, A.T.M., 2014. Investigation of thermal and viscoelastic properties of polymers relevant to hot melt extrusion - I: Polyvinylpyrrolidone and related polymers. J. Excipients Food Chem. 5, 32–45.

Gustafsson, C., Bonferoni, M.C., Caramella, C., Lennholm, H., Nyström, C., 1999. Characterisation of particle properties and compaction behaviour of hydroxypropyl methylcellulose with different degrees of methoxy/hydroxypropyl substitution. Eur. J. Pharm. Sci. 9, 171–184. https://doi.org/10.1016/S0928-0987(99)00054-8

Hayashi, T., Kanbe, H., Okada, M., Suzuki, M., Ikeda, Y., Onuki, Y., Kaneko, T., Sonobe, T., 2005. Formulation study and drug release mechanism of a new theophylline sustained-release preparation. Int. J. Pharm. 304, 91–101. https://doi.org/10.1016/j.ijpharm.2005.07.022

Jamróz, W., Szafraniec, J., Kurek, M., Jachowicz, R., 2018. 3D printing in pharmaceutical and medical applications. Pharm. Res. 35, 1–22.

Jiang, J., Xu, X., Stringer, J., 2018. Support Structures for Additive Manufacturing: A Review. J. Manuf. Mater. Process. 2018, Vol. 2, Page 64 2, 64. https://doi.org/10.3390/JMMP2040064

Jones, D.S., Woolfson, A.D., Brown, A.F., 1997. Textural, viscoelastic and mucoadhesive properties of pharmaceutical gels composed of cellulose polymers. Int. J. Pharm. 151, 223–233. https://doi.org/10.1016/S0378-5173(97)04904-1

Joshi, S.C., 2011. Sol-gel behavior of hydroxypropyl methylcellulose (HPMC) in ionic media including drug release. Materials (Basel). 4, 1861–1905. https://doi.org/10.3390/ma4101861

Kadry, H., Al-hilal, T.A., Keshavarz, A., Alam, F., Joy, A., Ahsan, F., 2018. Multi-Purposable Filaments of HPMC for 3D Printing of Medications with Tailored Drug Release and Timed-Absorption Department of Pharmaceutical Sciences , School of Pharmacy , Texas Tech University Health Sciences Center , 1300 Coulter Dr ., Amarillo , TX-. Int. J. Pharm. https://doi.org/10.1016/j.ijpharm.2018.04.010

Khaled, S.A., Alexander, M.R., Irvine, D.J., Wildman, R.D., Wallace, M.J., Sharpe, S., Yoo, J., Roberts, C.J., 2018. Extrusion 3D Printing of Paracetamol Tablets from a Single Formulation with Tunable Release Profiles Through Control of Tablet Geometry. AAPS PharmSciTech 19, 3403–3413. https://doi.org/10.1208/s12249-018-1107-z

Khaled, S.A., Burley, J.C., Alexander, M.R., Roberts, C.J., 2014. Desktop 3D printing of controlled release pharmaceutical bilayer tablets. Int. J. Pharm. 461, 105–111. https://doi.org/10.1016/j.ijpharm.2013.11.021

Khaled, S.A., Burley, J.C., Alexander, M.R., Yang, J., Roberts, C.J., 2015a. 3D printing of tablets containing multiple drugs with defined release profiles. Int. J. Pharm. 494, 643–650. https://doi.org/10.1016/j.ijpharm.2015.07.067

Khaled, S.A., Burley, J.C., Alexander, M.R., Yang, J., Roberts, C.J., 2015b. 3D printing of five-in-one dose combination polypill with defined immediate and sustained release profiles. J. Control. Release 217, 308–314. https://doi.org/10.1016/j.jconrel.2015.09.028

Khalil, S., Nam, J., Sun, W., 2005. Multi-nozzle deposition for construction of 3D biopolymer tissue scaffolds. Rapid Prototyp. J. 11, 9–17. https://doi.org/10.1108/13552540510573347

Kim, H.W., Lee, J.H., Park, S.M., Lee, M.H., Lee, I.W., Doh, H.S., Park, H.J., 2018. Effect of Hydrocolloids on Rheological Properties and Printability of Vegetable Inks for 3D Food Printing. J. Food Sci. 83, 2923–2932. https://doi.org/10.1111/1750-3841.14391

Kollamaram, G., Croker, D.M., Walker, G.M., Goyanes, A., Basit, A.W., Gaisford, S., 2018. Low temperature fused deposition modeling (FDM) 3D printing of thermolabile drugs. Int. J. Pharm. 545, 144–152. https://doi.org/10.1016/j.ijpharm.2018.04.055

Kotta, S., Nair, A., Alsabeelah, N., 2018. 3D Printing Technology in Drug Delivery: Recent Progress and Application. Curr. Pharm. Des. 24, 5039–5048. https://doi.org/10.2174/1381612825666181206123828

Kuo, C.-C., Qin, H., Acuña, D.F., Cheng, Yiliang, Jiang, X., Shi, X., 2019. Printability of Hydrogel Com- posites Using Extrusion-Based 3D Printing and Post-Processing with Calcium Chloride. HSOA J. Food Sci. Nutr. https://doi.org/10.24966/FSN-1076/100051

Kyobula, M., Adedeji, A., Alexander, M.R., Saleh, E., Wildman, R., Ashcroft, I., Gellert, P.R., Roberts, C.J., 2017. 3D inkjet printing of tablets exploiting bespoke complex geometries for controlled and tuneable drug release. J. Control. Release 261, 207–215. https://doi.org/10.1016/j.jconrel.2017.06.025

Li, L., Thangamathesvaran, P.M., Yue, C.Y., Tam, K.C., Hu, X., Lam, Y.C., 2001. Gel Network Structure of Methylcellulose in Water. Langmuir 17, 8062–8068. https://doi.org/10.1021/la010917r

Li, Q., Guan, X., Cui, M., Zhu, Z., Chen, K., Wen, H., Jia, D., Hou, J., Xu, W., Yang, X., Pan, W., 2018. Preparation and investigation of novel gastro-floating tablets with 3D extrusion-based printing. Int. J. Pharm. 535, 325–332. https://doi.org/10.1016/j.ijpharm.2017.10.037

Lille, M., Nurmela, A., Nordlund, E., Metsä-Kortelainen, S., Sozer, N., 2018. Applicability of protein and fiber-rich food materials in extrusion-based 3D printing. J. Food Eng. 220, 20–27. https://doi.org/10.1016/j.jfoodeng.2017.04.034

Liu, J., Sun, L., Xu, W., Wang, Q., Yu, S., Sun, J., 2019. Current advances and future perspectives of 3D printing natural-derived biopolymers. Carbohydr. Polym. 207, 297–316. https://doi.org/10.1016/j.carbpol.2018.11.077

Maroni, A., Melocchi, A., Parietti, F., Foppoli, A., Zema, L., Gazzaniga, A., 2017. 3D printed multi-compartment capsular devices for two-pulse oral drug delivery. J. Control. Release 268, 10–18. https://doi.org/10.1016/j.jconrel.2017.10.008

Melocchi, A., Parietti, F., Loreti, G., Maroni, A., Gazzaniga, A., Zema, L., 2015. 3D printing by fused deposition modeling (FDM) of a swellable/erodible capsular device for oral pulsatile release of drugs. J. Drug Deliv. Sci. Technol. 30, 360–367. https://doi.org/10.1016/j.jddst.2015.07.016

Mischnick, P., Momcilovic, D., 2010. Chemical Structure Analysis of Starch and Cellulose Derivatives, Advances in Carbohydrate Chemistry and Biochemistry. Elsevier Inc. https://doi.org/10.1016/S0065-2318(10)64004-8

Mitchell, K., Ford, J.L., Armstrong, D.J., Elliott, P.N.C., Hogan, J.E., Rostron, C., 1993. The influence of substitution type on the performance of methylcellulose and hydroxypropylmethycellulose in gels and matrices. Int. J. Pharm. 100, 143–154. https://doi.org/10.1016/0378-5173(93)90085-T

Norman, J., Madurawe, R.D., Moore, C.M.V., Khan, M.A., Khairuzzaman, A., 2017. A new chapter in pharmaceutical manufacturing: 3D-printed drug products. Adv. Drug Deliv. Rev. 108, 39–50. https://doi.org/10.1016/j.addr.2016.03.001

Peyron, M.A., Maskawi, K., Woda, A., Tanguay, R., Lund, J.P., 1997. Effects of food texture and sample thickness on mandibular movement and hardness assessment during biting in man. J. Dent. Res. 76, 789–795. https://doi.org/10.1177/00220345970760031201

Pietrzak, K., Isreb, A., Alhnan, M.A., 2015. A flexible-dose dispenser for immediate and extended release 3D printed tablets. Eur. J. Pharm. Biopharm. 96, 380–387. https://doi.org/10.1016/j.ejpb.2015.07.027

Polamaplly, P., Cheng, Y., Shi, X., Manikandan, K., Zhang, X., Kremer, G.E., Qin, H., 2019. 3D printing and characterization of hydroxypropyl methylcellulose and methylcellulose for biodegradable support structures. Polymer (Guildf). 173, 119–126. https://doi.org/10.1016/j.polymer.2019.04.013

Ramachandran, S., Chen, S., Etzler, F., 1999. Rheological characterization of hydroxypropylcellulose gels. Drug Dev. Ind. Pharm. 25, 153–161. https://doi.org/10.1081/DDC-100102155

Roshan, H., Asef, M.R., 2010. Characteristics of oilwell cement slurry using CMC. SPE Drill. Complet. 25, 328–335. https://doi.org/10.2118/114246-PA

Sadia, M., Sośnicka, A., Arafat, B., Isreb, A., Ahmed, W., Kelarakis, A., Alhnan, M.A., 2016. Adaptation of pharmaceutical excipients to FDM 3D printing for the fabrication of patient-tailored immediate release tablets. Int. J. Pharm. 513, 659–668. https://doi.org/10.1016/j.ijpharm.2016.09.050

Skowyra, J., Pietrzak, K., Alhnan, M.A., 2015. Fabrication of extended-release patient-tailored prednisolone tablets via fused deposition modelling (FDM) 3D printing. Eur. J. Pharm. Sci. 68, 11–17. https://doi.org/10.1016/j.ejps.2014.11.009

Solanki, N.G., Tahsin, M., Shah, A. V, Serajuddin, A.T.M., 2018. Formulation of 3D Printed Tablet for Rapid Drug Release by Fused Deposition Modeling: Screening Polymers for Drug Release, Drug-Polymer Miscibility and Printability. J. Pharm. Sci. 107, 390–401. https://doi.org/10.1016/j.xphs.2017.10.021

Tan, D.K., Maniruzzaman, M., Nokhodchi, A., 2018. Advanced pharmaceutical applications of hot-melt extrusion coupled with fused deposition modelling (FDM) 3D printing for personalised drug delivery. Pharmaceutics 10. https://doi.org/10.3390/pharmaceutics10040203

Trenfield, S.J., Goyanes, A., Telford, R., Wilsdon, D., Rowland, M., Gaisford, S., Basit, A.W., 2018. 3D printed drug products : Non-destructive dose veri fi cation using a rapid point-and-shoot approach. Int. J. Pharm. 549, 283–292. https://doi.org/10.1016/j.ijpharm.2018.08.002

Viridén, A., Abrahmsén-Alami, S., Wittgren, B., Larsson, A., 2011. Release of theophylline and carbamazepine from matrix tablets - Consequences of HPMC chemical heterogeneity. Eur. J. Pharm. Biopharm. 78, 470–479. https://doi.org/10.1016/j.ejpb.2011.02.003

Water, J.J., Bohr, A., Boetker, J., Aho, J., Sandler, N., Nielsen, H.M., Rantanen, J., 2015. Three-dimensional printing of drug-eluting implants: Preparation of an antimicrobial polylactide feedstock material. J. Pharm. Sci. 104, 1099–1107. https://doi.org/10.1002/jps.24305

Tables and Figures

Table 3.1 Estimated yield stress (determined through the oscillatory stress sweep test - linear viscoelastic region) of different excipients: K4M and E4M with varying concentrations and theophylline dosages. Values are presented as mean ± SD (n=3). Means that have no superscript in common are significantly different from each other (Tukey's HSD, P<0.05)

Excipient	Concentration % (w/w)	Dosage (mg)			
		0	75	100	125
K4M	10	1954.0±5.3^{e}	1985.7±45.7^{e}	2025.1±37.0^{e}	1906.8±101.2^{e}
	12	3270.2±53.6^{a}	3022.2±49.8^{b}	3100.8±35.0^{b}	2977.1±107.6^{b}
E4M	10	1455.647±19.3^{g}	1623.807±4.7^{f}	1640.0±12.7^{f}	1524.1±11.2^{fg}
	12	2295.2±29.3^{d}	2342.6±13.7^{cd}	2434.0±49.9^{cd}	2468.2±29.9^{c}

Table 3.2 Textural profile analysis parameters for HPMC K4M and E4M with varying concentrations and theophylline dosages. Values are presented as mean ± SD (n=3). Means that have no superscript in common are significantly different from each other (Tukey's HSD, P<0.05).

Excipient	Concentration % (w/w)	Dosage (mg)	Hardness (g)	Adhesiveness (g·s)	Cohesiveness	Springiness
K4M	10%	0	342.7±39.0^{g}	-366.6±27.3^{a}	1.0^{cd}	0.9^{b}
		75	422.4±22.2f^{g}	-503.6±30.8^{ab}	1.1^{cd}	0.9^{b}
		100	456.2±11.7^{fg}	-549.8±24.2^{abc}	1.0^{de}	0.9^{b}
		125	555.4±27.7^{defg}	-655.1±12.8^{bcde}	1.0^{de}	0.9^{b}
	12%	0	471.3±65.1^{efg}	-563.5±35.7^{abcd}	1.0^{de}	0.9^{b}
		75	565.1±40.5^{defg}	-670.9±25.9^{bcde}	1.0^{de}	0.9^{b}
		100	677.2±55.1^{cdefg}	-797.2±55.4^{cdef}	1.0^{de}	0.9^{b}
		125	814.9±52.3^{bcde}	-853.6±91.8^{ef}	0.9^{e}	0.9^{b}
E4M	10%	0	533.3±200.8^{defg}	-488.8±112.6^{ab}	1.3^{a}	1.0^{a}
		75	1018.2±99.6^{bc}	-850.4±52.8^{ef}	1.1^{bc}	1.0^{a}
		100	1155.0±83.3^{ab}	-961.1±32.3^{fg}	1.1^{bcd}	1.0^{a}
		125	1471.7±210.7^{a}	-1186.3±138.2^{g}	1.1^{bcd}	1.0^{a}
	12%	0	395.4±269.3^{fg}	-459.0±243.4^{ab}	1.2^{ab}	0.9^{b}
		75	727.3±105.7^{cdef}	-841.2±118.8^{def}	1.1^{bcd}	0.9^{b}
		100	837.0±57.9^{bcd}	-852.3±115.0^{ef}	1.1^{bdc}	0.9^{b}
		125	948.5±77.9^{bc}	-1018.3±33.2^{fg}	1.1^{bc}	0.9^{b}

Table 3.3 The correlation coefficient (R^2) of theophylline release kinetic models from *in vitro* dissolution test

Excipient	Concentration % (w/w)	Dosage (mg)	Zero-order	First-order	Korsmeyer-Peppas	Higuchi	Hixson-Crowell
K4M	10%	75	0.69	0.99	0.94	0.93	0.96
		100	0.77	0.99	0.98	0.96	0.97
		125	0.80	0.98	0.98	0.98	0.96
	12%	75	0.76	0.99	0.98	0.96	0.96
		100	0.79	0.98	0.98	0.97	0.96
		125	0.84	0.98	0.99	0.99	0.98
E4M	10%	75	0.58	0.99	0.88	0.86	0.88
		100	0.69	1.00	0.94	0.93	0.94
		125	0.76	1.00	0.97	0.96	0.95
	12%	75	0.80	0.99	0.97	0.98	0.96
		100	0.83	0.98	0.98	0.99	0.94
		125	0.76	0.94	0.96	0.96	0.99

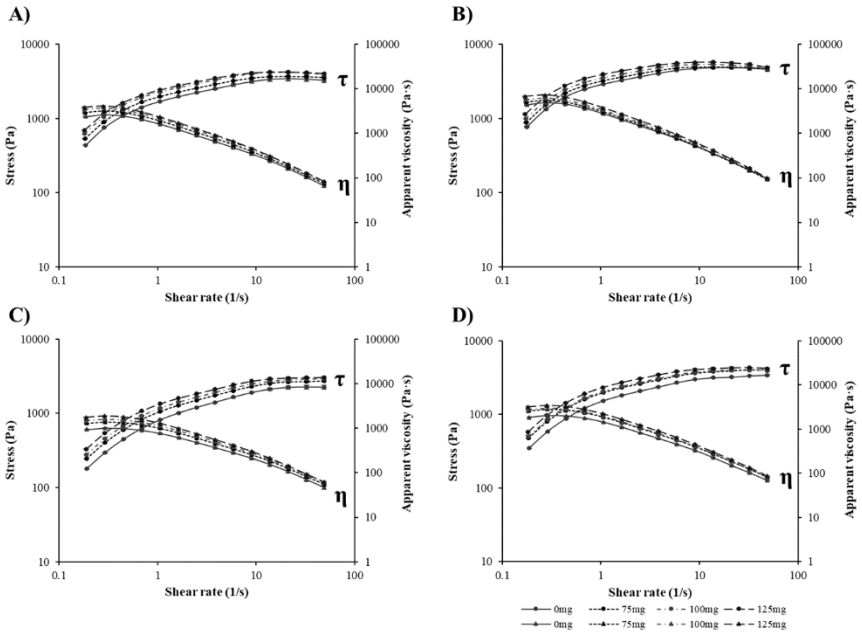

Figure 3.1 Shear stress (τ) and apparent viscosity (η) versus shear rate profiles of HPMC K4M and E4M with different theophylline dosages (0, 75, 100, 125 mg) at different excipient concentrations: A) K4M10%, B) K4M12%, C) E4M 10%, and D) E4M 12% (w/w).

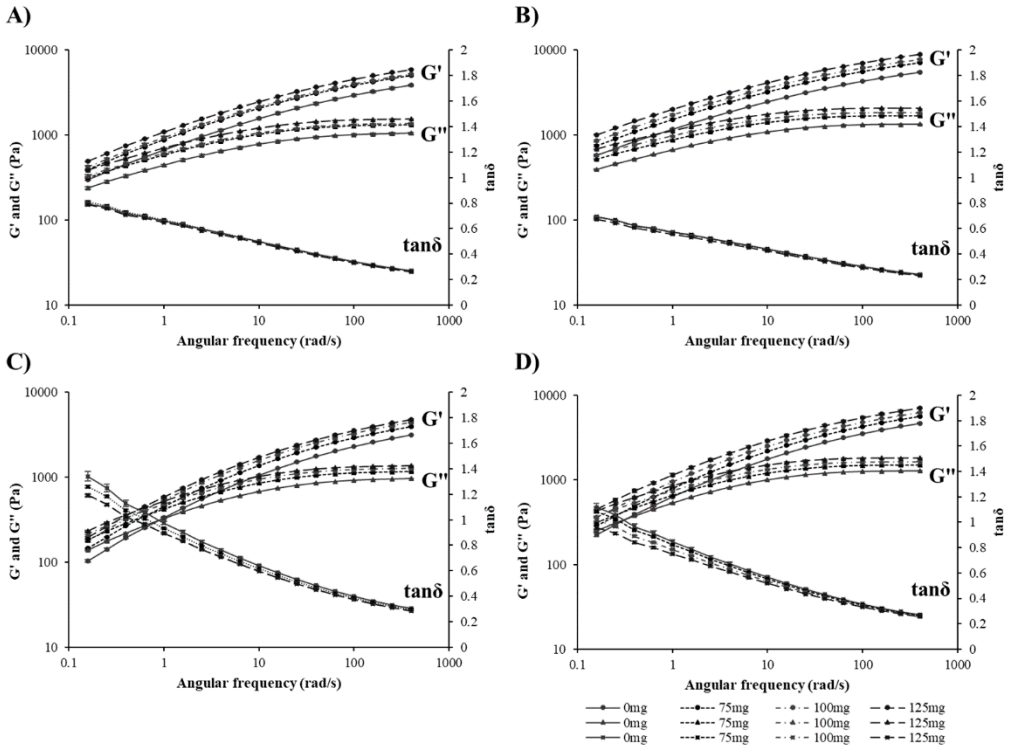

Figure 3.2 Storage modulus (G'), loss modulus (G") and tanδ versus frequency profile of HPMC K4M and E4M with different theophylline dosages (0, 75, 100, 125 mg) at different excipient concentrations: A) K4M10%, B) K4M12%, C) E4M 10%, and D) E4M 12% (w/w).

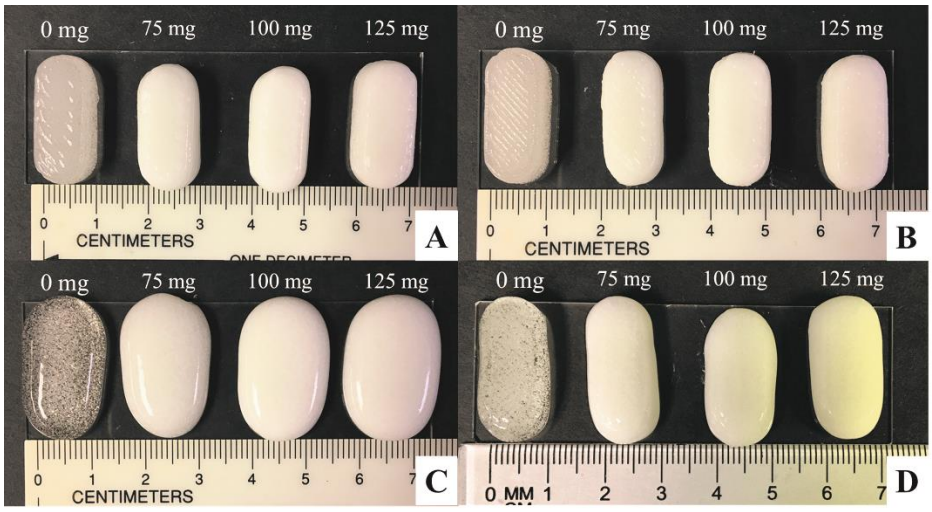

Figure 3.3 The appearance of printed tablets with different formulas: A) K4M10%, B) K4M12%, C) E4M 10%, and D) E4M 12% (w/w).

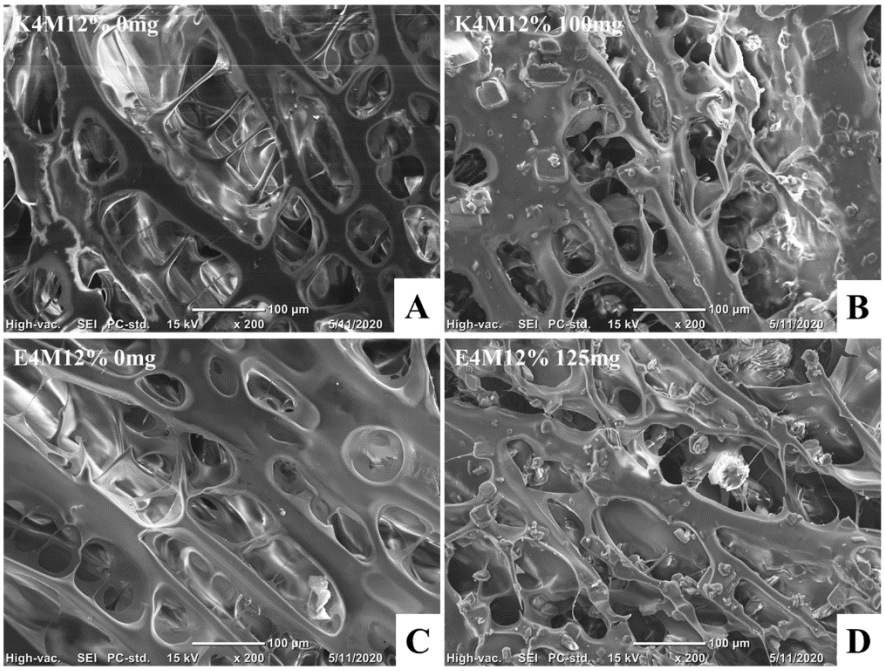

Figure 3.4 SEM image of the printed tablets' top surface with different formulations.

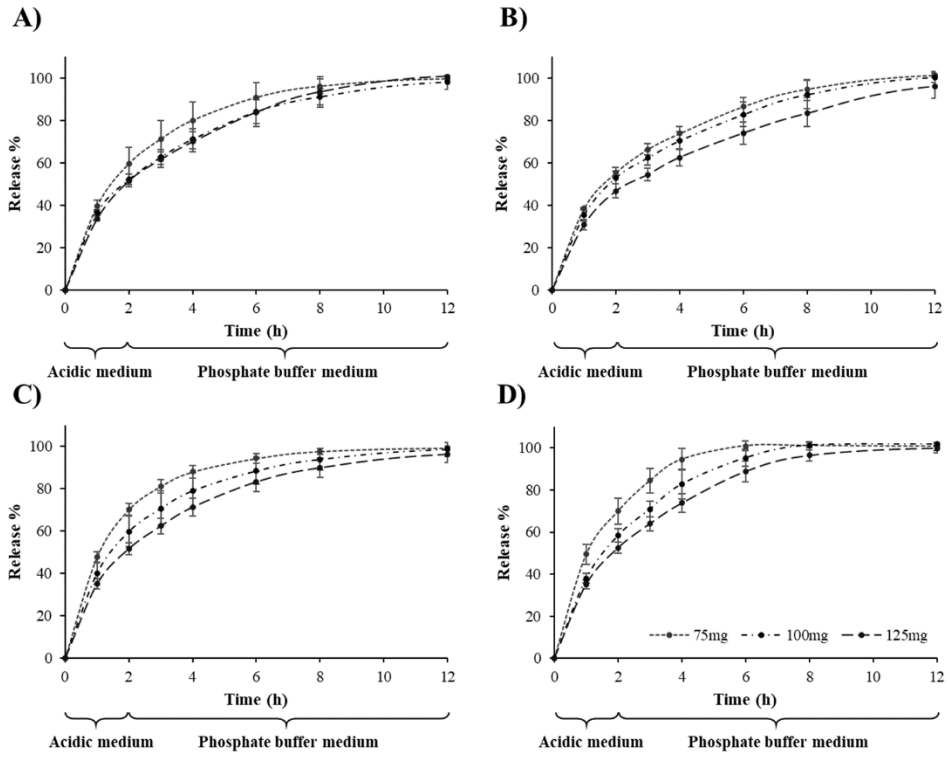

Figure 3.5 The cumulative release profiles of theophylline from 3D printed tablets with different formulas: A) K4M10%, B) K4M12%, C) E4M 10%, and D) E4M 12% (w/w).

CHAPTER 4. PRINTABILITY OF A CELLULOSE DERIVATIVE FOR EXTRUSION-BASED 3D PRINTING: THE APPLICATION ON A BIODEGRADABLE SUPPORT MATERIAL

Yiliang Cheng[1], Xiaolei Shi[1]*, Xuepeng Jiang[2], Xiaohui Wang[1], Hantang Qin[2]*

[1] Food Science and Human Nutrition Department, Iowa State University, Ames, IA, 50011, USA

[2] Industrial and Manufacturing Systems Engineering Department, Iowa State University, Ames, IA, 50011, USA

Modified from a manuscript published in *Frontiers in Materials*

Abstract

Support material plays a leading role in the application of 3D printing to avoid deformation and enhance stability. This study aimed to fabricate the support structure by using hydroxypropyl methylcellulose (HPMC), which has advantages over conventional material such as low cost, low printable temperature, and high biodegradability. Once dissolved in water over gelling temperature, the HPMC based hydrogel exhibited shear-thinning behavior with decreasing apparent viscosity values at higher shear rates. The shear-dependent viscosity makes the HPMC hydrogel extrudable throughout the printing process and the printed structure stable enough without deformation. As concentration increased, apparent viscosity and storage modulus both subsequently increased. These rheological properties indicated that the concentration of HPMC K4M hydrogel significantly influenced the printability and shape retention ability, which is associated with the mechanical strength of printed filaments. The highest concentration, 12% w/v, should have the best ability to hold the printed shape over time due to the highest G' and lowest loss tangent. The printability test also showed that K4M 12% w/v could be printed into

different fill density (100%, 75%, and 50%) with different patterns, i.e., rectilinear and Hilbert curve. The selection of fill density and pattern both have an effect on surface roughness and porosity. The printed support material was compatible with acrylonitrile butadiene styrene (ABS), which is the material to fabricate the main structure for 3D printing. The support material made of HPMC can be easily removed by peeling off from the main structure without visible residual.

Introduction

In recent years, 3D printing has been widely applied in many fields. A support structure is used to prevent the deformation or collapse caused by gravity or other external forces during the printing process (Jiang et al., 2018). As additive manufacturing is developing, it is necessary to find out a proper sacrificial support material that includes advantages such as low waste and cost. Cellulose is one of the most abundant polymers made from plants. It attracts wide attention as a biodegradable polymer in additive manufacturing fields. Cellulose derivatives are modified from cellulose by substitution of hydroxyl groups with hydroxypropyl groups and methoxyl groups using chemical reactions. Such chemical modifications improve the water solubility, thus overcome certain material limitations for the technical applications. Cellulose derivatives have been widely used as a coating material, emulsifier, thickener, binder, and filler for food and drug production (Banks et al., 2014; Ding et al., 2014); however, their usages in the area of additive manufacturing is still in its infancy.

While polylactic acid (PLA) is the most mature support materials used in Fused Deposition Modeling (FDM) 3D printing technology, cellulose-based biopolymer materials have a relatively lower cost (<10$/kg) compared to PLA (20-30$/kg) (Sanandiya et al., 2018; Baran and Erbil, 2019). As a thermoplastic polymer, PLA material requires a high printing temperature (180-200 °C) to become printable and achieves desirable quality (Valerga et al., 2018). But the

previous study demonstrated that the cellulose-based hydrogel could be printable under ambient process temperature and showed excellent shape retention ability (Polamaplly et al., 2019). Besides, cellulose-based polymers showed high degradability and dissolubility due to the behavior of hydrolytic degradation in cold water (Luo et al., 2019). Compared with cellulose polymers, it is less environmentally friendly to remove PLA supportive structure from the main structure by soaking in the chemical solution of isopropyl alcohol and potassium hydroxide (Jiang et al., 2018).

The main difference between different cellulose derivatives depends on their substituted groups. Additionally, the degree of substituted groups results in unique properties. Hydroxypropyl methylcellulose (HPMC) is one of the most common types of commercially available grades of cellulose derivatives. The hydroxypropyl group from HPMC material significantly increased the thermostability when compared with other cellulose derivatives, such as methylcellulose (MC), carboxymethyl cellulose (CMC), and hydroxyethylcellulose (HEC) (Li et al., 1999).

Currently, the field is limited by a lack of the printability test of cellulose derivatives materials which could be potentially applied as biodegradable support structure for extrusion-based 3D printing. To fill in the knowledge gap, we hypothesize the HPMC hydrogels can be 3D printed to provide mechanical support to the main structure, and then easily removed without a negative effect on the main structure quality. Our previous study indicated that the hydrogels made from HPMC K4M showed rheological properties that are suitable for 3D printing, and the printed filaments can be dissolved by water (Polamaplly et al., 2019). The aim of this paper is to investigate the viscoelastic properties and mechanical strength of HPMC K4M hydrogels with

different concentrations and explore the potential of using HPMC as supportive material in the application of 3D printing technology.

Material and methods

HPMC K4M was provided by J. Rettenmaier USA LP (Schoolcraft, MI). The degree of substitution for the methoxyl groups is 19-24%, for the hydroxypropyl groups is 4-12%. The 4M terminology indicates the viscosity of this material is in the range of 3000-5600 mPa·s in 2% solution at 20°C under 20rpm. The dissolving and gelling temperatures are 25-30 °C and 77 °C, respectively. The aqueous solutions were prepared with 80°C water into three different concentrations: 8%, 10%, and 12% w/v. After cooling down to ambient temperature (25 °C), all samples were centrifuged at 5000 rpm for 10 minutes to remove air bubbles.

The rheological properties test was carried out using Rheometer (TA Instruments Discovery HR-2, USA) with parallel geometry plates at a gap size of 1mm under ambient temperature. The flow ramp test was conducted to determine the apparent viscosity under the increased shear rate (0.1 to 100 1/s). The apparent viscosity was measured and plotted as a function of the shear rate. The oscillatory frequency sweep test was used to characterize the materials' dynamic modulus with sweep strain increased from 1 to 100%. The rheological properties, i.e., shear rate, apparent viscosity, angular frequency, storage modulus (G'), loss modulus (G"), and loss tangent (tan δ =G"/G'), were recorded by the Trios Software (TA Instruments, USA). All rheological properties tests were conducted in triplicates.

The printability test was conducted using the extrusion-based syringe that was configured on the platform of the Velleman K8200 3D printer (Velleman Inc., Fort Worth, Texas). The test was designed to print geometries with different fill-in patterns, i.e., rectilinear and Hilbert curve, and densities (100, 75, and 50%). **Fig. 4.1** shows the sketch of the extrusion-based 3D printer. The printer settings were as follows: speed was 5mm/s, nozzle diameter was 0.437 mm,

extrusion multilayer was 0.05, print under ambient temperature, and the number of layers was twelve. To study the morphology and the pore structure of the printed objects, the freeze-dried HPMC K4M12% sample (100% fill-in density with rectilinear pattern) was coated with gold (SBC-12 Sputter coater) to improve the conductivity. The SEM images were observed on JEOL (JCM-6000). The average pore size (width and length) of K4M12% object's surface was acquired by measuring 5 pores with image J software (version Java 1.8.0).

Results and discussion

As shown in **Fig. 4.2A**, the apparent viscosity of all the materials decreased as the shear rate increased, which means the materials behave as shear-thinning fluids (Polamaplly et al., 2019). The property of shear stress-dependent viscosity makes the HPMC gel printable through the extrusion-based printer once the applied stress exceeds the yield stress. Then the printed filament showed the shape retention ability that is associated with the high apparent viscosity after extrusion (Gunasekaran and Ak, 2000; Rao, 2014; Yang et al., 2018). The G' and G" are functions of frequency, and both gradually increased with the increasing oscillatory frequency, as shown in **Fig. 4.2B**. The G' and G" used to describe the magnitude of energy stored and lost per cycle of deformation (Gunasekaran and Ak, 2000). Under the same concentration, G' is higher than G" which indicated the deformation through this material is permanently elastic or recoverable (Rao, 2014). When the concentration increased, both G' and G" increased, which indicated the strength of the material network structure increased, and the material behaved more solid-like (Yang et al., 2018). The reason is the increased concentration of HPMC brings stronger intermolecular hydrogen bonding (Ranganathan et al., 2018). The G' for HPMC gel increased when the formation of the gel network was more completed, and the dense network structure contributed to the stronger gel strength (Joshi, 2011). The decreased G' of materials

improved the flowability when extruding from the syringe nozzle, but it is not helpful for the shape retention ability (Wang et al., 2018).

The loss tangent values for all three different concentrations are less than 1, which means the materials have predominant solid-like behavior. The loss tangent decreased as HPMC K4M concentration increased, which indicated the G' become dominant, i.e., materials showed more solid-like behavior due to water content decreased (Liu et al., 2018). Gao et al. (2019) claimed that the gelatin-alginate composite hydrogels showed optimal compromise between structural integrity and extrusion uniformity with a tanδ in the range of 0.25 to 0.45. According to the rheological properties of HPMC hydrogel, the increased concentration made the value of tanδ fall into this critical range under relatively lower angular frequency. In general, the rheological properties of HPMC K4M demonstrated concentration played a significant role in the mechanical strength of printed filaments. The highest concentration, 12% w/v HPMC K4M hydrogel, showed the highest G' (3072 Pa) and lowest loss tangent (0.55) at 1 rad/s.

For shear-thinning materials, it has been reported that increasing the material concentration could conducive to the resolution of printed objects. Because the increased content of HPMC polymer brings more available interaction sites to form hydrogen bonding which led to resolution improvement (Wilson et al., 2017). Meanwhile, the filament diameter during the printing process also decreased as HPMC hydrogel concentration increased, which also enhanced the resolution of printed objects and inhibited the extrude swell or die swell phenomenon (Cloitre et al., 1998; Polamaplly et al., 2019). Polamaplly et al. (2019) indicated that the decreasing shape fidelity factor of printed filaments attributed to an increase in the storage modulus of materials. The 12% w/v HPMC hydrogel showed the highest G' value, which should exhibit the lowest shape fidelity factor correspondingly, i.e., the printed filaments could stack up in layers without

sagging or deformation. In this case, the 12% w/v HPMC hydrogel had been selected to do the printability test due to the optimal shape retention ability and buildability. According to the previous study, when compared with other nozzles with different diameters ranging from 0.437mm to 1.0mm, the smallest one showed the smallest diameter of printed filaments which subsequently improved the geometries' resolution (Polamaplly et al., 2019). As a result, the nozzle with 0.437mm diameter was chosen to print the objects for the printability test because of the desired resolution and surface quality.

The rectilinear pattern makes the printer nozzle move into simple parallel lines at a 45° angle. Not like the clear surface of the rectilinear pattern, the geometries filled in with the Hilbert curve pattern showed less straight and distinct peripheral lines (**Fig. 4.3 A, B, C**). The main reason may be the short traveling distance of the nozzle caused the printed filaments to have less tensile strength (Fafenrot et al., 2017; Akhoundi and Behravesh, 2019). The nozzle could be moved more smoothly through the x and y direction when using a rectilinear fill-in pattern. Besides, the printing process of the Hilbert curve pattern took a remarkably long time to fill in the printed geometries. **Fig. 4.3D** showed the surface of extruded K4M12% filaments was porous with uneven oblong shape pores. The average length and width of the pores are 267 μm and 173 μm, respectively. These microscale pores have composed a net structure of K4M hydrogel which contained high water content before sublimation. When mixing with the water over gelling temperature, the power-like K4M material firstly dissolved into solvent as a liquid then converted into a semi-solid state as a hydrogel. The gelation formed as the self-aggregation between methyl groups and water because of the relative hydrophobic property. The aggregation is expedited by increased temperature which promotes the formation of hydrogen bonds (Joshi, 2011). The hydrophobic interaction induced the gelation of the HPMC solution and resulted in a

three-dimensional network as evidenced in **Fig. 4.3D**. The porous network structure also showed the potential of the application for pharmaceutical purposes, because the cross-linked net structure may work as a micro-scale barrier to control the active pharmaceutical ingredients release profile from HPMC based hydrogel matrix (Ali et al., 2015).

For the rectilinear pattern, the 50% fill density geometry showed uneven surface and twisted filaments compared with other densities. The reason may be the lower density left more space for printed material to fill in. The Hilbert curve developed much higher porosity than the rectilinear pattern under the same level of density. The high porosity should favor the penetration rate of gas or liquid in future applications.

Fig. 4.4 showed the combination between the 12% w/v K4M based support structure and the main structure made of ABS. The support structure was sticky and provided excellent adhesiveness to attach the surface of ABS. These two printed parts could hold together and are supposed to provide high integrity and stability during the printing process. Also, the K4M supportive structure can be thoroughly peeled off from the main structure without visible residual. According to the rheological properties, K4M 12% w/v hydrogel showed the best shape retention ability. The relatively high G' of this concentration also denotes more solid-like property and higher mechanical rigidity.

Conclusion

Compared with the most common filaments for 3D printing, such as polylactic acid (PLA) and acrylonitrile butadiene styrene (ABS), cellulose derivatives-based filament has a bunch of advantages such as low-cost, ambient temperature printable, and eco-friendly processing. The HPMC K4M hydrogel showed excellent printability by using the extrusion-based 3D printer. The shape retention ability during printing attributed to an increase in the concentration of HPMC K4M. The shear-thinning and viscoelastic properties confer printability on the printed

geometries allowing them to be printed with different fill-in patterns and densities. There are several critical rheological parameters that play the leading role when building the relationship between flowability and shape retention ability. The higher concentration of printed hydrogel is desirable due to the optimal value of apparent viscosity, storage modulus, and loss tangent. The HPMC K4M 12% w/v material had been selected for the printability test with consideration of the highest G' and lowest loss tangent. The selection between fill-in patterns and densities depends on the purpose of the support structure. The rectilinear surface fill is clearer and more distinct, and the Hilbert curve fill-in pattern could provide a more rough contact surface. The printing process time and structure porosity could be modified by adjusting the fill-in density. In other words, the printed geometries suffer from extreme pitting with a grid-like pattern of holes in the surface once the fill-in density was lower than 75%. The support material made of HPMC K4M can be easily removed by peeling off from the ABS-based structure without visible residual. The future potential of this edible material will move on the application with human consumption, such as drug delivery systems and bio-scaffold printing. The biocompatibility, mechanical strength, porosity, and drug loading/release profile need to be investigated based on the research purpose.

References

Akhoundi, B., and Behravesh, A. H. (2019). Effect of filling pattern on the tensile and flexural mechanical properties ofFDM3D printed products. *Exp. Mech*. 59, 883–897. doi: 10.1007/s11340-018-00467-y

Ali, L., Ahmad, M., and Usman, M. (2015). Evaluation of cross-linked hydroxypropyl methylcellulose graft-methacrylic acid copolymer as extended release oral drug carrier. *Cell. Chem. Technol.* 49, 143–151.

Banks, S. R., Pygall, S. R., Bajwa, G. S., Doughty, S. W., Timmins, P., and Melia, C. D. (2014). The influence of substituted phenols on the sol: gel transition of hydroxypropyl methylcellulose (HPMC) aqueous solutions. *Carbohydr. Polym.* 101, 1198–1204. doi: 10.1016/j.carbpol.2013.10.061

Baran, E. H., and Erbil, H. Y. (2019). Surface modification of 3D printed PLA objects by fused deposition modeling: a review. *Colloids Interfaces* 3:43. doi: 10.3390/colloids3020043

Cloitre, M., Hall, T., Mata, C., and Joseph, D. D. (1998). Delayed-die swell and sedimentation of elongated particles in wormlike micellar solutions. *J. Nonnewton. Fluid Mech.* 79, 157–171. doi: 10.1016/S0377-0257(98)00103-7

Ding, C., Zhang, M., and Li, G. (2014). Rheological properties of collagen/hydroxypropyl methylcellulose (COL/HPMC) blended solutions. *J. Appl. Polym. Sci.* 131, 1–10. doi: 10.1002/app.40042

Fafenrot, S., Grimmelsmann, N., Wortmann, M., and Ehrmann, A. (2017). Three-dimensional (3D) printing of polymer-metal hybrid materials by fused deposition modeling. *Materials (Basel)* 10:1199. doi: 10.3390/ma10101199

Gao, T., Gillispie, G. J., Copus, J. S., Kumar, A., Rajan, P., Seol, Y., et al. (2019). Optimization ofgelatin-alginate composite bioink printability using rheological parameters: a systematic approach. *Biofabrication* 10:034106. doi: 10.1088/ 1758-5090/aacdc7.Optimization

Gunasekaran, S., and Ak, M. M. (2000). Dynamic oscillatory shear testing of foods Ð selected applications. *Trends Food Sci. Technol.* 11, 115–127. doi: 10.1016/ s0924-2244(00)00058-3

Jiang, J., Xu, X., and Stringer, J. (2018). Support Structures for additive manufacturing: a review. *J. Manuf. Mater. Process.* 2:64. doi: 10.3390/ JMMP2040064

Joshi, S. C. (2011). Sol-gel behavior of hydroxypropyl methylcellulose (HPMC) in ionic media including drug release. *Materials (Basel).* 4, 1861–1905. doi: 10.3390/ma4101861

Li, X., Huang, M., and Bai, H. E. (1999). Thermal decomposition of cellulose ethers. *Appl. Polym.* 73, 2927–2936. doi: 10.1002/(sici)1097-4628(19990929)73: 14<2927::aid-app17>3.0.co;2-k

Liu, Z., Zhang, M., Bhandari, B., and Yang, C. (2018). Impact of rheological properties of mashed potatoes on 3D printing. *J. Food Eng.* 220, 76–82. doi: 10.1016/j.jfoodeng.2017.04.017

Luo, Y., Lin, Z., and Guo, G. (2019). Biodegradation assessment of poly (Lactic Acid) filled with functionalized titania nanoparticles (PLA/TiO 2) under compost conditions. *Nanoscale Res. Lett.* 14:59. doi: 10.1186/s11671-019- 2891-4

Polamaplly, P., Cheng, Y., Shi, X., Manikandan, K., Zhang, X., Kremer, G. E., et al. (2019). 3D printing and characterization ofhydroxypropyl methylcellulose and methylcellulose for biodegradable support structures. *Polymer (Guildf.)* 173, 119–126. doi: 10.1016/j.polymer.2019.04.013

Ranganathan, N., Joseph Bensingh, R., Abdul Kader, M., and Nayak, S. K. (2018). "Synthesis and properties of hydrogels prepared by various polymerization reaction systems," in *Cellulose-Based Superabsorbent Hydrogels. Polymers and Polymeric Composites: A Reference Series*, ed. M. Mondal (Cham: Springer), 1–25. doi: 10.1007/978-3-319-77830-3_18

Rao, A. M. (2014*). Rheology of Fluid, Semisolid, and Solid Foods Principles and Applications*, 3rd Edn, ed. G. V. Barbosa-Canovas (New York, NY: Springer).

Sanandiya, N. D., Vijay, Y., Dimopoulou, M., Dritsas, S., and Fernandez, J. G. (2018). Large-scale additive manufacturing with bioinspired cellulosic materials. *Sci. Rep.* 8:8642. doi: 10.1038/s41598-018-26985-2

Valerga, A. P., Batista, M., Salguero, J., and Girot, F. (2018). Influence of PLA filament conditions on characteristics of FDM parts. *Materials (Basel)* 11:1322. doi: 10.3390/ma11081322

Wang, L., Zhang, M., Bhandari, B., and Yang, C. (2018). Investigation on fish surimi gel as promising food material for 3D printing. *J. Food Eng.* 220, 101–108. doi: 10.1016/j.jfoodeng.2017.02.029

Wilson, S. A., Cross, L. M., Peak, C. W., and Gaharwar, A. K. (2017). Shear- thinning and thermo-reversible nanoengineered inks for 3D bioprinting. *ACS Appl. Mater. Interfaces* 9, 43449–43458. doi: 10.1021/acsami.7b13602

Yang, F., Zhang, M., Bhandari, B., and Liu, Y. (2018). Investigation on lemon juice gel as food material for 3D printing and optimization of printing parameters. *LWT Food Sci. Technol.* 87, 67–76. doi: 10.1016/j.lwt.2017.08.054

Figures

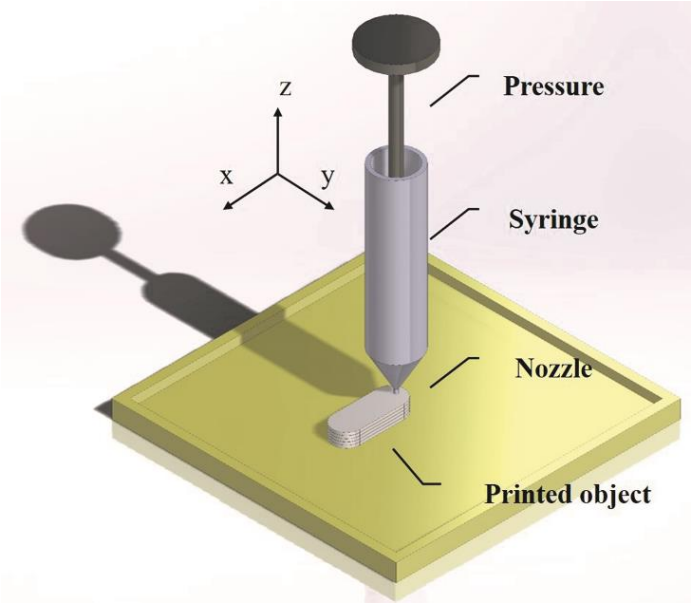

Figure 4.1 Semi-solid extrusion-based 3D printer schematic.

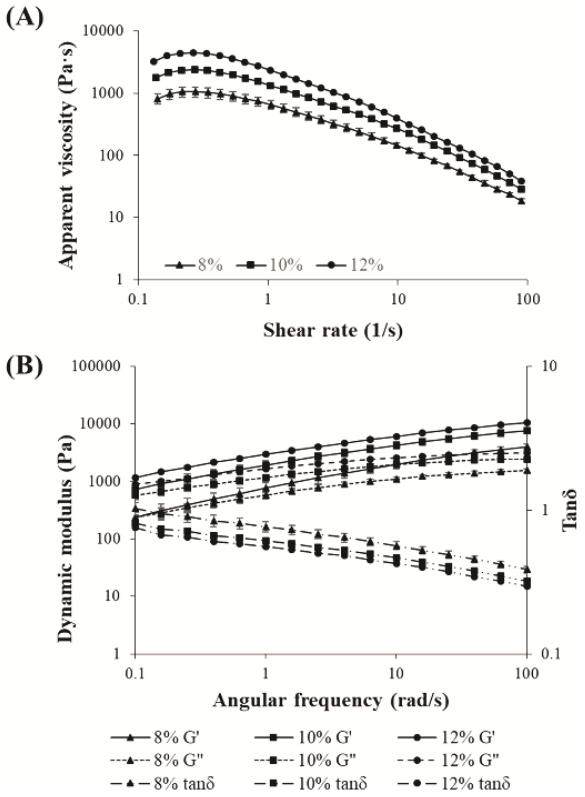

Figure 4.2 (A) Flow ramp test data: apparent viscosity versus shear rate profiles. (B) Frequency sweep test data: dynamic modulus and loss tangent versus angular frequency profiles of HPMC K4M under different concentrations (8, 10, and 12% w/v).

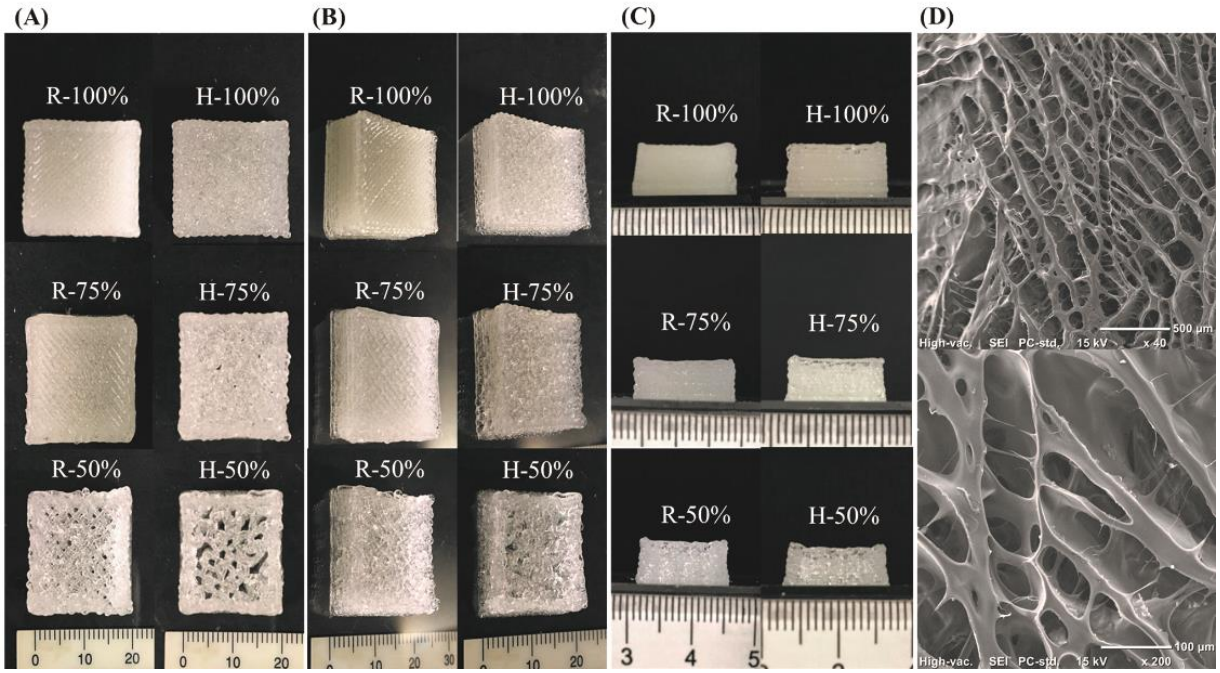

Figure 4.3 K4M 12% w/v printed geometries with different fill-in patterns (R means rectilinear fill-in patterns and H means Hilbert curve fill-in patterns) and densities (100, 75, and 50%). (A) Top view; (B) Side view; (C) Front view; (D) SEM micrographs of HPMC K4M 12% (R-100%).

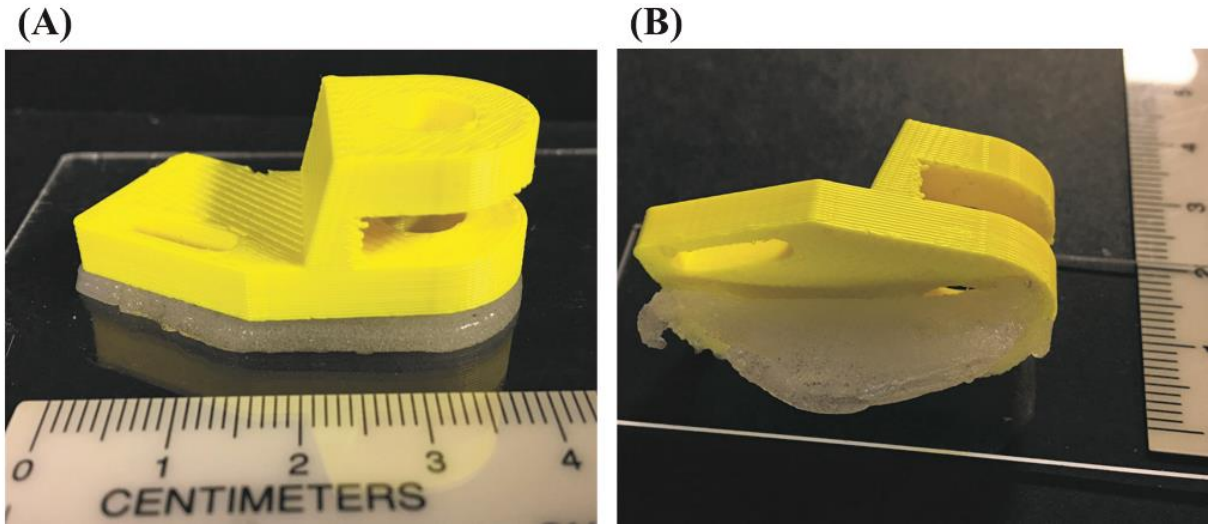

Figure 4.4 K4M 12% w/v based support structure (a) attached with ABS based main structure and (b) peeled off from the main structure without visible residual.

CHAPTER 5. GENERAL CONCLUSION

The overall objective of this research was to investigate the feasibility of using SSE-based 3D printing technology to fabricate the semi-solid materials and to explore the relation between rheological properties and 3D printability of hydrogels. The first project, Chapter 2, focused on the development of MC A4M-based tablets, and the second project, Chapter 3, investigated the feasibility of using HPMC K4M and E4M as matrixes to load API. These two projects both selected the cellulose derivatives materials as target excipient, and these two materials also showed unique characteristics.

The concentration and type of excipient played predominate roles in determining the 3D printing potential, which was related to the rheological and textural properties. The excipient concentration 10% (w/w) for MC A4M and 12% (w/w) for HPMC K4M and E4M were the most optimal levels to balance between the extrudability and shape retention ability of the 3D printed objects. With the same concentration, MC A4M showed the best printing quality, followed by HPMC K4M and E4M. The gelling ability of cellulose derivatives led these biopolymers to providing the three-dimensional porous structures after gelation as potential matrices for drug loading. As shown in the SEM images, the theophylline clusters were attached to the cellulose derivatives matrices. This finding also explained that the 3D printability predominantly depended on both excipient concentration and type. Due to the difference in water solubility, these three excipients also showed different drug release rates. But all of these three excipients could extend the release time of theophylline over 12 hours. More importantly, these 3D printed tablets showed similar release profiles and release mechanisms compared to the tablets prepared by conventional direct compression and FDM 3D printing technology. SSE-based 3D printing offers significant advantages compared with other techniques in terms of low process temperature

(ambient temperature), rapid fabrication, customized dosage, lower environmental impact, and cost-effective approach as it saves up to 80% usage of excipients. The finding of this study will support the development of patient-tailored medicines with improved efficacy.

Considering the low cost and high biodegradability of cellulose derivatives, HPMC also attracted full attention as a biodegradable polymer in the additive manufacturing field. The third project, Chapter 4, aimed to investigate the viscoelastic properties and mechanical strength of HPMC K4M hydrogel as supportive material in the application of 3D printing technology. This study indicated that cellulose derivatives-based filament had a bunch of advantages such as low-cost, being ambient temperature printable, and eco-friendly processing. Thus, this biopolymer may have the potential to replace petroleum-based materials and high-cost biopolymers, such as acrylonitrile butadiene styrene (ABS) and polylactic acid (PLA) in manufacturing industries.

Due to the success in tablet fabrication of using SSE 3D printer with cellulose derivatives based hydrogel, the future work could focus on the feasibility of loading bioactive compounds, such as vitamins, probiotics, and proteins in the 3D printed hydrogel matrices. Besides, the release profile, physical properties, and moisture content of 3D printed tablets with post-processing, such as freeze-drying or coating, should be conducted to explore the different drug release profiles and the possibility of long-term preservation.

APPENDIX A. SUPPLYMENTARY MATERIALS OF MC A4M-BASED TABLETS

Chromatogram and Results

Injection Details

Injection Name:	**R2_MC10%allmg1,2htest**	*Run Time (min):*	**12.00**
Vial Number:	**RD1**	*Injection Volume:*	**20.00**
Injection Type:	**Unknown**	*Channel:*	**UV_VIS_1**
Calibration Level:		*Wavelength:*	**272**
Instrument Method:	**A_RT12mHPLC Test_1.2FR**	*Bandwidth:*	**2**
Processing Method:	**FSHN410**	*Dilution Factor:*	**1.0000**
Injection Date/Time:	**29/Jan/20 16:29**	*Sample Weight:*	**1.0000**

Chromatogram

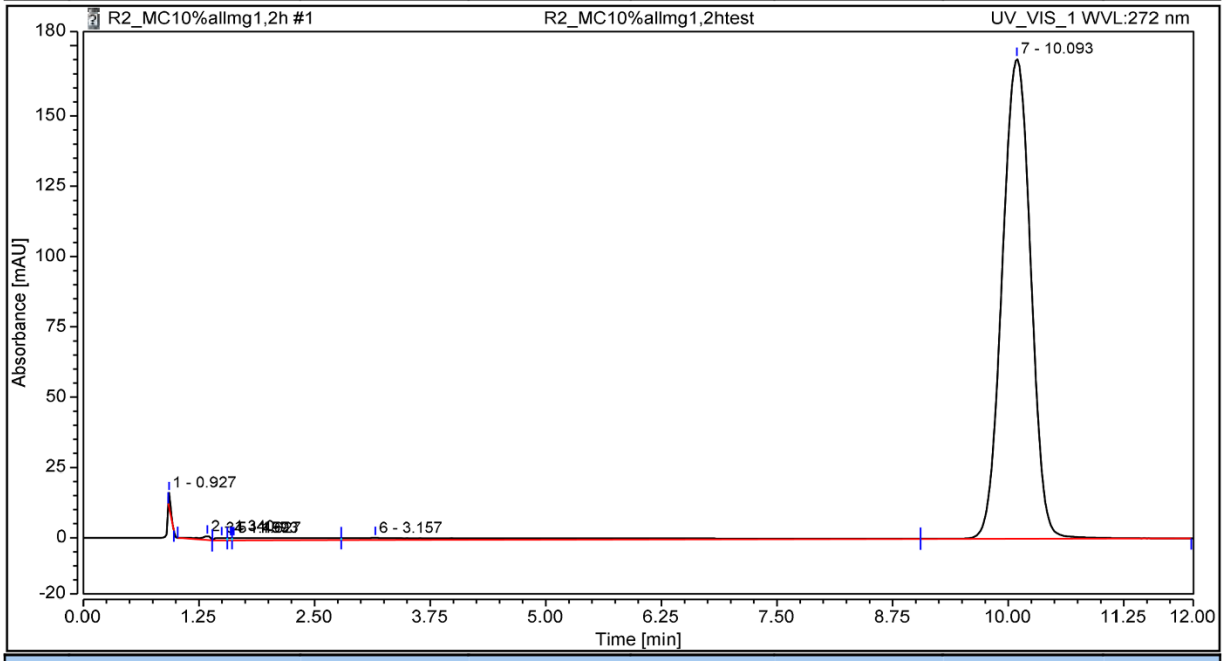

Integration Results

No.	Peak Name	Retention Time min	Area mAU*min	Height mAU	Relative Area %	Relative Height %	Amount n.a.
1		0.927	0.140	5.390	0.22	2.98	n.a.
2		1.340	0.185	1.332	0.28	0.74	n.a.
3		1.497	0.123	0.861	0.19	0.48	n.a.
4		1.593	0.042	0.846	0.06	0.47	n.a.
5		1.627	0.903	0.844	1.39	0.47	n.a.
6		3.157	2.563	0.789	3.94	0.44	n.a.
7		10.093	61.085	170.716	93.92	94.43	n.a.
Total:			**65.040**	**180.778**	**100.00**	**100.00**	

Figure A.1 HPLC chromatogram of 3D printed tablet MC10% 75mg.

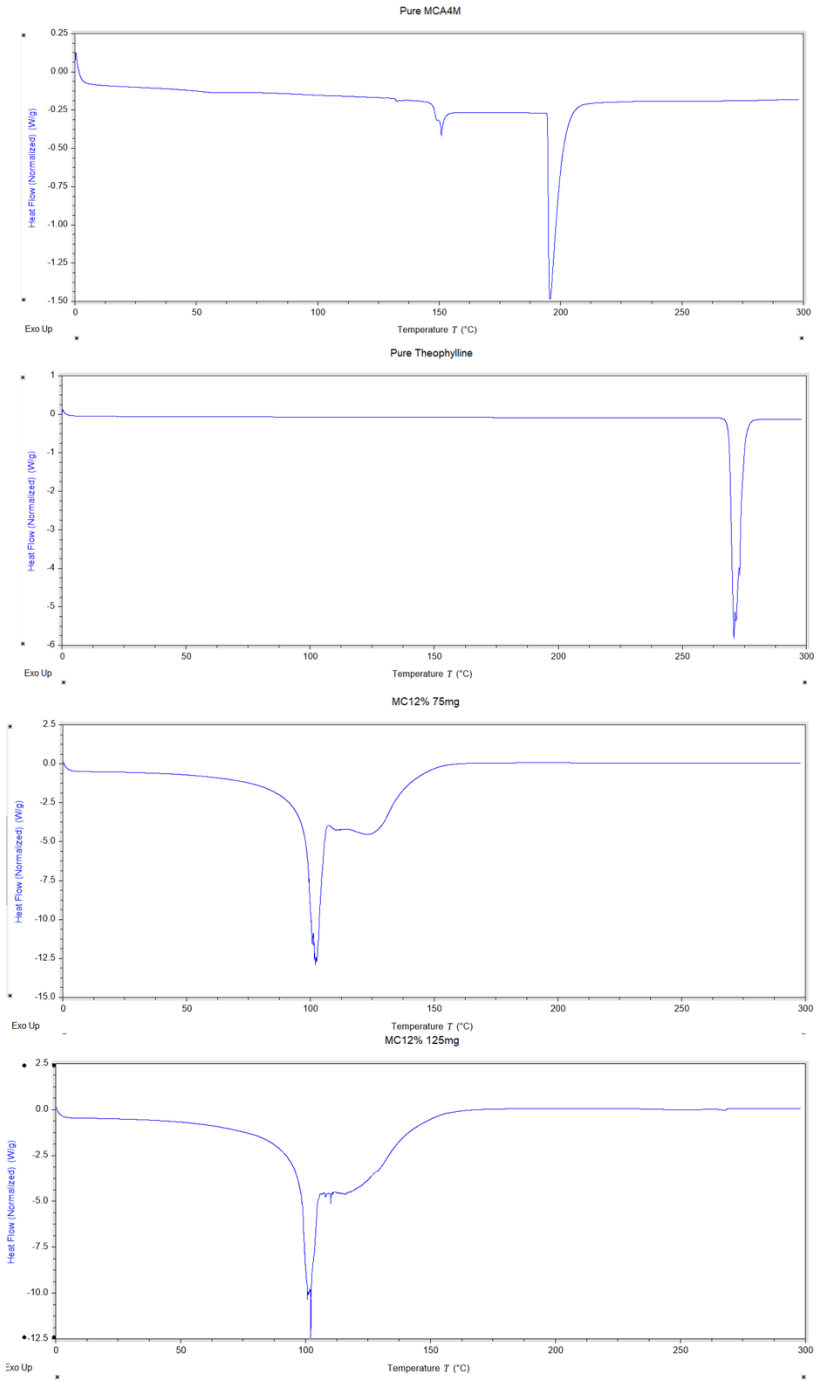

Figure A.2 DSC results of pure MC A4M, pure theophylline and therapeutic pastes with two formulations (MC12% 75mg and MC12% 125mg).

APPENDIX B. HPMC BASED TABLETS WITH 8% (W/W) CONCENTRATION RHEOLOGICAL DATA AND TABLETS APPEARANCE

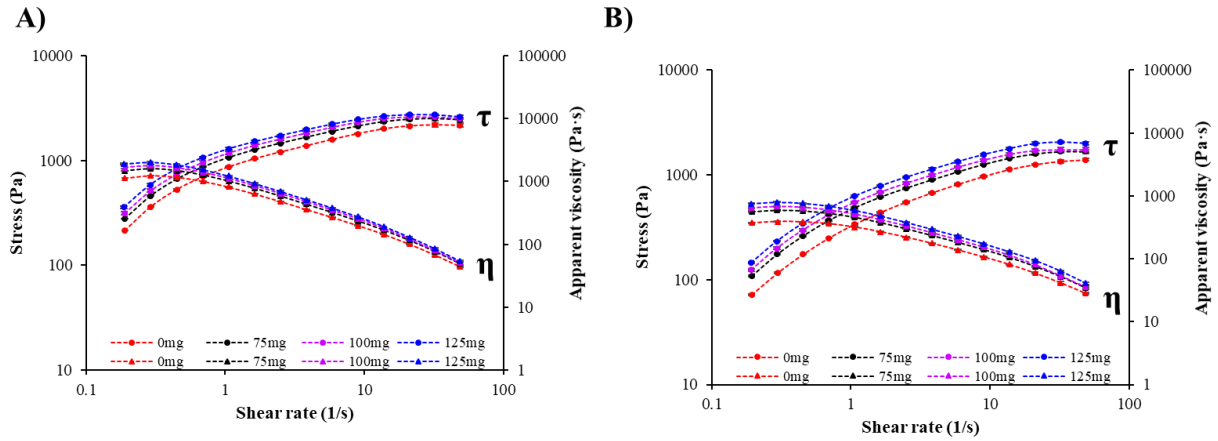

Figure B.1 Shear stress (τ) and apparent viscosity (η) versus shear rate profiles of HPMC K4M and E4M with different theophylline dosages (0, 75, 100, 125 mg) at different excipient concentrations: A) K4M8% and B) E4M8% (w/w).

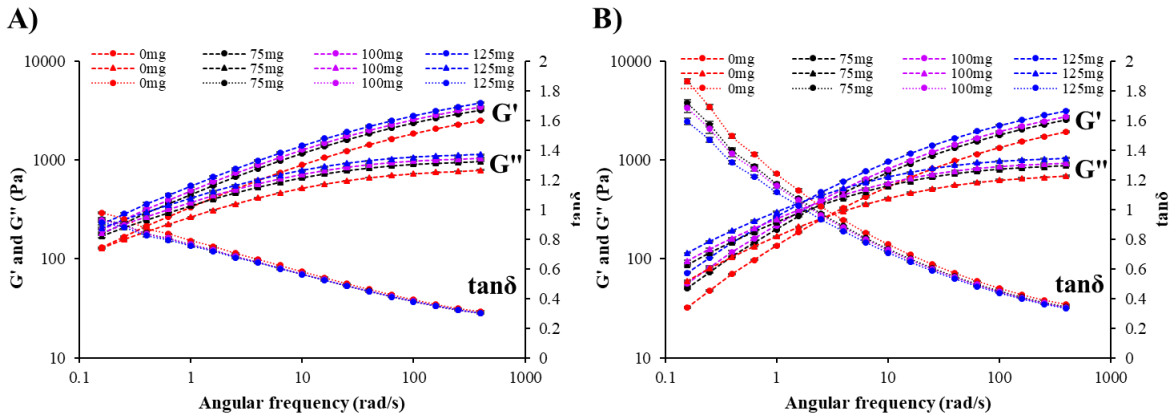

Figure B.2 Storage modulus (G'), loss modulus (G") and tanδ versus frequency profile of HPMC K4M and E4M with different theophylline dosages (0, 75, 100, 125 mg) at different excipient concentrations: A) K4M8% and B) E4M8% (w/w).

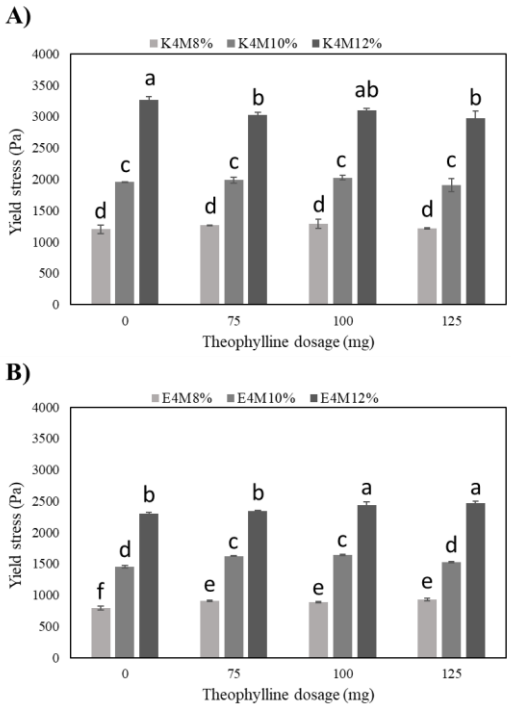

Figure B.3 Estimated yield stress (determined through the oscillatory stress sweep test - linear viscoelastic region) of different excipients: K4M and E4M with varying concentrations and theophylline dosages.

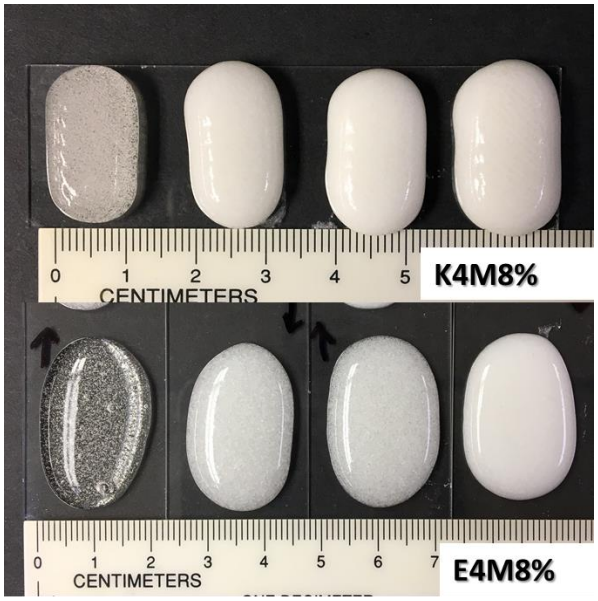

Figure B.4 The appearance of printed tablets with K4M and E4M 8% (w/w).

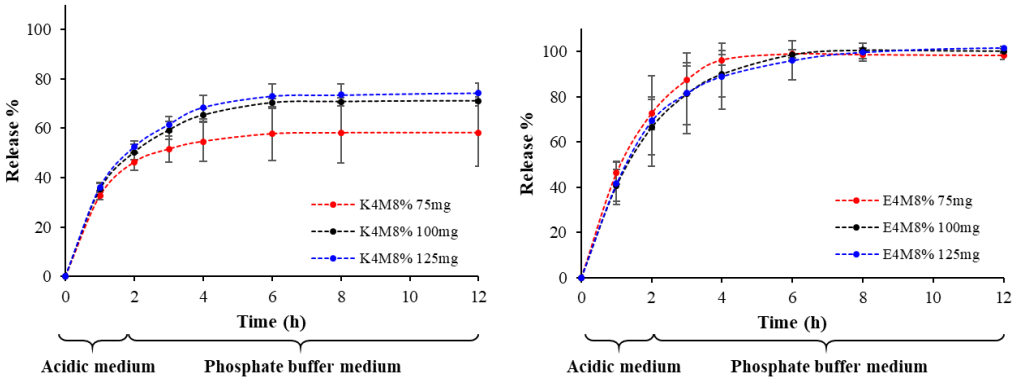

Figure B.5 The cumulative release profiles of theophylline from 3D printed tablets with different formulas: K4M and E4M 8% (w/w).

APPENDIX C. PRELIMINARY TEST RESULTS OF FREEZE DRIED TABLETS

Figure C.1 K4M12% (w/w) 100 mg tablets after freeze dry process.

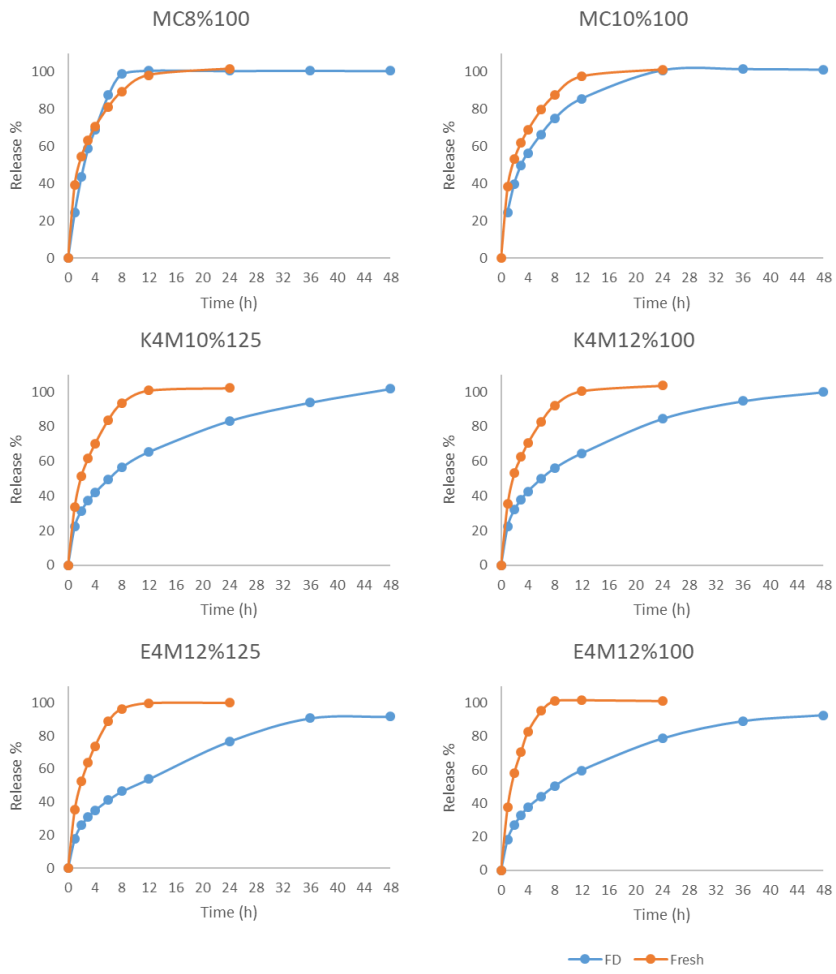

Figure C.2 Comparison of *in vitro* dissolution test results between 3D printed tablets before and after freeze dry process (orange line fresh means without freeze dry process; blue line FD means with freeze dry process).

Table C.1 Results of fitting *in vitro* release profile to different kinetic models from freeze dried tablets

Concentration % (w/w)	**Zero-order (R^2)**	**First-order (R^2)**	**Korsmeyer -Peppas (R^2)**	**Release exponent n**	**Higuchi (R^2)**
MC8% 100mg	0.82	0.92	0.95	0.76	0.96
MC10% 100mg	0.84	0.99	0.98	0.60	0.99
K4M10% 125mg	0.82	0.97	0.99	0.46	0.97
K4M12% 100mg	0.81	0.88	0.99	0.47	0.97
E4M12% 125mg	0.86	0.98	0.99	0.49	0.98
E4M12% 100mg	0.83	0.99	0.99	0.51	0.97

APPENDIX D. SEMI-SOLID EXTRUSION BASED 3D PRINTER

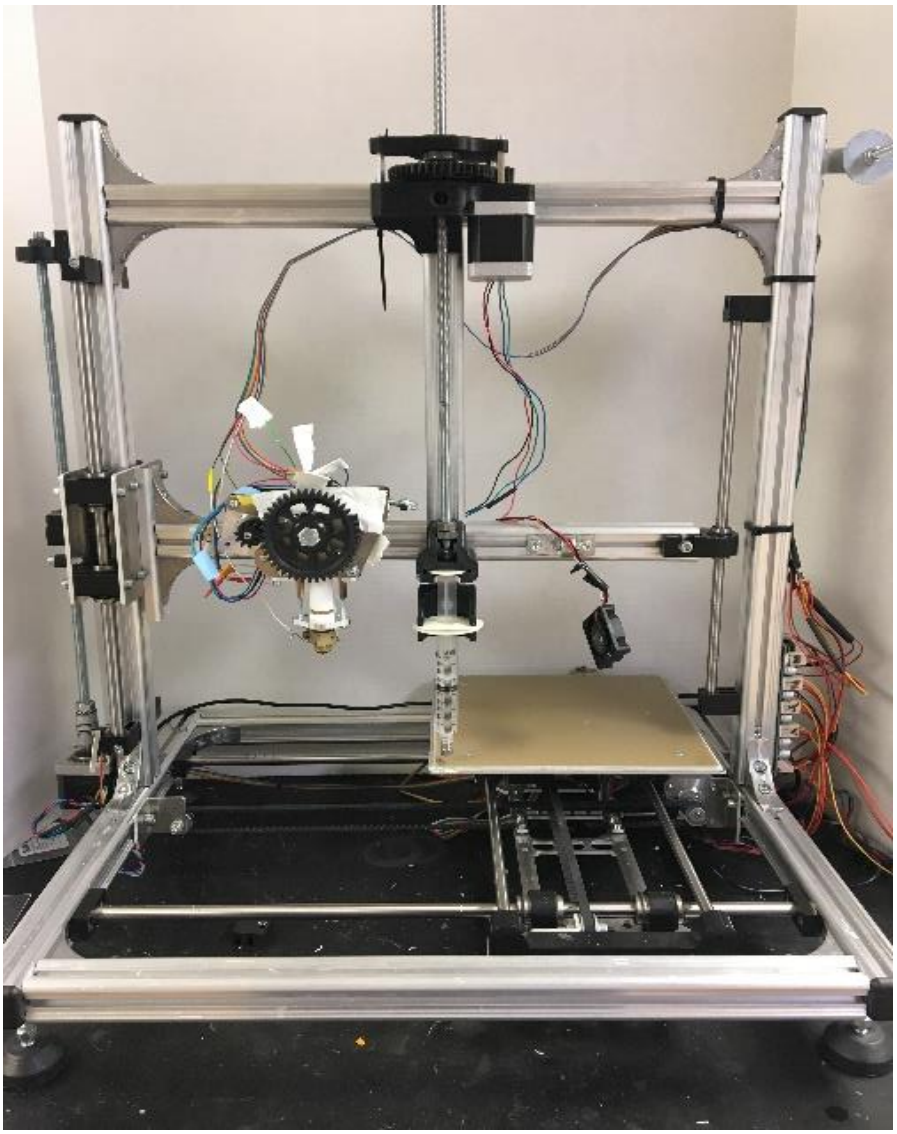

APPENDIX E. FIGURE CITATION APPROVAL

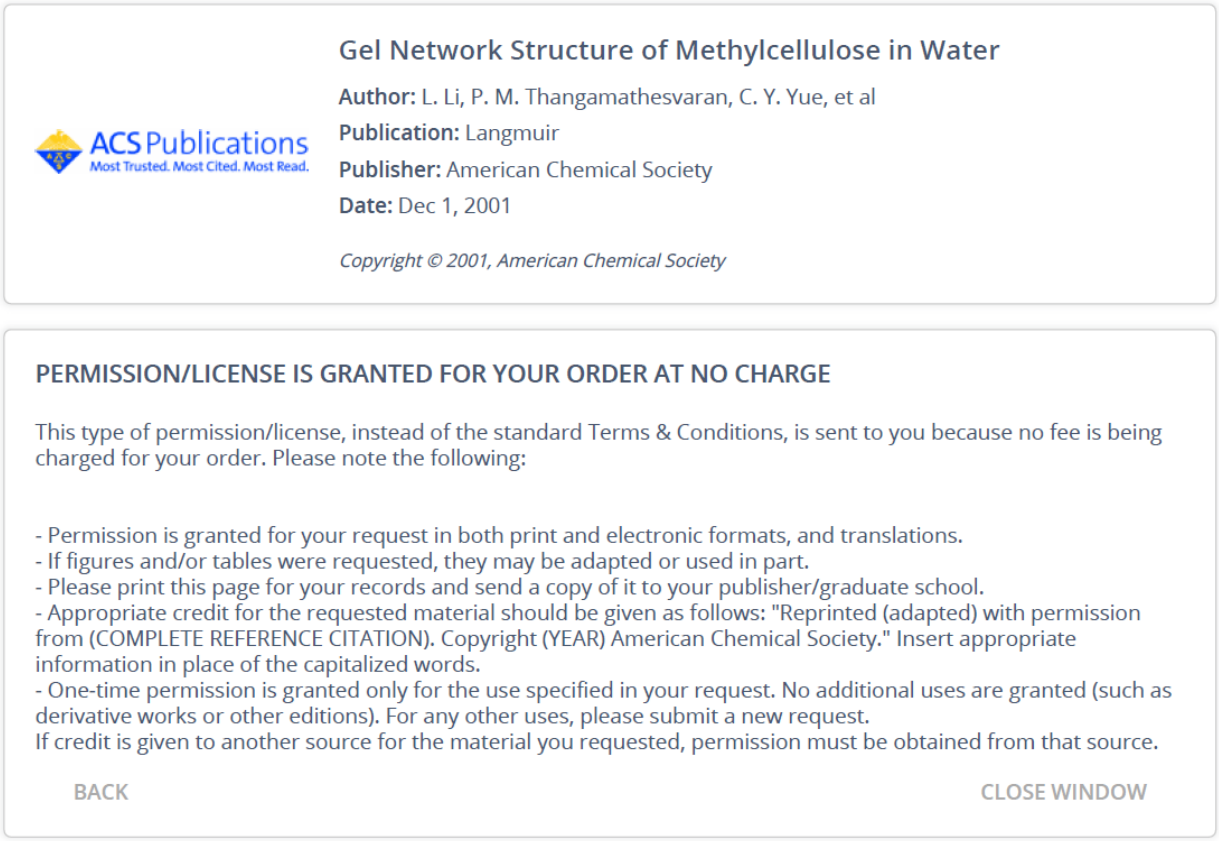

Gel Network Structure of Methylcellulose in Water

Author: L. Li, P. M. Thangamathesvaran, C. Y. Yue, et al
Publication: Langmuir
Publisher: American Chemical Society
Date: Dec 1, 2001

PERMISSION/LICENSE IS GRANTED FOR YOUR ORDER AT NO CHARGE

This type of permission/license, instead of the standard Terms & Conditions, is sent to you because no fee is being charged for your order. Please note the following:

- Permission is granted for your request in both print and electronic formats, and translations.
- If figures and/or tables were requested, they may be adapted or used in part.
- Please print this page for your records and send a copy of it to your publisher/graduate school.
- Appropriate credit for the requested material should be given as follows: "Reprinted (adapted) with permission from (COMPLETE REFERENCE CITATION). Copyright (YEAR) American Chemical Society." Insert appropriate information in place of the capitalized words.
- One-time permission is granted only for the use specified in your request. No additional uses are granted (such as derivative works or other editions). For any other uses, please submit a new request.

If credit is given to another source for the material you requested, permission must be obtained from that source.

BACK CLOSE WINDOW